The interplay of chaos and dissipation in driven quantum systems

Zur Erlangung des akademischen Grades eines
Doktors der Naturwissenschaften
der Mathematisch-Naturwissenschaftlichen Fakultät
der Universität Augsburg vorgelegte

Dissertation

von
Dipl.-Phys. Sigmund Kohler
aus
Ehingen (Donau)

Augsburg, im Februar 1999

Erster Berichter:	Prof. Dr. Peter Hänggi
Zweiter Berichter:	Prof. Dr. Thomas Dittrich
Tag der mündlichen Prüfung:	5. März 1999

Contents

1 Introduction **1**

2 Driven quantum systems and Floquet theory **5**
2.1 Discrete time-translation and Floquet ansatz 5
2.2 Composite Hilbert space 7
2.3 Properties of Floquet states 9
2.4 The propagator 11
2.5 Numerical computation of Floquet states 11
2.5.1 Floquet-matrix methods 12
2.5.2 Propagator methods 12

3 Quantum dissipation and Markov approximation **15**
3.1 The system-bath model 15
3.2 Quantum Langevin equation 16
3.3 Influence functional 18
3.4 Markovian master equation 20

4 Driving and dissipation: Floquet-Markov theory **23**
4.1 Simple inclusion of the driving 23
4.2 An improved Markovian master equation 24
4.3 Decomposition into Floquet basis 25
4.3.1 Matrix elements 25
4.3.2 Rotating-wave approximation 27
4.4 The dissipative quantum map and its numerical implementation . . . 28

5 The parametrically driven harmonic oscillator **31**
5.1 The model and its classical dynamics 31
5.2 Floquet states in stable regimes 34
5.3 Floquet-Markov description in full RWA 36
5.4 Basis-independent description beyond RWA 38
5.4.1 Wigner representation and Fokker-Planck equation 39
5.4.2 Wigner-Floquet solutions 40
5.4.3 Influence of the driving on the master equation 41
5.5 Asymptotics 43
5.5.1 The conservative limit 43

5.5.2 The high-temperature limit 44
5.6 Numerical results 45
5.7 Conclusion 48

6 The harmonically driven double-well potential 51
6.1 The model 52
6.1.1 Symmetries 53
6.1.2 Tunneling, driving, and dissipation 55
6.1.3 The onset of chaos 56
6.2 Chaotic tunneling near singlet-doublet crossings 58
6.2.1 Three-level crossings 58
6.2.2 Dissipative chaos-assisted tunneling 65
6.2.3 Asymptotic state 67
6.3 Signatures of chaos in the asymptotic state 72
6.3.1 Classical attractor 72
6.3.2 Quantum attractor 75

7 Summary and outlook 79

A The harmonic oscillator 81
A.1 Number states as a basis set 82
A.2 Coherent states 83
A.3 Quasiprobabilities 83
A.3.1 Wigner function 84
A.3.2 Husimi function and Wehrl entropy 85

B The density operator 87
B.1 Lindblad form 87
B.2 Coherence and entropy 88

C Solution of the Fokker-Planck equation 89

References 93

Acknowledgment 101

1 Introduction

The interplay of classical chaos and dissipation in a quantum system bears interesting effects at the border between classical and quantum mechanics like, e.g., the suppression of classical chaos by quantum interference [1] or its restauration by dissipation [2]. While the mutual influence of quantum coherence and classical chaos has been an extensive field of research since many years, the additional effects caused by coupling the chaotic system to an environment, namely dissipation and decoherence, have been studied only rarely. A reason may be the fact that by including dissipation, the computational effort grows drastically, since one has to deal with density matrices instead of wave functions.

In classical Hamiltonian systems, the transition from regular motion to chaos is most clearly visible in the change of the phase-space structure: With increasing nonlinearity, regular tori start to dissolve in a chaotic layer which grows in size until it covers the whole phase space. While the motion along regular tori is stable and predictable for long times, chaotic dynamics is characterized by a sensitive dependence on the initial conditions: Neighboring phase-space points start to diverge exponentially in time and a completely deterministic system evolves in a practically diffusive manner on a chaotic sea [3].

On a quantum level, the position-momentum uncertainty does not allow for the arbitrarily fine classical phase-space structures and results in coarse-graining over an area which is given by Planck's quantum of action. Thus, the classical dynamics leaves in the corresponding quantum system, at most, its signatures like, e.g., scars along unstable periodic orbits in the wave functions [4], or the centering of Husimi functions on classical manifolds [5]. Another characteristic quantum feature is the discreteness of the energy levels in bounded systems. In complex systems, eigenenergies are effectively random numbers whose statistical properties depend on the integrability of the corresponding classical dynamics [6–8]. In the fully chaotic case, the eigenenergies are anticorrelated and the inverse of their mean spacing defines a time scale, the so-called break time, after which the quantum dynamics becomes quasiperiodic and thus, classical chaos is suppressed [1]. This suppression of chaos relies on the perfect coherence of a superposition which remains for arbitrary long times. Therefore, any disruption of coherence, like it occurs due to the coupling to an environment, restores the characteristics of classical features at least to some extent [2].

One of the most intriguing quantum effects is tunneling, the coherent transport through a potential barrier. It was originally proposed by Hund [9] to explain the ammonium spectrum and studied since then in various modifications. A generic setting for the observation of tunneling is a symmetric bistable potential whose wells are separated by a static energy barrier. A time-dependent external field acting on

such a system may entail dramatic consequences for the quantum dynamics, even if its effect is barely visible in the classical phase space. Depending on the driving amplitude and frequency, an external driving can modify the tunnel rate by orders of magnitude or even bring tunneling to a complete standstill [10]. Tunneling is particularly sensitive to any disruption of coherence—in presence of dissipation it becomes a transient effect that fades out on a finite time scale [11, 12].

Driving the double-well potential with a frequency near the classical resonances results in even more significant consequences. They are apparent already in the classical phase space since chaos comes into play and the separatrix which encloses the wells is replaced by a chaotic layer. In the corresponding quantum system, we therefore observe chaotic tunneling—coherent transport between regular islands which are separated by a chaotic layer, rather than by a static barrier. The small but finite overlap of the tunnel doublets with the chaotic states, i.e., with states which are localized in the chaotic layer, typically increases the tunnel splittings and, consequently, the tunnel rates—the essence of chaos-assisted tunneling [13–15]. As soon as the chaotic layer grows in size and attains a significant overlap with the tunnel doublets, the tunnel splittings become of the order of the mean level spacing [16] and tunneling is replaced by chaotic diffusion [16–18].

The most successful approach to dissipation in quantum mechanics, consistent with the fundamental laws of quantum mechanics, is based on the coupling of the conservative system to external degrees of freedom. Probably the first proof that such a system-bath scheme results in dissipative quantum mechanics was given by Magalinskiĭ [19] for a harmonic oscillator. Using a perturbative approach, Zwanzig [20] derived from this model a Markovian master equation for a general classical system subject to weak dissipation. Master equations of this kind have been applied to various problems in solid state physics, quantum optics, and chemistry. Later, Caldeira and Leggett eliminated the bath exactly [11, 21], which enabled studying dissipative quantum systems, beyond a weak-coupling limit. However, even a partially analytical solution of the resulting path-integral expression is only feasible for the simplest systems, like harmonic potentials or two-level systems—the investigation of dissipative systems with complex dynamics requires to fall back to the weak-coupling regime.

Thus, for the description of strongly driven, nonlinear systems subject to weak dissipation, it is desirable to combine a Markovian approach to quantum dissipation, leading to a master equation for the density operator, with the Floquet formalism that allows to treat time-periodic forces of arbitrary strength and frequency [22]. While the Floquet formalism is exact and essentially amounts to using an optimal representation for the treatment of time-periodic problems [23–25], the simplification brought about by the Markovian description is achieved only at the expense of accuracy. Here, a subtle technical difficulty lies in the fact that the truncation of the long-time memory introduced by the bath, and the inclusion of the driving, do not commute. This implies that the result of the Markov approximation depends on whether the driving is considered in its derivation or not [26, 27].

Within the present work, we will implement a Markovian approach to quan-

tum dissipation based on the Floquet formalism to the investigation of two different systems, for each of which we have, besides other interesting aspects, one central question in mind: The *parametrically driven harmonic oscillator*, will serve predominantly to test different approximation schemes for the Floquet-Markov master equation and to study the modification of its dissipative part brought about by the driving. For this linear system, all approximative steps can be reliably checked since an exact solution is at hand [28]. Besides being an exactly solvable model with yet nontrivial dynamics, this system is interesting in its own right, since it describes the motion of an ion in a Paul trap. These traps have gained new interest very recently, since they form the central system in a scheme for a quantum computer [29] whose experimental realization is currently attempted. Thereby the main obstacle is, besides the preparation of the ground state, the loss of coherence once the computation has started.

The *harmonically driven quartic double-well potential*, a system which exhibits complex nonlinear dynamics, will be used as a working model for the investigation of chaotic tunneling in presence of dissipation. Recent studies of non-dissipative chaotic tunneling suggest that tunneling is accelerated by the influence of chaotic states, replacing a doublet structure by a three-level dynamics [30–33]. The bath, in turn, couples these states indirectly to all other states of the system and, thus, we expect to observe a novel dissipative tunnel scenario which is on the one hand richer than the conservative dynamics and on the other hand substantially different from the familiar two-state tunneling.

This thesis is organized as follows: In Chapter 2 we give an introduction to Floquet theory for quantum systems with periodic time-dependence. A brief review of the system-bath model for quantum dissipation and a derivation of a Markovian master equation is provided in Chapter 3 and combined with Floquet theory in Chapter 4 to obtain a Markovian description of periodically driven quantum systems subject to weak dissipation. Within this Floquet-Markov approach, we investigate the dynamics of the parametrically driven harmonic oscillator and the driven double-well potential in Chapters 5 and 6, respectively. Chapter 7 serves to summarize the main results. A number of merely technical issues is deferred to the appendix. Parts of this thesis have already been published in Refs. [27, 34].

2 Driven quantum systems and Floquet theory

Interactions of quantum systems with strong laser fields are characterized by two properties of the field: On the one hand, the influence of the field on the system is typically so strong that a treatment beyond perturbation theory becomes necessary, but the back-action of the system on the field is negligible. On the other hand, the field is in a coherent state with large mean photon number and, thus, can be described adequately by its expectation value, given by a function harmonic in time. This implies that an explicit time dependence of the Hamiltonian serves as a substitute for a canonical degree of freedom and raised interest in a theory for quantum systems with explicit periodic time dependence, thus an extension of Floquet theory [35] from classical to quantum mechanics. One-dimensional driven systems also play an important role as models for (quantum) chaos: Their "one and a half degrees of freedom" represent the minimal requirement for non-integrable dynamics [36]. Thus, they exemplify the simplest quantum systems with chaotic classical counterpart.

In this chapter we give an introduction to Floquet theory for quantum systems with periodic time dependence [12, 23–25, 36, 37], where we put strong focus on the properties of Floquet states and numerical methods which we use in subsequent chapters.

2.1 Discrete time-translation and Floquet ansatz

To reduce the complexity of a physical system, its symmetries are analyzed to obtain a proper *ansatz* for the symmetry-reduced solutions. In quantum mechanics, symmetry is expressed by an operator $\mathcal{S}$ which leaves the Schrödinger equation

$$\left(H(t) - \mathrm{i}\hbar\frac{\partial}{\partial t}\right)|\psi(t)\rangle = 0 \tag{2.1}$$

invariant, i.e., commutes with the operator $H(t) - \mathrm{i}\hbar\partial_t$. Thus, the solutions of the Schrödinger equation are, besides a time-dependent phase factor, also eigenfunctions of the symmetry operator [38].

For a Hamiltonian with T-periodic time dependence,

$$H(t) = H(t+T), \quad T = \frac{2\pi}{\Omega}, \tag{2.2}$$

the related symmetry operation is a discrete time translation by one period of the driving,

$$\mathcal{S}_T : t \to t + T. \tag{2.3}$$

As symmetry operations have to conserve the norm of any wavefunction, the eigenvalues of $\mathcal{S}$ are pure phase factors and we may assume for an eigenfunction $|\psi(t)\rangle$ the eigenvalue $\exp(-\mathrm{i}\theta)$, $\theta \in \mathbb{R}$,

$$\mathcal{S}_T|\psi(t)\rangle = |\psi(t+T)\rangle = \mathrm{e}^{-\mathrm{i}\theta}|\psi(t)\rangle. \tag{2.4}$$

By inserting this eigenvalue equation into the *ansatz*

$$|\psi(t)\rangle = \mathrm{e}^{-\mathrm{i}\epsilon t/\hbar}|\phi(t)\rangle, \quad \epsilon = \hbar\theta/T, \tag{2.5}$$

we obtain the condition

$$|\phi(t)\rangle = |\phi(t+T)\rangle, \tag{2.6}$$

which means that $|\phi(t)\rangle$ is periodic in time, alike the Hamiltonian. Thus for a system which obeys discrete time-translational symmetry, there exists a complete set $\{|\psi_\alpha(t)\rangle\}$ of solutions of the Schrödinger equation which have Floquet structure, i.e., they are of the form

$$|\psi_\alpha(t)\rangle = \mathrm{e}^{-\mathrm{i}\epsilon_\alpha t/\hbar}|\phi_\alpha(t)\rangle, \tag{2.7}$$

$$|\phi_\alpha(t)\rangle = |\phi_\alpha(t+T)\rangle. \tag{2.8}$$

However, a general solution of the Schrödinger equation (2.1) is given by a superposition of many Floquet states,

$$|\psi(t)\rangle = \sum_\alpha u_\alpha \mathrm{e}^{-\mathrm{i}\epsilon_\alpha t/\hbar}|\phi_\alpha(t)\rangle, \tag{2.9}$$

and is in general not of the form (2.5). The Floquet states $|\phi_\alpha(t)\rangle$ are, in contrast to the $|\psi_\alpha(t)\rangle$, not solutions of the Schrödinger equation. The ϵ_α have the dimension energy and in periodically driven systems play a role analogous to the eigenenergies in time-independent systems. In analogy to the quasimomentum of electrons in spatially periodic systems, they are called quasienergies. We emphasize that the T-periodic time-dependence of the Floquet states is only relevant for the dynamics within a period of the driving, whereas the long-time dynamics is governed by the phase factors $\exp(-\mathrm{i}\epsilon_\alpha t/\hbar)$.

Inserting (2.5) into the Schrödinger equation yields the eigenvalue equation for the Floquet states [23, 39, 40]

$$\mathcal{H}(t)|\phi(t)\rangle = \epsilon|\phi(t)\rangle \tag{2.10}$$

with the Hermitian Floquet Hamiltonian [40]

$$\mathcal{H}(t) = H(t) - \mathrm{i}\hbar\frac{\partial}{\partial t}. \tag{2.11}$$

Technically, the determination of the Floquet states from (2.10) is one of the main tasks in dealing with periodically time-dependent systems.

From a group-theoretical point of view, each Floquet state $|\phi_\alpha(t)\rangle$ belongs to an irreducible representation of an Abelian group, characterized by the Floquet exponent $\theta_\alpha = \epsilon_\alpha T/\hbar$ [40]. This exponent allows for an interpretation as a Berry phase [41].

Solutions of Floquet structure are found for dynamical systems that can be described by differential equations with periodically time-dependent coefficients [35, 42]. We also use this fact for the solution of classical equations of motion and for the solution of Fokker-Planck equations in subsequent chapters. In these cases, however, the eigenvalue equation which corresponds to (2.10) is in general non-Hermitian, thus the Floquet indices may be complex.

2.2 Composite Hilbert space

The state $|\psi(t)\rangle$ of a system, as well as the Floquet states $|\phi_\alpha(t)\rangle$, are elements of a Hilbert space $\mathcal{R}$, which describes the system's degrees of freedom. For a bounded particle moving in a potential, $\mathcal{R}$ is the space of square-integrable functions [43]. In many cases, $\mathcal{R}$ can be approximated by a Hilbert space with finite dimension.

It is possible to describe the time dependence of the Floquet states within the framework of a Hilbert space theory. According to (2.8), the Floquet states are elements of the space of T-periodic functions, denoted by $\mathcal{T}$ [40]. An inner product on $\mathcal{T}$ is defined by

$$(f, g) = \frac{1}{T}\int_0^T \mathrm{d}t\, f^*(t)\, g(t), \tag{2.12}$$

and a set of orthonormalized basis functions reads [43]

$$\varphi_n(t) = \mathrm{e}^{-\mathrm{i}n\Omega t}, \quad \Omega = \frac{2\pi}{T}, \quad n \in \mathbb{Z}. \tag{2.13}$$

For a basis independent notation, we define the vectors $|n\rangle_{\mathcal{T}}$ by

$$\varphi_n(t) = \langle t|n\rangle_{\mathcal{T}}. \tag{2.14}$$

To avoid confusion with elements of configuration space $\mathcal{R}$, we mark these vectors by an index $\mathcal{T}$. The basis set $\{\varphi_n\}$ is orthonormalized and complete [43],

$$(\varphi_n, \varphi_{n'}) = \delta_{n,n'}\,, \tag{2.15}$$

$$\frac{1}{T}\sum_n \varphi_n^*(t)\,\varphi_n(t') = \delta_T(t - t'), \tag{2.16}$$

where δ_T denotes the T-periodic delta function.

We combine the periodic time dependence of the Floquet states with their spatial degrees of freedom and interpret them as elements of a composite Hilbert space $\mathcal{R} \otimes \mathcal{T}$. The inner product (2.12) is extended accordingly,

$$\langle\langle\phi|\phi'\rangle\rangle = \frac{1}{T}\int_0^T \mathrm{d}t\, \langle\phi(t)|\phi'(t)\rangle. \tag{2.17}$$

The elements of this composite Hilbert space, written in "time representation," are T-periodic states,

$$\langle t|\phi\rangle\rangle \equiv |\phi(t)\rangle = |\phi(t+T)\rangle. \tag{2.18}$$

By this introduction of a Hilbert space structure for the time dependence, we formally traced back the computation of Floquet states to the computation of eigenstates of a time-independent Hamiltonian with an additional degree of freedom. The methods known for the computation of energy eigenstates of a time-independent Hamiltonian, like e.g., perturbation theory, can be applied accordingly [39, 40].

The decomposition of a state $|\phi(t)\rangle$ into the set of basis functions (2.13) is equivalent to its representation as a Fourier series,

$$|\phi_\alpha(t)\rangle = \sum_n \mathrm{e}^{-\mathrm{i}n\Omega t}\,|c_{\alpha,n}\rangle, \tag{2.19}$$

$$|c_{\alpha,n}\rangle = \frac{1}{T}\int_0^T \mathrm{d}t\,\mathrm{e}^{\mathrm{i}n\Omega t}\,|\phi_\alpha(t)\rangle. \tag{2.20}$$

The Fourier modes in this context are also called Floquet channels.

Semiclassical interpretation of the Floquet states

A time-dependent Hamiltonian is usually obtained from a time-independent theory by substituting a part of the system by its classical limit [25]. This allows for a semiclassical interpretation of the vectors $|n\rangle_{\mathcal{T}}$ and the Floquet states [40]. We restrict ourselves to the case of a linearly coupled driving field with cosine shape.

A system S, which couples via dipole interaction to a single-mode laser with frequency Ω, can be described by the Hamiltonian [44]

$$H = H_S + \mu x(a + a^+) + \hbar\Omega a^+ a. \tag{2.21}$$

We assume in the semiclassical limit that the state of the laser field is a coherent one (see Appendix A) and that it possesses a very high mean photon number,

$$|z\rangle = |\sqrt{n_0}\exp(\mathrm{i}\Omega t)\rangle\,, \quad n_0 \gg 1. \tag{2.22}$$

Under this condition, the description of the system can be simplified in two ways:

1. We replace the operators a and a^+ by their expectation values (see Appendix A) and obtain a driven system with a time-dependent Hamiltonian. The corresponding Floquet Hamiltonian reads

$$\mathcal{H} = H_S + 2\mu x\sqrt{n_0}\cos(\Omega t) + \hbar\Omega n_0 - \mathrm{i}\hbar\partial_t, \tag{2.23}$$

decomposed into the basis set $\{|n\rangle_{\mathcal{T}}\}$,

$$\mathcal{H}_{n,n'} = H_S\delta_{n,n'} + \mu x\sqrt{n_0}\,(\delta_{n,n'+1} + \delta_{n,n'-1}) + \hbar\Omega(n_0 - n)\delta_{n,n'}. \tag{2.24}$$

2. We decompose the Hamiltonian H, whose eigenfunctions are the so-called dressed states, into the number states (A.10) of the laser mode to obtain

$$H_{n,n'} = H_S\delta_{n,n'} + \mu x\left(\sqrt{n+1}\,\delta_{n,n'+1} + \sqrt{n}\,\delta_{n,n'-1}\right) + \hbar\Omega n\,\delta_{n,n'}. \tag{2.25}$$

If the state of the laser field is the highly exited coherent state (2.22), we get relevant contributions only for $n \approx n_0 \gg 1$. The prefactors $\sqrt{n}$ and $\sqrt{n+1}$ in this limit become $\sqrt{n_0} + \mathcal{O}(n_0^{-1/2})$.

The Floquet Hamiltonian (2.24) agrees—besides a shift in the index—with the Hamiltonian (2.25). Therefore the basis states $|n\rangle_{\mathcal{T}}$ allow for an interpretation as the semiclassical limit of the number states of the laser field and the Floquet states as the semiclassical limit of the dressed states.

2.3 Properties of Floquet states

Equivalent representations

Assuming that $|\phi(t)\rangle$ is an eigenvector of $\mathcal{H}(t)$ with eigenvalue ϵ,

$$\mathcal{H}(t)\,|\phi(t)\rangle = \epsilon|\phi(t)\rangle, \tag{2.26}$$

the state

$$|\phi^{(n)}(t)\rangle = \mathrm{e}^{\mathrm{i}n\Omega t}|\phi(t)\rangle \tag{2.27}$$

obeys

$$\begin{aligned}\mathcal{H}(t)\,|\phi^{(n)}(t)\rangle &= (H(t) + \partial_t)\,\mathrm{e}^{\mathrm{i}n\Omega t}|\phi(t)\rangle &(2.28)\\ &= (\epsilon + n\hbar\Omega)\,\mathrm{e}^{\mathrm{i}n\Omega t}|\phi(t)\rangle. &(2.29)\end{aligned}$$

This means that $|\phi^{(n)}(t)\rangle$ is also an eigenvector of the Floquet Hamiltonian $\mathcal{H}(t)$, i.e., a Floquet state, but with eigenvalue

$$\epsilon^{(n)} = \epsilon + n\hbar\Omega. \tag{2.30}$$

The respective solutions of the Schrödinger equation,

$$\begin{aligned}|\psi^{(n)}(t)\rangle &= \mathrm{e}^{-\mathrm{i}(\epsilon+n\hbar\Omega)t/\hbar}|\phi^{(n)}(t)\rangle &(2.31)\\ &= |\psi(t)\rangle &(2.32)\end{aligned}$$

are identical. Thus, there exists a class of equivalent Floquet states whose quasienergies differ only by integer multiples of $\hbar\Omega$. They all describe the same physical state. Therefore, it is sufficient to take only those Floquet states into account, whose quasienergies lie within a single Brillouin zone $\hbar\omega_{\mathrm{BZ}} \le \epsilon < \hbar(\omega_{\mathrm{BZ}} + \Omega)$.

In the following, we denote by $\{|\phi_\alpha(t)\rangle\}$ a complete set of Floquet states with corresponding quasienergies $\{\epsilon_\alpha\}$. They are orthonormalized with respect to the inner product (2.17),

$$\langle\langle\phi_\alpha|\phi_{\alpha'}\rangle\rangle = \delta_{\alpha,\alpha'}. \tag{2.33}$$

Orthonormalization on $\mathcal{R}$

The inner product of two non-equivalent Floquet states on $\mathcal{R}$ obeys the T-periodicity of the Floquet states and can be written as a Fourier series,

$$\langle\phi_\alpha(t)|\phi_{\alpha'}(t)\rangle = \sum_n \kappa_n \mathrm{e}^{-\mathrm{i}n\Omega t}. \tag{2.34}$$

The Fourier coefficients read

$$\kappa_n = \frac{1}{T}\int_0^T \mathrm{d}t'\, \mathrm{e}^{\mathrm{i}n\Omega t'} \langle\phi_\alpha(t')|\phi_{\alpha'}(t')\rangle \tag{2.35}$$

$$= \langle\langle\phi_\alpha|\phi_{\alpha'}^{(n)}\rangle\rangle = \delta_{\alpha,\alpha'}\delta_{n,0}\,, \tag{2.36}$$

where the time integration has been expressed by the inner product (2.17). Thus, we get

$$\langle\phi_\alpha(t)|\phi_{\alpha'}(t)\rangle = \delta_{\alpha,\alpha'}\,. \tag{2.37}$$

This means that from the orthonormalization of the Floquet states with respect to the inner product (2.17) on $\mathcal{R}\otimes\mathcal{T}$ we obtain orthonormalization with respect to the inner product on $\mathcal{R}$ at equal times. Here however, caution is appropriate: The orthonormalization on $\mathcal{R}$ is in general only valid for equal times and is in particular not valid for the Fourier components (2.20).

Mean energy

Due to the Brillouin-zone structure (2.30), quasienergies do not allow for global ordering. The instantaneous energies

$$E_\alpha(t) = \langle\psi_\alpha(t)|H(t)|\psi_\alpha(t)\rangle \tag{2.38}$$

$$= \langle\phi_\alpha(t)|H(t)|\phi_\alpha(t)\rangle \tag{2.39}$$

do not either, since they vary with time. A quantity that is defined on the full real axis and therefore does allow for a complete ordering is the mean energy [12, 23–25]

$$E_\alpha = \frac{1}{T}\int_0^T \mathrm{d}t\, E_\alpha(t) \tag{2.40}$$

$$= \epsilon_\alpha + \mathrm{i}\hbar\langle\langle\phi_\alpha|\frac{\partial}{\partial t}|\phi_\alpha\rangle\rangle, \tag{2.41}$$

which results from averaging over one period of the driving. By use of the Fourier representation (2.19) we obtain

$$E_\alpha = \sum_n (\epsilon_\alpha + n\hbar\Omega)\langle c_{\alpha,n}|c_{\alpha,n}\rangle \tag{2.42}$$

Thus the nth Floquet channel gives a contribution $\epsilon_\alpha + n\hbar\Omega$, weighted by the squared modulus $\langle c_{\alpha,n}|c_{\alpha,n}\rangle$ of the corresponding Fourier coefficient.

2.4 The propagator

The time evolution of a quantum system can be written by use of a unitary operator $U(t,t')$, which is a solution of the Schrödinger equation,

$$\mathrm{i}\hbar\frac{\partial}{\partial t}U(t,t') = H(t)\,U(t,t'), \tag{2.43}$$

$$U(t,t) = \mathsf{1}. \tag{2.44}$$

A formal integration yields

$$U(t,t') = \mathsf{T}\exp\left(-\frac{\mathrm{i}}{\hbar}\int_{t'}^{t}\mathrm{d}t''H(t'')\right), \tag{2.45}$$

where T denotes time ordering. Due to the time dependence of the Hamiltonian, $U(t,t')$ depends explicitly on both times t and t', not only on their difference.

Expressed in terms of the Floquet states, the propagator reads

$$U(t,t') = \sum_{\alpha}\mathrm{e}^{-\mathrm{i}\epsilon_\alpha(t-t')/\hbar}|\phi_\alpha(t)\rangle\langle\phi_\alpha(t')|, \tag{2.46}$$

as this expression obviously solves the Schrödinger equation and the initial condition (2.44) is ensured by the completeness of the Floquet states.

The propagator $U(T,0)$ defines a quantum map for the propagation over a full period of the driving,

$$U(T,0) = \sum_{\alpha}\mathrm{e}^{-\mathrm{i}\epsilon_\alpha T/\hbar}|\phi_\alpha(0)\rangle\langle\phi_\alpha(0)|, \tag{2.47}$$

$$U(nT,0) = \sum_{\alpha}\mathrm{e}^{-\mathrm{i}n\epsilon_\alpha T/\hbar}|\phi_\alpha(0)\rangle\langle\phi_\alpha(0)| \tag{2.48}$$

$$= [U(T,0)]^n, \tag{2.49}$$

To obtain the last line, we used the T-periodicity of the Floquet states and their completeness and orthogonality at equal times. The propagator $U(T,0)$ is indispensable for the investigation of the long-time dynamics of driven quantum systems [23, 25].

The Floquet states at time t are instantaneous eigenstates of the one-period propagator $U(t+T,t)$,

$$U(t+T,t)|\phi_\alpha(t)\rangle = \mathrm{e}^{-\mathrm{i}\epsilon_\alpha T/\hbar}|\phi_\alpha(t)\rangle, \tag{2.50}$$

as can easily be seen by inserting the Floquet-state representation (2.46) of the propagator.

2.5 Numerical computation of Floquet states

Among the methods for the computation of Floquet states of bounded systems, we essentially discern two classes [37]: The first class consists of methods based directly

on the solution of the eigenvalue equation (2.10) of the Floquet Hamiltonian. A second class of methods starts with the computation of the Floquet propagator $U(T,0)$, followed by the solution of the eigenvalue equation (2.50) for the propagator. In the present work, we treat systems subject to a cosine-shaped driving. Accordingly, we elucidate the numerical methods for the case of a Hamiltonian of the structure

$$H(t) = H_0 + 2H_1 \cos(\Omega t), \tag{2.51}$$

where we have introduced a factor 2 for ease of notation. They can be generalized straightforwardly.

2.5.1 Floquet-matrix methods

The Floquet Hamiltonian for (2.51) decomposed into the basis $\{|n\rangle_{\mathcal{T}}\}$ reads

$$\mathcal{H}_{n,n'} = (H_0 + n\hbar\Omega)\delta_{n,n'} + H_1(\delta_{n,n'+1} + \delta_{n,n'-1}), \tag{2.52}$$

or in matrix notation,

$$\mathcal{H} = \begin{pmatrix} \ddots & \vdots & \vdots & \vdots & \vdots & \vdots & \\ \cdots & H_0 + 2\hbar\Omega & H_1 & 0 & 0 & 0 & \cdots \\ \cdots & H_1 & H_0 + \hbar\Omega & H_1 & 0 & 0 & \cdots \\ \cdots & 0 & H_1 & H_0 & H_1 & 0 & \cdots \\ \cdots & 0 & 0 & H_1 & H_0 - \hbar\Omega & H_1 & \cdots \\ \cdots & 0 & 0 & 0 & H_1 & H_0 - 2\hbar\Omega & \cdots \\ & \vdots & \vdots & \vdots & \vdots & \vdots & \ddots \end{pmatrix}. \tag{2.53}$$

The eigenvectors of (2.53) are the Fourier components $|c_{\alpha,n}\rangle$ of the Floquet states, as the decomposition into $\{|n\rangle_{\mathcal{T}}\}$ corresponds to Fourier representation. Due to the Brillouin-zone like structure, it is sufficient to compute all eigenvectors whose eigenvalues lie in an interval of size $\hbar\Omega$.

As a basis set for the Hilbert space $\mathcal{R}$, one commonly uses M eigenstates of the undriven Hamiltonian H_0, which itself has been decomposed into the eigenfunctions of the harmonic oscillator (see Appendix A). Thus, for N Floquet channels the dimension of the Floquet matrix is NM and the computational effort for the matrix diagonalization is proportional to $(NM)^3$.

A further efficient method for the computation of eigenvectors of the tridiagonal matrix (2.53) are matrix continued fractions [25,45]. We shall not apply this method.

2.5.2 Propagator methods

The quasienergies and the Floquet states at time $t = 0$ can be extracted from the one-period propagator by use of the eigenvalue equation (2.50) of the unitary operator $U(T,0)$. In numerical calculations, however, it is advantageous to diagonalize the Hermitian operator

$$V = \mathrm{i}\frac{1 + U(T,0)}{1 - U(T,0)}. \tag{2.54}$$

Being a function of $U(T,0)$, V possesses the same eigenvectors as $U(T,0)$, namely the Floquet states $|\phi_\alpha(0)\rangle$. It is straightforward to show that the corresponding eigenvalues read $\cot(\epsilon_\alpha T/2\hbar)$.

For the computation of the mean energies and to determine the coefficients of the master equation for the dissipative dynamics (see next chapter), it is necessary to know the Floquet states' Fourier coefficients $|c_{\alpha,n}\rangle$. They are obtained by propagating the $|\phi_\alpha(0)\rangle$ over one period of the driving, which yields $|\psi_\alpha(t)\rangle = \exp(-\mathrm{i}\epsilon_\alpha t/\hbar)|\phi_\alpha(t)\rangle$, for t in the range $[0,T]$. The $|c_{\alpha,n}\rangle$ result from Fourier decomposition, according to their definition (2.20). The propagation can be performed in various ways. In the following, we sketch the methods implemented in this work.

Direct integration of the Schrödinger equation

The most simple method for the computation of the propagator is the direct integration of the Schrödinger equation by use of a Runge-Kutta routine, where the initial condition is the unit matrix. An extension of this method to other shapes of driving is rather easy.

It emerges that the numerical effort for the propagation is proportional to NM^3, however with a much larger prefactor compared to the diagonalization of the Floquet matrix. Therefore, computing the Floquet states by direct integration is well-suited if a large number of Floquet channels is required.

The (t,t')-formalism

A very efficient numerical method for the computation of the propagator for a Hamiltonian of the form (2.51) is derived from the (t,t')-formalism [38,46,47]. There, the Schrödinger is extended by a second time coordinate to read

$$\mathrm{i}\hbar\frac{\partial}{\partial t}|\psi(t,t')\rangle = \left(H(t') - \mathrm{i}\hbar\frac{\partial}{\partial t'}\right)|\psi(t,t')\rangle. \tag{2.55}$$

The time t' is treated formally like an additional canonical coordinate of a time-independent problem. We postulate T-periodic boundary conditions in t', which enables decomposition into the basis set (2.13). Being a solution of (2.55), $|\psi(t,t')\rangle$, on the cut $t'=t$ where $\partial t'/\partial t = 1$, obeys

$$\mathrm{i}\hbar\frac{\partial}{\partial t}|\psi(t,t)\rangle = \mathrm{i}\hbar\left(\frac{\partial}{\partial t} + \frac{\partial}{\partial t'}\right)|\psi(t,t')\rangle\Big|_{t'=t} \tag{2.56}$$

$$= H(t)|\psi(t,t)\rangle. \tag{2.57}$$

Thus $|\psi(t,t)\rangle$ is a solution of the "true" Schrödinger equation (2.1). In an analogous way, from the propagator

$$\mathcal{U}(t-t_0) = \mathrm{e}^{-\mathrm{i}\mathcal{H}(t-t_0)/\hbar} \tag{2.58}$$

of the extended Schrödinger equation (2.55) one can extract the "true" propagator. It reads

$$U(t,t_0) = {}_{\mathcal{T}}\langle 0|\mathcal{U}(t-t_0)|t'\rangle_{\mathcal{T}}|_{t'=t} \tag{2.59}$$

$$= \sum_n {}_{\mathcal{T}}\langle 0|\mathcal{U}(t-t_0)|n\rangle_{\mathcal{T}}\, \mathrm{e}^{\mathrm{i}n\Omega t}. \tag{2.60}$$

This is so because on the one hand it fulfills the initial condition

$$U(t_0,t_0) = \sum_n {}_{\mathcal{T}}\langle 0|1_{\mathcal{R}\otimes\mathcal{T}}|n\rangle_{\mathcal{T}} \mathrm{e}^{\mathrm{i}n\Omega t_0} = 1_{\mathcal{R}}, \tag{2.61}$$

and on the other hand solves the Schrödinger equation,

$$\mathrm{i}\hbar\frac{\partial}{\partial t}U(t,t_0) = \mathrm{i}\hbar\left(\frac{\partial}{\partial t}+\frac{\partial}{\partial t'}\right) {}_{\mathcal{T}}\langle 0|\mathcal{U}(t-t_0)|t'\rangle_{\mathcal{T}}\Big|_{t'=t} \tag{2.62}$$

$$= H(t)U(t,t_0). \tag{2.63}$$

Here the time ordering, which we have to consider explicitly in (2.45), is intrinsic.

By Taylor expansion of the extended propagator $\mathcal{U}$ one obtains for the time step from t to $t+\tau$

$$U(t+\tau,t) = \sum_n \mathrm{e}^{\mathrm{i}n\Omega(t+\tau)} {}_{\mathcal{T}}\langle 0|\mathcal{U}(\tau)|n\rangle_{\mathcal{T}} \tag{2.64}$$

$$= \sum_n \mathrm{e}^{\mathrm{i}n\Omega(t+\tau)} \sum_{\nu=0}^{\infty} \mathcal{U}_{0,n}^{(\nu)}(\tau), \tag{2.65}$$

with

$$\mathcal{U}_{0,n}^{(\nu)}(\tau) = \frac{1}{\nu!}\left(-\frac{\mathrm{i}\tau}{\hbar}\right)^{\nu} {}_{\mathcal{T}}\langle 0|\mathcal{H}^{\nu}|n\rangle_{\mathcal{T}}. \tag{2.66}$$

For a sufficiently small time step τ, it is possible to truncate the sum over ν after $N+1$ terms. Due to the tridiagonal structure of $\mathcal{H}$, in the sum over n all terms with $|n| > N$ vanish. Typically, already a few Floquet channels are sufficient to obtain numerical convergence [47].

In the special case $N = 1$ we obtain $U(t+\tau,t) = 1 - \mathrm{i}H(t+\tau)\tau/\hbar$, the first term of the Taylor expansion of the time-ordered exponential (2.45). For larger N, the time ordering results in a more complicated expression.

3 Quantum dissipation and Markov approximation

Within the framework of classical mechanics, dissipation can be introduced phenomenologically just by adding a velocity-proportional friction force. Although an extension of the Lagrange formalism to this model of dissipation is possible [48], quantization results in unphysical properties, e.g., a time-dependent mass, or doesn't handle the uncertainty relation properly [49].

The most successful approach to dissipation in quantum mechanics, consistent with the fundamental laws of quantum mechanics, is based on the coupling of the conservative system to external degrees of freedom. Probably the first proof that such a system-bath scheme results in dissipative quantum mechanics was given by Magalinskiĭ [19] for a harmonic oscillator. Zwanzig generalized this concept within the framework of classical stochastic processes to arbitrary potentials and derived a Markovian master equation for the dynamics of the dissipative system by the so-called projector formalism [20]. By similar approaches, master equations for quantum systems [50–52] were derived and applied in laser physics [50] and to nuclear magnetic resonance and electron-spin resonance. Later, Caldeira and Leggett rediscovered the system-bath model in the context of dissipative tunneling [11] and, in a path-integral formulation, eliminated the bath exactly [21,53]. This enabled the investigation of dissipative quantum systems, beyond a weak-coupling limit. Strong system-bath correlations result in interesting effects, among them most prominently the algebraic decay of correlation functions at zero temperature [54, 55].

However, as soon as nonlinear forces come into play, the path-integral approach requires to resort to extensive and sophisticated numerics, such as Monte-Carlo calculations [56–58], with their own shortcomings. Thus, for the description of nonlinear systems subject to weak dissipation, it is desirable to to treat the influence of the bath in perturbation theory, leading to a Markovian master equation for the density operator [50–52]. In this chapter, we introduce the system-bath model and derive a Markovian master equation for the reduced density operator for the case of a static central system.

3.1 The system-bath model

To achieve a microscopic model of dissipation, we couple the system bilinearly to a bath of non-interacting harmonic oscillators with masses m_ν, frequencies ω_ν, momenta p_ν, and coordinates x_ν, with the coupling strength c_ν [11, 19, 59]. The total Hamiltonian of system and bath is then given by

$$H = H_{\rm S} + H_{\rm SB} + H_{\rm B}, \tag{3.1}$$

where H_{S} denotes the Hamiltonian of the central system and

$$H_{\mathrm{B}} = \sum_{\nu} \left(\frac{p_\nu^2}{2m_\nu} + \frac{1}{2} m_\nu \omega_\nu^2 x_\nu^2 \right), \tag{3.2}$$

$$H_{\mathrm{SB}} = -x \sum_{\nu} c_\nu x_\nu + x^2 \sum_{\nu} \frac{c_\nu^2}{2m_\nu \omega_\nu^2}, \tag{3.3}$$

describe the heat bath and its coupling to the system. The second term in H_{SB}, which depends only on the position x of the system, serves to cancel a renormalization of the potential due to the coupling [49, 53, 59].

For the time evolution we choose an initial condition of the Feynman-Vernon type: at $t = t_0$, the bath is not correlated to the system and canonically distributed with respect to the free bath Hamiltonian, i.e., the density operator W of system plus bath reads

$$W(t_0) = \varrho(t_0) \otimes \frac{\mathrm{e}^{-H_{\mathrm{B}}/k_{\mathrm{B}}T}}{\operatorname{tr} \mathrm{e}^{-H_{\mathrm{B}}/k_{\mathrm{B}}T}}, \tag{3.4}$$

where ϱ is the density operator of the system and $k_{\mathrm{B}}T$ denotes Boltzmann's constant times temperature. Although this choice is somewhat artificial, it is favorable due to its technical simplicity. Other initial conditions, like e.g. the canonical ensemble of the whole system including the coupling [60], are more realistic. However, below we will deal with driven systems where specifying a more sophisticated preparation is not meaningful without specifying an onset of the driving.

Due to the bilinearity of the bath and its coupling to the system, one can eliminate the bath variables to get an exact, closed integro-differential equation for the dynamics of the central system, subject to dissipation. The elimination can be performed in two ways, which are the subjects of the following sections.

3.2 Quantum Langevin equation

From the system-bath Hamiltonian (3.1) we derive the Heisenberg equations of motion for the system and the bath operators and solve the latter formally. This results in a dissipative differential equation for the Heisenberg position operator of the system, which is driven by an operator-valued stochastic force. Although in general, this quantum Langevin equation cannot be solved exactly and thus is of limited practical use, it offers a possibility for interpretations.

The Heisenberg equations of motion for the position operators of the system and of the bath oscillators read

$$\ddot{x} + \frac{1}{m} V'(x) = \frac{1}{m} \sum_{\nu} c_\nu \left(x_\nu - \frac{c_\nu}{m_\nu \omega_\nu^2} x \right), \tag{3.5}$$

$$\ddot{x}_\nu + \omega_\nu^2 x_\nu = \frac{c_\nu}{m_\nu} x. \tag{3.6}$$

Equation (3.6) is easily integrated to yield the formal solution

$$x_\nu(t) = x_\nu(t_0)\cos\omega(t-t_0) + \frac{p_\nu(t_0)}{m_\nu\omega_\nu}\sin\omega_\nu(t-t_0) + \frac{c_\nu}{m_\nu\omega_\nu}\int_{t_0}^{t}\mathrm{d}t'\sin\omega_\nu(t-t')\,x(t'). \tag{3.7}$$

After integration by parts, inserting into (3.5) results in the so-called quantum Langevin equation [61–64]

$$\ddot{x}(t) + \int_{t_0}^{t}\mathrm{d}t'\gamma(t-t')\dot{x}(t') + \frac{1}{m}V'(x(t)) = \frac{1}{m}\xi(t) - \gamma(t)x(t_0) \tag{3.8}$$

with the damping kernel

$$\gamma(t) = \frac{1}{m}\sum_\nu \frac{c_\nu^2}{m_\nu\omega_\nu^2}\cos\omega_\nu(t-t_0) \tag{3.9}$$

and the operator-valued fluctuating force

$$\xi(t) = \sum_\nu c_\nu\left(x_\nu(t_0)\cos\omega_\nu(t-t_0) + \frac{p_\nu(t_0)}{m_\nu\omega_\nu}\sin\omega_\nu(t-t_0)\right). \tag{3.10}$$

The last term in (3.8) gives rise to an initial slip due to the sudden coupling of the system and the bath at time t_0 [19, 61, 64]. It will be omitted in the following as we will not study preparation effects within this framework. The influence of the fluctuating force on the system is fully characterized by its symmetric autocorrelation function, the noise kernel

$$K(t-t') = \frac{1}{2\hbar}\langle\xi(t)\xi(t') + \xi(t')\xi(t)\rangle, \tag{3.11}$$

$$= \sum_\nu \frac{c_\nu^2}{2m_\nu\omega_\nu}\coth\left(\frac{\hbar\omega_\nu}{2k_\mathrm{B}T}\right)\cos\omega_\nu(t-t'). \tag{3.12}$$

To obtain the last line, we have made use of the equilibrium expectation values

$$\frac{1}{2}m_\nu\omega_\nu^2\langle x_\nu x_{\nu'}\rangle = \frac{1}{2m_\nu}\langle p_\nu p_{\nu'}\rangle = \frac{\hbar\omega_\nu}{4}\coth\left(\frac{\hbar\omega_\nu}{2k_\mathrm{B}T}\right)\delta_{\nu\nu'} \tag{3.13}$$

for the bath operators in the canonical ensemble. As the system-bath Hamiltonian (3.1) is bilinear in the bath coordinates x_ν, the Gaussian property holds, i.e., we can express moments and correlations of higher order by products of K's. The correlation function $K(\tau)$ decays within a time

$$\tau_\mathrm{B} = \hbar/k_\mathrm{B}T, \tag{3.14}$$

which also marks the time scale below which correlations between system and bath are relevant. In the limit of zero temperature, τ_B diverges and these correlations play a dominant role [54, 55].

At this point it is convenient to introduce the spectral density of the system-bath coupling

$$I(\omega) = \pi \sum_{\nu} \frac{c_\nu^2}{2m_\nu\omega_\nu}\delta(\omega - \omega_\nu). \tag{3.15}$$

In a continuum limit for the heat bath we assume $I(\omega)$ to be a smooth function. The damping and the noise kernel can be expressed by the spectral function to read

$$\gamma(t) = \frac{2}{\pi m}\int_0^\infty \mathrm{d}\omega \frac{I(\omega)}{\omega}\cos\omega t \tag{3.16}$$

$$K(t) = \frac{1}{\pi}\int_0^\infty \mathrm{d}\omega\, I(\omega)\coth\left(\frac{\hbar\omega}{2k_\mathrm{B}T}\right)\cos\omega t. \tag{3.17}$$

Both are not independent of each other since they obey the so-called second fluctuation-dissipation relation [49], which in Fourier representation reads

$$K(\omega) = \frac{1}{2}m\hbar\omega\gamma(\omega)\coth\left(\frac{\hbar\omega}{2k_\mathrm{B}T}\right). \tag{3.18}$$

In the classical limit $k_\mathrm{B}T \gg \hbar\omega$, Eq. (3.18) reads $K(\omega) = m\gamma(\omega)k_\mathrm{B}T$ and the quantum Langevin equation becomes in the long-time limit formally equivalent to the corresponding classical Langevin equation [49, 62, 63].

As a prototypical model for damping, we use the Ohmic friction kernel $\gamma(t) = 2\gamma\delta(t)$, where the memory of the friction in (3.8) drops to zero. This corresponds to the Ohmic spectral density $I(\omega) = m\gamma\omega$. An Ohmic spectral density is often used as an approximation to a more complicated one and therefore in literature sometimes appears as "first Markov approximation" [50]. The assumption of an increasing spectral density for arbitrarily high frequencies, however, is not only somewhat artificial, but also results in divergent integrals. We regularize them, if required, by a cutoff in the spectral density,

$$I(\omega) = m\gamma\omega\frac{\omega_\mathrm{D}^2}{\omega^2 + \omega_\mathrm{D}^2}, \tag{3.19}$$

which defines the Drude model. The cutoff frequency ω_D introduces a short but finite memory $\tau_\mathrm{D} = 1/\omega_\mathrm{D}$ for the friction.

3.3 Influence functional

Despite the fact that the quantum Langevin equation (3.8) appears quite simple, its practical use is limited to the very rare cases where it can be integrated directly. A more useful approach is the elimination of the heat bath in the equation of motion for the full density operator W, which results in an equation of motion for the reduced density operator $\varrho = \mathrm{tr}_\mathrm{B}\, W$ of the central system subject to dissipation, where tr_B denotes the trace over the bath variables. For an exact elimination of the

heat bath, the path-integral formulation of quantum mechanics has proved to be more convenient than operator notation [11, 53].

We start with the time evolution of the full density matrix,

$$W(t) = \mathrm{e}^{-\mathrm{i}H(t-t_0)/\hbar} W(t_0) \mathrm{e}^{\mathrm{i}H(t-t_0)/\hbar}, \tag{3.20}$$

which in position representation reads

$$\begin{aligned} W(x_\mathrm{f}, \boldsymbol{x}_\mathrm{f}, x_\mathrm{f}', \boldsymbol{x}_\mathrm{f}', t) &\equiv \langle x_\mathrm{f}, \boldsymbol{x}_\mathrm{f} | W(t) | x_\mathrm{f}', \boldsymbol{x}_\mathrm{f}' \rangle & (3.21) \\ &= \int \mathrm{d}x_0 \, \mathrm{d}x_0' \, \mathrm{d}\boldsymbol{x}_0 \, \mathrm{d}\boldsymbol{x}_0' \, U(x_\mathrm{f}, \boldsymbol{x}_\mathrm{f}, t; x_0, \boldsymbol{x}_0, t_0) & (3.22) \\ &\quad \times U^*(x_\mathrm{f}', \boldsymbol{x}_\mathrm{f}', t; x_0', \boldsymbol{x}_0', t_0) W(x_0, \boldsymbol{x}_0, x_0', \boldsymbol{x}_0', t_0). & (3.23) \end{aligned}$$

The propagator $U(x, \boldsymbol{x}, t; x_0, \boldsymbol{x}_0, t_0)$ of the system plus the bath is given by the path integral expression [11, 49, 65]

$$U(x_\mathrm{f}, \boldsymbol{x}_\mathrm{f}, t; x_0, \boldsymbol{x}_0, t_0) = \int_{x(t_0)=x_0}^{x(t)=x_\mathrm{f}} \mathcal{D}x \int_{\boldsymbol{x}(t_0)=\boldsymbol{x}_0}^{\boldsymbol{x}(t)=\boldsymbol{x}_\mathrm{f}} \mathcal{D}\boldsymbol{x} \exp\left(\frac{\mathrm{i}}{\hbar} S[x] + \frac{\mathrm{i}}{\hbar} S_\mathrm{B}[x, \boldsymbol{x}] \right). \tag{3.24}$$

The variable $\boldsymbol{x}$ is a shorthand for all bath coordinates x_ν and $\mathcal{D}\boldsymbol{x}$ denotes path integration over all of them. The actions

$$S[x] = \int_{t_0}^{t} \mathrm{d}t' \left(\frac{m}{2} \dot{x}^2(t') - V(x(t')) \right), \tag{3.25}$$

$$S_\mathrm{B}[x, \boldsymbol{x}] = \sum_\nu \int_{t_0}^{t} \mathrm{d}t' \left(\frac{m_\nu}{2} \dot{x}_\nu(t')^2 - \frac{1}{2} m_\nu \omega_\nu^2 \left(x_\nu(t') - \frac{c_\nu}{m_\nu \omega_\nu^2} x(t') \right)^2 \right), \tag{3.26}$$

correspond to the Hamiltonian H_S of the central system and $H_\mathrm{B} + H_\mathrm{SB}$ for the bath plus system-bath coupling, respectively. We insert the initial condition (3.4) and evaluate the path integral over the bath variables. After tracing out the bath variables by integrating over all the bath coordinates $\boldsymbol{x}_\mathrm{f}$, we obtain [11, 21, 49]

$$\varrho(x_\mathrm{f}, x_\mathrm{f}', t) = \int \mathrm{d}x_0 \, \mathrm{d}x_0' \, J(x_\mathrm{f}, x_\mathrm{f}', t; x_0, x_0', t_0) \varrho(x_0, x_0', t_0), \tag{3.27}$$

$$\begin{aligned} J(x_\mathrm{f}, x_\mathrm{f}', t; x_0, x_0', t_0) = &\int_{x(t_0)=x_0}^{x(t)=x_\mathrm{f}} \mathcal{D}x \int_{x'(t_0)=x_0'}^{x'(t)=x_\mathrm{f}'} \mathcal{D}x' \exp\left(\frac{\mathrm{i}}{\hbar} S[x] - \frac{\mathrm{i}}{\hbar} S[x'] \right) \\ &\times \exp\left(-\frac{1}{\hbar} \phi_\mathrm{FV}[x, x'] \right). \end{aligned} \tag{3.28}$$

The propagator $J(x_\mathrm{f}, x_\mathrm{f}', t; x_0, x_0', t_0)$ describes the time-evolution of the dissipative system. The entire influence of the bath is subsumed in the so-called influence functional [21] $\phi_\mathrm{FV}[x, x']$,

$$\mathrm{Re}\, \phi_\mathrm{FV}[x, x'] = \int_{t_0}^{t} \mathrm{d}t' \int_{t_0}^{t'} \mathrm{d}t'' \Big(x(t') - x'(t') \Big) K(t' - t'') \Big(x(t'') - x'(t'') \Big), \tag{3.29}$$

$$\operatorname{Im}\phi_{\mathrm{FV}}[x,x'] = -\frac{m}{2}\int_{t_0}^{t}\mathrm{d}t'\int_{t_0}^{t'}\mathrm{d}t''\Big(x(t')-x'(t')\Big)\gamma(t'-t'')\Big(\dot{x}(t'')+\dot{x}'(t'')\Big) - \frac{m}{2}\int_{t_0}^{t}\mathrm{d}t'\Big(x(t')-x'(t')\Big)\gamma(t')\Big(x(t_0)+x'(t_0)\Big). \tag{3.30}$$

To obtain (3.30), we have integrated $\operatorname{Im}\phi_{\mathrm{FV}}$ by parts, canceling the potential renormalization in (3.26). The last term of the imaginary part gives the initial slip, known from Eq. (3.8), and is omitted in the following. The real part of the influence functional describes the noise, whereas the imaginary part gives rise to friction [49].

3.4 Markovian master equation

By perturbation theory for the propagator (3.28) up to lowest non-trivial order in the system-bath coupling, we derive a master equation of Markovian type, i.e., without memory. The steps to introduce this Markov approximation are usually performed in operator notation, starting from the full system-bath Hamiltonian (3.1). Here, we give a derivation from the path-integral expression (3.28). The present derivation requires essentially the same approximations as the standard projection technique approach, but has some advantages. First, one can here distinguish more clearly between the influence of friction and noise, because each of them is easily identified in the path integral expression (3.28) [49]. A second benefit is the exact cancellation of the potential renormalization in (3.30). And last but not least, one can show that for the case of an Ohmic spectral density, the friction part in the Markovian master equation becomes exact.

In standard perturbation theory for path integrals [65, 66], the exponent of the influence functional is approximated by a Taylor series,

$$\exp\left(-\frac{1}{\hbar}\phi_{\mathrm{FV}}[x,x']\right) \approx 1-\frac{1}{\hbar}\phi_{\mathrm{FV}}[x,x']. \tag{3.31}$$

The small parameter in this approximation is the effective coupling strength γ, which means that γ has to be the smallest frequency scale in the problem. Thus,

$$\gamma \ll 1/\tau_{\mathrm{B}} = k_{\mathrm{B}}T/\hbar, \tag{3.32}$$

$$\gamma \ll \Delta/\hbar, \tag{3.33}$$

where τ_{B} is the correlation time of the bath and Δ denotes any energy difference in the spectrum of the conservative problem.

The propagator for the density matrix is at order zero in the perturbation given by the first line of (3.28). It can be separated into two parts, one depending only on x, the other only on x'. They are easily identified as the propagator for the Schrödinger equation of the pure system and its complex conjugate,

$$J_0(x_{\mathrm{f}},x'_{\mathrm{f}},t;x_0,x'_0,t_0) = U_0(x_{\mathrm{f}},t;x_0,t_0)\,U_0^*(x'_{\mathrm{f}},t;x'_0,t_0). \tag{3.34}$$

In first order of perturbation (which is already second order in the coupling constants c_ν), the influence functionals (3.29) and (3.30) only yield contributions at times t' and t''. Thus we can dissect the path integral into an explicit integration over $x_1 = x(t')$ and $x_2 = x(t'')$ and free time evolution [65, 66] to get

$$\begin{aligned}\varrho(x_\mathrm{f}, x'_\mathrm{f}, t) = &\int \mathrm{d}x_0 \mathrm{d}x'_0\, J_0(x_\mathrm{f}, x'_\mathrm{f}, t; x_0, x'_0, t_0)\varrho(x_0, x'_0, t_0) \\ &- \frac{1}{\hbar}\int_{t_0}^{t}\mathrm{d}t' \int_{t_0}^{t'}\mathrm{d}t'' \int \mathrm{d}x_1\, \mathrm{d}x'_1\, \mathrm{d}x_2\, \mathrm{d}x'_2\, J_0(x_\mathrm{f}, x'_\mathrm{f}, t; x_1, x'_1, t')\,(x_1 - x'_1) \\ &\quad \times J_0(x_1, x'_1, t''; x_2, x'_2, t'')K(t' - t'')\,(x_2 - x'_2)\varrho(x_2, x'_2, t'') \\ &+ \frac{\mathrm{i}m}{2\hbar}\int_{t_0}^{t}\mathrm{d}t' \int_{t_0}^{t'}\mathrm{d}t'' \int \mathrm{d}x_1\, \mathrm{d}x'_1\, \mathrm{d}x_2\, \mathrm{d}x'_2\, J_0(x_\mathrm{f}, x'_\mathrm{f}, t; x_1, x'_1, t')\,(x_1 - x'_1) \\ &\quad \times J_0(x_1, x'_1, t''; x_2, x'_2, t'')\,\gamma(t' - t'')\,(\dot{x}_2 + \dot{x}'_2)\varrho(x_2, x'_2, t''), \end{aligned} \tag{3.35}$$

where we have assumed that path integration commutes with the integrals over t' and t''. By use of (3.27) and (3.34), we can express $\varrho(t'')$ in zeroth order of the perturbation by $\varrho(t)$,

$$\varrho(x_2, x'_2, t'') = \int \mathrm{d}x_0\, \mathrm{d}x'_0\, J_0(x_2, x'_2, t''; x_0, x'_0, t)\varrho(x_0, x'_0, t). \tag{3.36}$$

We insert into (3.35), differentiate with respect to t, and obtain the master equation

$$\begin{aligned}&\dot{\varrho}(x_\mathrm{f}, x'_\mathrm{f}, t) \\ &= -\frac{\mathrm{i}}{\hbar}\Big(H(x_\mathrm{f}) - H(x'_\mathrm{f})\Big)\varrho(x_\mathrm{f}, x'_\mathrm{f}, t) \\ &\quad - \frac{1}{\hbar}\int_{t_0}^{t}\mathrm{d}\tau\, K(\tau) \int \mathrm{d}x_1\, \mathrm{d}x'_1\, \mathrm{d}x_2\, \mathrm{d}x'_2\, (x_\mathrm{f} - x'_\mathrm{f})\, U_0(x_\mathrm{f}, t; x_2, t - \tau)U_0^*(x'_\mathrm{f}, t; x'_2, t - \tau) \\ &\qquad \times (x_2 - x'_2)\, U_0(x_2, t - \tau; x, t)\, U_0^*(x'_2, t - \tau; x', t)\, \varrho(x, x', t) \\ &\quad + \frac{\mathrm{i}m}{2\hbar}\int_{t_0}^{t}\mathrm{d}\tau\, \gamma(\tau) \int \mathrm{d}x_1\, \mathrm{d}x'_1\, \mathrm{d}x_2\, \mathrm{d}x'_2\, (x_\mathrm{f} - x'_\mathrm{f})\, U_0(x_\mathrm{f}, t; x_2, t - \tau)U_0^*(x'_\mathrm{f}, t; x'_2, t - \tau) \\ &\qquad \times (\dot{x}_2 + \dot{x}'_2)\, U_0(x_2, t - \tau; x, t)\, U_0^*(x'_2, t - \tau; x', t)\, \varrho(x, x', t), \end{aligned} \tag{3.37}$$

where the free propagator J_0 for the density matrix has been substituted by the propagator U_0 of the Schrödinger equation and the integration variable t'' by $\tau = t - t''$. This master equation is Markovian since $\dot{\varrho}(t)$ depends only on $\varrho(t)$, i.e., at equal times, not on the history of ϱ.

In the following chapters, we will solve the master equation in energy basis, in Floquet basis, or in Wigner representation, respectively. In all these cases, an operator notation is more convenient than a position representation. Deriving from (3.37)

the representation-free form is straightforward and yields

$$\frac{\mathrm{d}}{\mathrm{d}t}\varrho = -\frac{\mathrm{i}}{\hbar}[H_{\mathrm{S}}, \varrho] - \frac{1}{\hbar}\int_0^\infty \mathrm{d}\tau\, K(\tau)\,[x, [x_{\mathrm{H}}(t-\tau, t), \varrho]] + \frac{\mathrm{i}}{2\hbar}\int_0^\infty \mathrm{d}\tau\, \gamma(\tau)\,[x, [p_{\mathrm{H}}(t-\tau, t), \varrho]_+], \tag{3.38}$$

with the anticommutator $[A, B]_+ = AB + BA$. The Heisenberg position and momentum operators x_{H} and p_{H} are defined according to

$$\mathcal{O}_{\mathrm{H}}(t, t') = U_0^\dagger(t, t')\,\mathcal{O}\,U_0(t, t'), \tag{3.39}$$

where $U_0(t, t') = \exp(-\mathrm{i}H_{\mathrm{S}}(t-t')/\hbar)$ denotes the propagator of the conservative system. We have assumed further that the integration kernel $K(\tau)$ is practically zero for $\tau > \tau_{\mathrm{B}}$ [67] and extended the upper integration limit in (3.38) to infinity. This implicitly moved the preparation time $t_0 \to -\infty$, thus the master equation (3.38) describes only the system dynamics sufficiently close to equilibrium.

For an Ohmic spectral density $\gamma(\tau) = 2\gamma\delta(\tau)$, the integration in the second line of (3.38) can be evaluated and we obtain the Markovian master equation

$$\frac{\mathrm{d}}{\mathrm{d}t}\varrho = -\frac{\mathrm{i}}{\hbar}[H_{\mathrm{S}}, \varrho] + \left(\mathcal{L}_{\mathrm{friction}} + \mathcal{L}^0_{\mathrm{noise}}\right)\varrho. \tag{3.40}$$

The commutator in (3.40) gives the coherent dynamics, whereas the superoperators

$$\mathcal{L}_{\mathrm{friction}}\,\varrho = -\frac{\mathrm{i}\gamma}{2\hbar}[x, [p, \varrho]_+], \tag{3.41}$$

$$\mathcal{L}^0_{\mathrm{noise}}\,\varrho = -\frac{1}{\hbar}[x, [Q, \varrho]], \tag{3.42}$$

describe the influence of the the bath: friction and noise. The operator

$$Q = \int_0^\infty \mathrm{d}\tau\, K(\tau)\, x_{\mathrm{H}}(t-\tau, t), \tag{3.43}$$

is qualitatively the Heisenberg position operator x_{H} of the system in Fourier representation. Therefore $\mathcal{L}^0_{\mathrm{noise}}$ depends on the conservative dynamics (superscript ^{0}), thus on the energy spectrum of the central system. Note that Q is time independent, since for a static Hamiltonian $x_{\mathrm{H}}(t-\tau, t) = x_{\mathrm{H}}(-\tau)$.

The Markovian master equation (3.40) together with (3.41) and (3.42), does not exhibit Lindblad form (B.3), thus the positivity of the density operator is not guaranteed for all possible initial states. The violation of positivity due to a master equation in this case, however, is a transient effect which only arises for preparations far from equilibrium [68–71], where the conditions under which the master equation has been derived, are not fulfilled. (See Appendix B.1 for a more detailed discussion).

4 Driving and dissipation: Floquet-Markov theory

For a dissipative quantum system subject to external driving, even a partially analytical solution within the path-integral approach is feasible only for the very simplest systems, in particular, for the periodically driven, damped harmonic oscillator [28], or for driven dissipative two-level systems [72, 73]. Thus, for the description of strongly driven systems subject to weak dissipation, it is desirable to combine a Markovian approach to quantum dissipation, leading to a master equation for the density operator, with the Floquet formalism that allows to treat time-periodic forces of arbitrary strength and frequency. While the Floquet formalism amounts essentially to using an optimal representation and is exact [23], the simplification brought about by the Markovian description is achieved only at the expense of accuracy. Here, a subtle technical difficulty lies in the fact that the truncation of the long-time memory introduced by the bath and the inclusion of the driving do not commute: As pointed out in Refs. [26, 27], the result of the Markov approximation depends on whether it is made with respect to the eigenenergy spectrum of the central system without the driving, or with respect to the quasienergy spectrum obtained from the Floquet solution of the driven system. In the second case it cannot be treated as a system with proper eigenstates and eigenenergies. Figure 4.1 depicts the two different possibilities for including driving and dissipation to the description of a quantum system. Both approaches yield a Markovian master equation, but differ quantitatively. We will investigate this difference in detail for the case of a parametrically driven harmonic oscillator in Chapter 5.

A Floquet theory for dissipative driven systems based on the energy spectrum has been worked out and applied to intense-field excitations of atoms in Refs. [37,74]; a quasienergy spectrum approach has been implemented in recent work on driven Rydberg atoms [22, 75] and coherent destruction of tunneling [76–78].

4.1 Simple inclusion of the driving

A simple Markovian approach to dissipative driven quantum systems results directly from the master equation for the undriven system: We replace in (3.40) the static Hamiltonian $H_{\rm S}$ by the time-dependent Hamiltonian

$$H_{\rm S}(t) = H_0 + H_F(t) \tag{4.1}$$

which yields

$$\frac{\mathrm{d}}{\mathrm{d}t}\varrho = -\frac{\mathrm{i}}{\hbar}[H_{\rm S}(t), \varrho] + \left(\mathcal{L}_{\rm friction} + \mathcal{L}^0_{\rm noise}\right)\varrho. \tag{4.2}$$

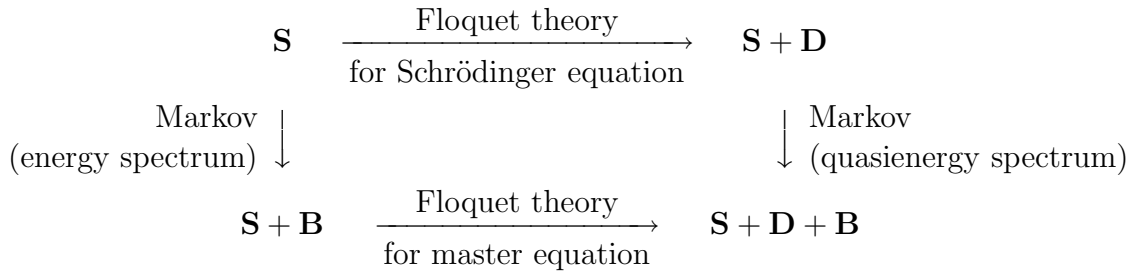

Figure 4.1: Successive inclusion of the driving (D) and the influence of a heat bath (B) to the description of a quantum system (S). The horizontal arrows denote exact Floquet treatment, whereas the vertical arrows mark an approximate step, namely the truncation of the long-time memory. The result depends on the route taken.

Here, the driving enters only the coherent part of the master equation, whereas $\mathcal{L}^0_{\text{noise}}$ has been derived from the undriven Hamiltonian H_0. Thus, we refer to this approach as the Markovian approach with respect to the unperturbed spectrum. For a periodically time-dependent driving, $H_F(t) = H_F(t+T)$, the master equation (4.2) allows for a Floquet treatment [37].

4.2 An improved Markovian master equation

We pointed out in Section 3.4, that the coherent dynamics of the central system plays an important role in the derivation of the Markovian master equation (3.40). This means that for a driven system the Markovian master equation depends on whether the driving is considered in its derivation or not.

To obtain an improved master equation whose dissipative kernel accounts for the influence of the driving, we start anew from the full system-bath Hamiltonian including the driving. Performing the same steps as in the preceeding chapter, but for an explicitly time-dependent Hamiltonian $H_{\text{S}}(t)$, we obtain the Markovian master equation

$$\frac{\mathrm{d}}{\mathrm{d}t}\varrho = -\frac{\mathrm{i}}{\hbar}[H_{\text{S}}(t), \varrho] + (\mathcal{L}_{\text{friction}} + \mathcal{L}_{\text{noise}})\,\varrho. \tag{4.3}$$

Friction and noise are described by the superoperators

$$\mathcal{L}_{\text{friction}}\,\varrho = -\frac{\mathrm{i}\gamma}{2\hbar}[x, [p, \varrho]_+], \tag{4.4}$$

$$\mathcal{L}_{\text{noise}}\,\varrho = -\frac{1}{\hbar}[x, [Q(t), \varrho]]. \tag{4.5}$$

Whereas $\mathcal{L}_{\text{friction}}$ is the same for both Markovian approaches, $\mathcal{L}_{\text{noise}}$ has acquired a time dependence which stems from the operator

$$Q(t) = \int_0^\infty \mathrm{d}\tau\, K(\tau)\, x_{\text{H}}(t-\tau, t), \tag{4.6}$$

where

$$x_{\mathrm{H}}(t,t') = U^{\dagger}(t,t')\, x\, U(t,t') \tag{4.7}$$

is the Heisenberg position operator of the driven system which depends explicitly on both times, t and t', not only on their difference. Therefore $\mathcal{L}_{\mathrm{noise}}$ is time dependent and does—in contrast to $\mathcal{L}^{0}_{\mathrm{noise}}$—not depend on the energy spectrum of the undriven system, but on the quasienergy spectrum of the driven system.

Since the role of the eigenenergies is now taken over by the quasienergies, we refer to this master equation as the Markovian approach with respect to the quasienergy spectrum. The influence of a driving force on $\mathcal{L}_{\mathrm{noise}}$ will be studied in detail for the case of a parametrically driven harmonic oscillator in Chapter 5.

4.3 Decomposition into Floquet basis

So far, we did not specify the time dependence of the system Hamiltonian in the derivation of the master equation. By assuming a T-periodic Hamiltonian, we are able to make use of the Floquet theorem and expand the reduced density operator ϱ into the time-periodic Floquet states $|\phi_\alpha(t)\rangle$ of the isolated driven system. They form a well-adapted basis for the case of weak dissipation. A master equation for the matrix elements

$$\varrho_{\alpha\beta} = \langle\phi_\alpha(t)|\varrho|\phi_\beta(t)\rangle \tag{4.8}$$

is derived from the basis-independent improved master equation (4.3).

4.3.1 Matrix elements

To decompose the master equation (4.3), we need to know the matrix elements of the operators x, p and $Q(t)$ in the Floquet basis. They all are T-periodic and can be expressed as a Fourier series,

$$X_{\alpha\beta}(t) \equiv \langle\phi_\alpha(t)|x|\phi_\beta(t)\rangle = \sum_n \mathrm{e}^{\mathrm{i}n\Omega t} X_{\alpha\beta,n}, \tag{4.9}$$

$$P_{\alpha\beta}(t) \equiv \langle\phi_\alpha(t)|p|\phi_\beta(t)\rangle = \sum_n \mathrm{e}^{\mathrm{i}n\Omega t} P_{\alpha\beta,n}, \tag{4.10}$$

$$Q_{\alpha\beta}(t) \equiv \langle\phi_\alpha(t)|Q(t)|\phi_\beta(t)\rangle = \sum_n \mathrm{e}^{\mathrm{i}n\Omega t} Q_{\alpha\beta,n}. \tag{4.11}$$

The Fourier coefficients of the position matrix elements read

$$X_{\alpha\beta,n} = \frac{1}{T}\int_0^T \mathrm{d}t\, \mathrm{e}^{-\mathrm{i}n\Omega t}\langle\phi_\alpha(t)|x|\phi_\beta(t)\rangle \tag{4.12}$$

$$= \langle\langle\phi_\alpha(t)|x|\phi_\beta^{(-n)}(t)\rangle\rangle. \tag{4.13}$$

Next, we will express the Fourier coefficients $P_{\alpha\beta,n}$ and $Q_{\alpha\beta,n}$ in terms of $X_{\alpha\beta,n}$.

For a Hamiltonian of the form $H = p^2/2m + V(x,t)$, the momentum operator can be expressed by a commutator,

$$p = \frac{m}{\mathrm{i}\hbar}[H,x] = \frac{m}{\mathrm{i}\hbar}[\mathcal{H},x], \tag{4.14}$$

where $\mathcal{H} = H - \mathrm{i}\hbar\partial/\partial t$ denotes the Floquet Hamiltonian. Thus we get

$$P_{\alpha\beta,n} = \frac{m}{\mathrm{i}\hbar}\langle\langle\phi_\alpha|p|\phi_\beta^{(-n)}\rangle\rangle \tag{4.15}$$

$$= \frac{m}{\mathrm{i}\hbar}(\epsilon_\alpha - \epsilon_\beta + n\hbar\Omega)X_{\alpha\beta,n}. \tag{4.16}$$

To obtain the last line, we made use of the eigenvalue equation (2.29) for the Floquet states after inserting (4.14).

The Fourier coefficients of the time-dependent matrix element $Q_{\alpha\beta}(t)$ read

$$\begin{aligned} Q_{\alpha\beta,n} &= \frac{1}{T}\int_0^T \mathrm{d}t\,\mathrm{e}^{-\mathrm{i}n\Omega t}\int_0^\infty \mathrm{d}\tau\,K(\tau)\langle\phi_\alpha(t)|x_{\mathrm{H}}(t-\tau,t)|\phi_\beta(t)\rangle \\ &= \int_0^\infty \mathrm{d}\tau\frac{m\gamma}{\pi}\int_0^\infty \mathrm{d}\omega\,\omega\coth\left(\frac{\hbar\omega}{2k_{\mathrm{B}}T}\right)\cos(\omega\tau)\mathrm{e}^{-\mathrm{i}(\epsilon_\alpha-\epsilon_\beta+n\hbar\Omega)\tau/\hbar}X_{\alpha\beta,n}, \end{aligned} \tag{4.17}$$

where we have inserted the spectral representation (3.17) of the noise kernel and made use of (4.12). The τ-integration is evaluated by using $\int_0^\infty \mathrm{d}\tau\exp(\mathrm{i}\omega\tau) = \pi\delta(\omega) + \mathrm{i}\mathsf{P}(1/\omega)$, where P denotes Cauchy's principal part. We end up with

$$Q_{\alpha\beta,n} = \frac{m\gamma}{2\hbar}(\epsilon_\alpha - \epsilon_\beta + n\hbar\Omega)\coth\left(\frac{\epsilon_\alpha-\epsilon_\beta+n\hbar\Omega}{2k_{\mathrm{B}}T}\right)X_{\alpha\beta,n}. \tag{4.18}$$

The contributions of the principal part result in quasienergy shifts of the order γ, the so-called Lamb shifts [50, 51], and have been neglected.

By use of the Fourier representations (4.9)–(4.11) we obtain from Eq. (4.3) the Floquet-Markov master equation [22, 27, 75]

$$\begin{aligned} \dot\varrho_{\alpha\beta}(t) &= \frac{\mathrm{d}}{\mathrm{d}t}\langle\phi_\alpha(t)|\varrho(t)|\phi_\beta(t)\rangle \\ &= -\frac{\mathrm{i}}{\hbar}(\epsilon_\alpha-\epsilon_\beta)\varrho_{\alpha\beta}(t) \\ &\quad + \sum_{\alpha'\beta'nn'}\mathrm{e}^{\mathrm{i}(n+n')\Omega t}\Big[(N_{\alpha\alpha',n}+N_{\beta\beta',-n'})X_{\alpha\alpha',n}\varrho_{\alpha'\beta'}X_{\beta'\beta,n'} \\ &\quad - N_{\beta'\alpha',n'}X_{\alpha\beta',n}X_{\beta'\alpha',n'}\varrho_{\alpha'\beta} - N_{\alpha'\beta',-n'}\varrho_{\alpha\beta'}X_{\beta'\alpha',n'}X_{\alpha'\beta,n}\Big]. \end{aligned} \tag{4.19}$$

Note that the coefficients of this differential equation are periodic in time with the period of the driving. The $N_{\alpha\beta,n}$ are given by

$$N_{\alpha\beta,n} = N(\epsilon_\alpha - \epsilon_{\alpha'} + n\hbar\Omega), \quad N(\epsilon) = \frac{m\gamma\epsilon}{\hbar^2}n_{\mathrm{th}}(\epsilon), \tag{4.20}$$

with the thermal occupation number

$$n_{\mathrm{th}}(\epsilon) = \frac{1}{\mathrm{e}^{\epsilon/k_{\mathrm{B}}T}-1} = \frac{1}{2}\left[\coth\left(\frac{\epsilon}{2k_{\mathrm{B}}T}\right)-1\right]. \tag{4.21}$$

For $\epsilon \gg k_{\mathrm{B}}T$, $N(\epsilon)$ approaches zero.

4.3.2 Rotating-wave approximation

We used the Floquet basis to formally eliminate a driving force of arbitrary strength from the coherent part of the master equation. However, the coefficients of the dissipative part are still time dependent and complicate the solution of the master equation. Here, we explore the conditions under which these coefficients can be replaced by their time average. This step effectively amounts to a rotating-wave approximation (RWA).

Moderate rotating-wave approximation

Assuming that dissipative effects are relevant only on a time scale much larger than the period $2\pi/\Omega$ of the driving, we average the likewise $2\pi/\Omega$-periodic coefficients of the master equation (4.19) over one period of the driving and end up with the equation of motion

$$\dot{\varrho}_{\alpha\beta}(t) = -\frac{\mathrm{i}}{\hbar}(\epsilon_\alpha - \epsilon_\beta)\varrho_{\alpha\beta}(t) + \sum_{\alpha'\beta'} \mathcal{L}_{\alpha\beta,\alpha'\beta'}\, \varrho_{\alpha'\beta'}(t), \tag{4.22}$$

with the dissipative transition rates

$$\begin{aligned}\mathcal{L}_{\alpha\beta,\alpha'\beta'} = &\sum_n \left(N_{\alpha\alpha',n} + N_{\beta\beta',n}\right) X_{\alpha\alpha',n} X_{\beta'\beta,-n} \\ &- \delta_{\beta\beta'} \sum_{\beta'',n} N_{\beta''\alpha',n} X_{\alpha\beta'',-n} X_{\beta''\alpha',n} - \delta_{\alpha\alpha'} \sum_{\alpha''n} N_{\alpha''\beta',n} X_{\beta'\alpha'',-n} X_{\alpha''\beta,n}.\end{aligned} \tag{4.23}$$

The time-independence of its coefficients reflects that the influence of the driving has been formally absorbed by decomposing into the Floquet basis. Note that diagonal and off-diagonal elements of the density matrix are not decoupled. It has also to be stressed that the rotating-wave approximation introduced here is less restrictive than the one in Refs. [22, 75], as detailed in the next paragraph.

Full rotating-wave approximation

In some cases one can even go one step further. We solve the coherent part of the master equation (4.22) by the *ansatz*

$$\varrho_{\alpha\beta}(t) = \mathrm{e}^{-\mathrm{i}(\epsilon_\alpha - \epsilon_\beta)t/\hbar}\sigma_{\alpha\beta}(t), \tag{4.24}$$

a transformation to the Heisenberg picture of the central system plus the driving. Inserting into (4.22) yields

$$\dot{\sigma}_{\alpha\beta}(t) = \sum_{\alpha'\beta'} \mathrm{e}^{\mathrm{i}(\epsilon_\alpha - \epsilon_\beta - \epsilon_{\alpha'} + \epsilon_{\beta'})t/\hbar} \mathcal{L}_{\alpha\beta,\alpha'\beta'}\, \sigma_{\alpha'\beta'}(t) \tag{4.25}$$

If dissipative effects are only relevant on a time scale much longer than all finite times $2\pi\hbar/(\epsilon_\alpha - \epsilon_\beta - \epsilon_{\alpha'} + \epsilon_{\beta'})$, we are allowed to replace the coefficients in (4.25) by their time average. Thus only the $\mathcal{L}_{\alpha\beta,\alpha'\beta'}$ which fulfill the full-RWA condition

$$\epsilon_\alpha - \epsilon_\beta = \epsilon_{\alpha'} - \epsilon_{\beta'}, \tag{4.26}$$

remain in (4.25) or (4.22), respectively. This condition is, however, much more restrictive than the one in the previous paragraph, since here, we have averaged over a longer time scale. Therefore the applicability of a full RWA is limited to very rare cases like, e.g., harmonic potentials with their equidistant (quasi-) energy levels.

Moreover, one can assume that for the case of a completely irregular spectrum where all quasienergies are effectively random numbers [8, 79], the quasienergy differences have no degeneracy at all. Then the full-RWA condition (4.26) results in [22, 75]

$$\alpha = \alpha', \quad \beta = \beta' \qquad \text{or} \qquad \alpha = \beta, \quad \alpha' = \beta'. \tag{4.27}$$

Inserting into (4.25) yields two decoupled sets of equations for the diagonal and the off-diagonal matrix elements,

$$\dot{\sigma}_{\alpha\alpha}(t) = \sum_{\alpha'} \mathcal{L}_{\alpha\alpha,\alpha'\alpha'}\, \sigma_{\alpha'\alpha'}(t), \tag{4.28}$$

$$\dot{\sigma}_{\alpha\beta}(t) = \mathcal{L}_{\alpha\beta,\alpha\beta}\, \sigma_{\alpha\beta}(t), \quad \alpha \neq \beta. \tag{4.29}$$

The second equation results in an exponential decay of the off-diagonal matrix elements. Therefore in the asymptotic limit, the density matrix becomes diagonal in the Floquet basis.

We will, however, find in Section 6.3 that even in a case where the dynamics of the system is fully chaotic and thus, a full RWA seems to be appropriate, the off-diagonal matrix elements play an important role for the asymptotic state.

4.4 The dissipative quantum map and its numerical implementation

The master equation (4.3) generates a dynamical semigroup for the time evolution of the density operator. Its coefficients share the T-periodicity of the driven system Hamiltonian $H_{\mathrm{S}}(t)$, i.e., Eq. (4.3) meets the conditions for a Floquet treatment. Therefore, it is possible to define a dissipative quantum map $\mathcal{G}(T)$ [25, 74, 80]—the analogue of the one-cycle propagator $U(T, 0)$ in the conservative case—which describes the stroboscopic dissipative time evolution of the density operator,

$$\varrho(nT) = [\mathcal{G}(T)]^n \varrho(0). \tag{4.30}$$

As the dynamics generated by (4.30) is dissipative, it converges in the long-time limit to an asymptotic state ϱ_∞, the "quantum attractor" which is the fixed point of the dissipative quantum map $\mathcal{G}(T)$.

Decomposing into the Floquet basis $\{|\phi_\alpha(t)\rangle\}$ yields the one-cycle propagation of the density matrix elements

$$\varrho_{\alpha\beta}((n+1)T) = \sum_{\alpha'\beta'} \mathcal{G}_{\alpha\beta,\alpha'\beta'}(T)\, \varrho_{\alpha'\beta'}(nT). \tag{4.31}$$

An equation of motion for the dissipative map,

$$\dot{\mathcal{G}}_{\alpha\beta,\alpha'\beta'}(t) = -\frac{\mathrm{i}}{\hbar}(\epsilon_\alpha - \epsilon_\beta)\mathcal{G}_{\alpha\beta,\alpha'\beta'}(t)\,\delta_{\alpha\alpha'}\,\delta_{\beta\beta'} + \sum_{\alpha''\beta''} \mathcal{L}_{\alpha\beta,\alpha''\beta''}\,\mathcal{G}_{\alpha''\beta'',\alpha'\beta'}(t) \qquad (4.32)$$

follows straightforwardly from (4.22). This form enables a numerical treatment of the master equation: We integrate (4.32) over one period of the driving T to obtain the dissipative map $\mathcal{G}(T)$. The time evolution of the density operator results from iteration according to (4.31).

5 The parametrically driven harmonic oscillator

In this chapter we investigate the properties and the quality of the different Markovian approaches to damped periodically driven quantum dynamics for a linear system where an exact path-integral solution is still available: The parametrically driven, damped harmonic oscillator allows for a very transparent and well-controlled investigation of the different approximation schemes introduced in Chapters 3 and 4. Here, their quality can be reliably checked since in this system, the quasienergy spectrum is sufficiently different from the unperturbed energy spectrum [81,82] (this feature is in contrast to the additively driven harmonic oscillator where the difference of two quasienergies does not depend on the driving parameters [83]), and a comparison with the known quantum path-integral solution [28] is possible.

Moreover, by switching to a phase-space representation such as the Wigner function, it is possible to elucidate the relationship of the quantal results to the corresponding classical Fokker-Planck dynamics. Since this relation is particularly close in the case of linear systems, this provides an additional consistency check. Therefore, a strong emphasis of this chapter is on the testing and thorough understanding of the available methods.

Forming a convenient "laboratory animal" due to its simplicity and linearity, the parametrically driven harmonic oscillator still shows nontrivial behavior, interesting in its own right. We give a brief review of the model, its classical dynamics, and its coherent quantum dynamics in Sections 5.1 and 5.2. In Section 5.3 we present the solution of the dissipative dynamics in Floquet-Markov description. A refined investigation within a basis-independent description, which allows for a detailed analysis of the influence of the driving on the dissipative terms of the master equation, is given in Section 5.4. Section 5.5 is devoted to a discussion of the asymptotics of the quantal solutions, such as the conservative and the high-temperature limits. Section 5.6 contains numerical results for a number of characteristic dynamical quantities as obtained for the alternative Markovian approaches, and the comparison to the path-integral solution. A summary of the various representations and levels of Markovian description, with their interrelations, is given in Section 5.7. A merely technical issue, the solution of a Fokker-Planck equation by the method of characteristics, is deferred to Appendix C.

5.1 The model and its classical dynamics

For a particle with mass m moving in a harmonic potential with time-dependent frequency, the Hamiltonian is given by

$$H_{\mathrm{S}}(t) = \frac{p^2}{2m} + \frac{1}{2}k(t)x^2, \tag{5.1}$$

where $k(t) = m\omega^2(t)$ is a periodic function with period T. An initial phase of the driving can be taken into account by a proper time translation. A special case is the Mathieu oscillator, where

$$\omega^2(t) = \omega_0^2 + \varepsilon \cos \Omega t, \quad \Omega = 2\pi/T. \tag{5.2}$$

This is an experimentally important case in view of the fact that it describes the Paul trap [84]. Depending on its frequency and amplitude, the driving can stabilize or destabilize the undriven oscillation. Figure 5.1 shows the zones of stable and unstable motion, respectively, for the Mathieu oscillator, in the ω_0^2-ε plane.

The equation of motion for a classical particle with Ohmic (i.e., velocity-proportional) dissipation in the potential given in (5.1) reads

$$\ddot{x} + \gamma\dot{x} + \frac{1}{m}k(t)x = 0. \tag{5.3}$$

By substituting $x = \xi \exp(-\gamma t/2)$, we can formally remove the damping to get an undamped equation with a modified potential

$$\ddot{\xi} + \left(\omega^2(t) - \gamma^2/4\right)\xi = 0. \tag{5.4}$$

Already here, on the level of the classical equations of motion, we can apply the Floquet theorem for second-order differential equations with time-periodic coefficients. It asserts [42, 85] that Eq. (5.4) has two solutions of the form

$$\xi_1(t) = \mathrm{e}^{\mathrm{i}\mu t}\varphi(t), \quad \xi_2(t) = \xi_1^*(t), \quad \varphi(t+T) = \varphi(t). \tag{5.5}$$

The solution $\xi_2(t)$ is related to $\xi_1(t)$ by the fact that the coefficients in the differential equation (5.4) are real. Being periodic in time, the classical Floquet function $\varphi(t)$ can be represented as a Fourier series,

$$\varphi(t) = \sum_{n=-\infty}^{\infty} c_n \mathrm{e}^{\mathrm{i}n\Omega t}. \tag{5.6}$$

The Floquet index μ depends on the shape of the driving $k(t)$ and is defined only $\bmod \Omega$. There exist driving functions for which μ is complex so that one of the solutions $\xi_i(t)$ becomes unstable (cf. Fig. 5.1). In stable regions μ is real. On the border between a stable and an unstable region, μ becomes a multiple of $\Omega/2$ and the solutions $\xi_1(t)$ and $\xi_2(t)$ are not linearly independent. For given $k(t)$, the functions $\varphi(t)$, $\xi_i(t)$ and the Floquet index μ still depend on the damping γ. We denote the limit $\gamma \to 0$ of $\varphi(t)$, $\xi_i(t)$, μ by $\varphi^0(t)$, $\xi_i^0(t)$, μ^0.

The normalization of the c_n is chosen such that the Wronskian $\mathcal{W}$, which is a constant of the motion, is given by

$$\mathcal{W} = \dot{\xi}_1(t)\xi_2(t) - \xi_1(t)\dot{\xi}_2(t) = 2\mathrm{i}, \tag{5.7}$$

resulting in the sum rule

$$\sum_{n=-\infty}^{\infty} c_n^2(\mu + n\Omega) = 1. \tag{5.8}$$

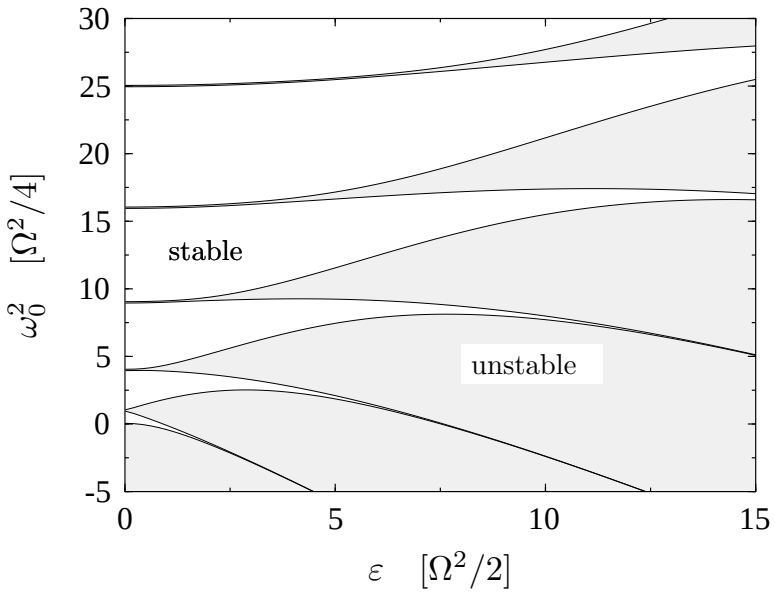

Figure 5.1: Stability of equation (5.3) with $\gamma = 0$ for the case of a Mathieu oscillator. In the white areas the Floquet index μ is real, which corresponds to stable solutions. In the shaded areas μ is complex and therefore one of the fundamental solutions (5.5) is unstable. On the borderlines, μ becomes a multiple of $\Omega/2$ and the motion is marginal stable.

Returning to the original x-coordinate, we find that the fundamental solutions of (5.3) read

$$f_i(t) = \mathrm{e}^{-\gamma t/2}\xi_i(t), \qquad i = 1, 2. \tag{5.9}$$

For constant frequency of the oscillator, $k(t) = \text{const} = m\omega_0^2$, the Floquet index and the periodic function become $\mu = (\omega_0^2 - \gamma^2/4)^{1/2}$ and $\varphi(t) = (\omega_0^2 - \gamma^2/4)^{-1/2}$, respectively, which reproduces the results for a damped harmonic oscillator without driving.

The Green function for Eq. (5.3) is constructed using Eqs. (5.6) and (5.7),

$$G(t,t') = \mathrm{e}^{-\gamma(t-t')/2}\Big(\xi_1(t)\xi_2(t') - \xi_2(t)\xi_1(t')\Big)/2\mathrm{i} \tag{5.10}$$

$$= \mathrm{e}^{-\gamma(t-t')/2}\sum_{n,n'} c_n c_{n'} \sin\Big(\mu(t-t') + \Omega(nt - n't')\Big). \tag{5.11}$$

In terms of this function, the solution of (5.3) with initial conditions $x(t_0) = x_0$ and $p(t_0) = p_0$, reads

$$x(t,t_0) = -x_0\frac{\partial G(t,t_0)}{\partial t_0} + \frac{p_0}{m}G(t,t_0). \tag{5.12}$$

Since the potential breaks continuous time-translational invariance, this solution depends explicitly on the initial time t_0.

5.2 Floquet states in stable regimes

It can be shown by group theoretical methods that the quantum mechanical quasienergy spectrum of a parametrically driven harmonic oscillator in a stable regime is equivalent to the energy spectrum of an undriven harmonic oscillator [83]. In unstable zones or on the borderlines, the quasienergy spectrum is equivalent to the energy spectrum of a parabolic barrier or of a free particle, respectively. The latter cases result in a continuous quasienergy spectrum. We restrict ourselves to the motion in stable regions.

In these regions of the parametrically driven harmonic oscillator (5.1), the Floquet solutions for the Schrödinger equation are derived in the literature in various ways [81, 86–90]. Here we sketch a derivation in the spirit of Ref. [86].

A solution of the classical equation of motion (5.3) in the non-dissipative case $\gamma = 0$ reads

$$x(t) = \sqrt{\frac{\hbar}{2m}}\Big(A^*\xi_1^0(t) + A\xi_2^0(t)\Big), \tag{5.13}$$

where A and A^* are complex normal coordinates. In a quantized version, they are replaced by the conjugate pair of operators

$$A(t) = \frac{\mathrm{i}}{\sqrt{2\hbar m}}\left(\xi_1^0(t)p - m\dot{\xi}_1^0(t)x\right), \tag{5.14}$$

$$A^+(t) = -\frac{\mathrm{i}}{\sqrt{2\hbar m}}\left(\xi_2^0(t)p - m\dot{\xi}_2^0(t)x\right), \tag{5.15}$$

which satisfy the canonical commutation relation

$$[A(t), A^+(t)] = 1. \tag{5.16}$$

In the limit of zero driving amplitude they reduce to the familiar shift operators (A.3), (A.4) of the time-independent harmonic oscillator.

The parametrically driven harmonic oscillator (5.1) possesses a T-periodic Hermitian invariant operator, the so-called Lewis invariant [86]

$$I(t) = A^+(t)A(t) = \frac{1}{2}\Big(x\,\dot{r}(t) - p\,r(t)\Big)^2 + \frac{x^2}{r^2(t)}, \tag{5.17}$$

$$r(t) = \sqrt{\xi_1^0(t)\,\xi_2^0(t)} = |\varphi^0(t)|. \tag{5.18}$$

The instantaneous eigenstates $\psi_\alpha(x,t)$ of this invariant coincide—besides a time-dependent phase factor—with the Floquet states of the system [86, 87, 91]. They can be constructed in analogy to the energy eigenstates of the time-independent harmonic oscillator: From the commutation relation (5.16) one obtains

$$A(t)\,\psi_\alpha(x,t) = \sqrt{\alpha}\,\psi_{\alpha-1}(x,t), \tag{5.19}$$

$$A^+(t)\,\psi_\alpha(x,t) = \sqrt{\alpha+1}\,\psi_{\alpha+1}(x,t). \tag{5.20}$$

Solving $A(t)\psi_0(x,t) = 0$ and iterating according to (5.20), we find for $I(t)$ the eigenfunctions

$$\begin{aligned}\psi_\alpha(x,t) &= \frac{(A^+(t))^\alpha}{\sqrt{\alpha!}}\psi_0(x,t) \qquad (5.21)\\ &= \left(\frac{\xi_2^0(t)}{\xi_1^0(t)}\right)^{\alpha/2}\sqrt{\frac{\sqrt{m/\pi\hbar}}{2^\alpha\alpha!\xi_1^0(t)}}\,H_\alpha\left(x\sqrt{m/\hbar\xi_1^0(t)\xi_2^0(t)}\right)\exp\left(\frac{\mathrm{i}m}{2\hbar}\frac{\dot{\xi}_1^0(t)}{\xi_1^0(t)}x^2\right),\end{aligned}$$

where H_α is the αth Hermite polynomial, $\alpha = 0, 1, 2, \ldots$. These states are solutions of the time-dependent Schrödinger equation [86] and in the undriven limit reduce to the position representation of the familiar eigenstates (A.10). Separating $\psi_\alpha(x,t)$ into a $2\pi/\Omega$-periodic function and an exponential prefactor, one finds the Floquet states

$$\phi_\alpha(x,t) = \sqrt{\frac{\sqrt{m/\pi\hbar}}{2^\alpha\alpha!\varphi^0(t)}}\,H_\alpha\left(\frac{x}{|\varphi^0(t)|}\sqrt{\frac{m}{\hbar}}\right)\exp\left(\frac{\mathrm{i}m}{2\hbar}\frac{\dot{\xi}_1^0(t)}{\xi_1^0(t)}x^2\right). \qquad (5.22)$$

The corresponding quasienergies

$$\epsilon_\alpha = \hbar\mu^0(\alpha + 1/2) \qquad (5.23)$$

are chosen such that in the undriven limit they reduce to the eigenenergies of the harmonic oscillator. Thus they do not lie within a single Brillouin zone.

The matrix elements of the position operator x with the Floquet states $|\phi_\alpha(t)\rangle$, which we will need to obtain the coefficients of the master equation, read

$$\begin{aligned}X_{\alpha\beta}(t) &= \langle\phi_\alpha(t)|x|\phi_\beta(t)\rangle \qquad (5.24)\\ &= \sum_n \mathrm{e}^{\mathrm{i}n\Omega t}X_{\alpha\beta,n}, \qquad (5.25)\\ X_{\alpha\beta,n} &= \frac{1}{T}\int_0^T \mathrm{d}t\,\mathrm{e}^{-\mathrm{i}n\Omega t}\langle\phi_\alpha(t)|x|\phi_\beta(t)\rangle. \qquad (5.26)\end{aligned}$$

To obtain Eqs. (5.25) and (5.26), the periodicity of the Floquet states $|\phi_\alpha(t)\rangle$ has been used. The Fourier components $X_{\alpha\beta,n}$ are preferably evaluated in the spatial representation,

$$\begin{aligned}X_{\alpha\beta}(t) &= \int_{-\infty}^{\infty}\mathrm{d}x\,\phi_\alpha(x,t)\,x\,\phi_\beta(x,t) \qquad (5.27)\\ &= \sqrt{\frac{\hbar}{2m}}\left(\sqrt{\beta}\,\varphi^0(-t)\delta_{\alpha,\beta-1} + \sqrt{\alpha}\,\varphi^0(t)\delta_{\alpha,\beta+1}\right), \qquad (5.28)\end{aligned}$$

by inserting the Fourier expansion (5.6) for $\varphi^0(t)$, to give

$$X_{\alpha\beta,n} = \sqrt{\frac{\hbar}{2m}}\left(\sqrt{\beta}\,c_{-n}\delta_{\alpha,\beta-1} + \sqrt{\alpha}\,c_n\delta_{\alpha,\beta+1}\right). \qquad (5.29)$$

5.3 Floquet-Markov description in full RWA

In the full rotating-wave approximation (RWA) introduced in Section 4.3.2, we neglect all contributions with $\epsilon_\alpha - \epsilon_\beta \neq \epsilon_{\alpha'} - \epsilon_{\beta'}$ in Eq. (4.25). Thus in the present case of an equidistant quasienergy spectrum, we have to keep all terms with $(\alpha - \beta) = (\alpha' - \beta')$.

Substituting Eq. (5.29) in Eq. (4.23), we obtain from (4.25) the time-independent master equation

$$\dot{\sigma}_{\alpha\beta} = \frac{\gamma}{2}\left\{(N+1)\left(2\sqrt{(\alpha+1)(\beta+1)}\sigma_{\alpha+1,\beta+1} - (\alpha+\beta)\sigma_{\alpha\beta}\right)\right.$$
$$\left. + N\left(2\sqrt{\alpha\beta}\sigma_{\alpha-1,\beta-1} - (\alpha+\beta+2)\sigma_{\alpha\beta}\right)\right\}. \tag{5.30}$$

The effective thermal-bath occupation number

$$N = \sum_n \left(c_n^0\right)^2 (\mu^0 + n\Omega)\, n_{\rm th}(\hbar\mu^0 + n\hbar\Omega) \tag{5.31}$$

reduces to $N = n_{\rm th}(\hbar\omega_0)$ in the undriven limit.

Formally, this master equation coincides with the one for the undriven dissipative harmonic oscillator in rotating-wave approximation [50]. It has the stationary solution

$$\sigma^\infty_{\alpha\beta} = \varrho^\infty_{\alpha\beta} = \frac{1}{N+1}\left(\frac{N}{N+1}\right)^\alpha \delta_{\alpha\beta}. \tag{5.32}$$

The density operator of the asymptotic solution is diagonal in this representation and reads

$$\varrho_\infty(t) = \sum_{\alpha=0}^\infty \varrho^\infty_{\alpha\alpha} |\phi_\alpha(t)\rangle\langle\phi_\alpha(t)|. \tag{5.33}$$

The basis $\{|\phi_\alpha(t)\rangle\}$ corresponds to the "generalized Floquet states" introduced in Ref. [26], i.e., they are centered on the classical asymptotic solution and diagonalize the asymptotic density operator.

To get the variances of (5.33), we switch to the Wigner representation. There, the asymptotic state reads

$$W_\infty(x,p,t) = \sum_{\alpha=0}^\infty \varrho^\infty_{\alpha\alpha} W_\alpha(x,p,t), \tag{5.34}$$

where

$$W_\alpha(x,p,t) = \frac{(-1)^\alpha}{\pi} {\rm e}^{-z^2} L_\alpha(2z^2), \tag{5.35}$$
$$z^2 = \frac{1}{\hbar}\left(m\dot{\xi}^0_1(t)\dot{\xi}^0_2(t)x^2 - \left(\dot{\xi}^0_1(t)\xi^0_2(t) + \xi^0_1(t)\dot{\xi}^0_2(t)\right)px + \xi^0_1(t)\xi^0_2(t)p^2/m\right),$$

is the Wigner function corresponding to $|\phi_\alpha(t)\rangle$ [89], with the αth Laguerre polynomial L_α. Using the sum rule [92]

$$\sum_{\alpha=0}^\infty \kappa^\alpha L_\alpha(x) = (1-\kappa)^{-1} \exp\left(\frac{x\kappa}{\kappa-1}\right), \tag{5.36}$$

we obtain the asymptotic solution in Wigner representation as

$$W_\infty(x,p,t) = \frac{1}{\pi(2N+1)} \mathrm{e}^{-z^2/(2N+1)}. \tag{5.37}$$

It is a Gaussian with the variances

$$\sigma_{xx}(t) = \frac{\hbar}{m}(N+1/2)\xi_1^0(t)\xi_2^0(t), \tag{5.38}$$

$$\sigma_{xp}(t) = \hbar(N+1/2)\left(\dot{\xi}_1^0(t)\xi_2^0(t) + \xi_1^0(t)\dot{\xi}_2^0(t)\right)/2, \tag{5.39}$$

$$\sigma_{pp}(t) = \hbar m(N+1/2)\dot{\xi}_1^0(t)\dot{\xi}_2^0(t). \tag{5.40}$$

To enable a comparison between the different equations of motions for the dissipative quantum system, we also give for the master equation in RWA, Eq. (5.30), the corresponding partial differential equation in Wigner representation. For a derivation, we use the shift properties (5.19) and (5.20) of the operators A and A^+, to obtain the corresponding basis-free operator equation from the master equation (5.30) for the density matrix elements $\sigma_{\alpha\beta}$

$$\begin{aligned}\dot{\varrho} = &-\frac{\mathrm{i}}{\hbar}[H_\mathrm{S}(t),\varrho] \\ &+\frac{\gamma}{2}\Big\{(N+1)\left(2A\varrho A^+ - A^+A\varrho - \varrho A^+A\right) \\ &\qquad + N\left(2A^+\varrho A - AA^+\varrho - \varrho AA^+\right)\Big\}.\end{aligned} \tag{5.41}$$

The dissipative part of this equation is the same as for the undriven dissipative harmonic oscillator [50], but with the shift operators for Floquet states instead of the usual creation and annihilation operators. Obviously, this master equation is of Lindblad form [93] (see Appendix B.1).

By substituting (5.14), (5.15), we get an operator equation which only consists of position and momentum operators. Applying the transformations (A.25)–(A.28) yields for the Wigner function the differential equation

$$\partial_t W(x,p,t) = \mathcal{L}_\mathrm{RWA}(t)\, W(x,p,t), \tag{5.42}$$

with the differential operator

$$\begin{aligned}\mathcal{L}_\mathrm{RWA}(t) = &-\frac{1}{m}p\partial_x + \frac{\gamma}{2}(\partial_x x + \partial_p p) + k(t)x\partial_x \\ &+\frac{\gamma}{2}\Big(D_{xx}(t)\partial_x^2 + D_{xp}(t)\partial_x\partial_p + D_{pp}(t)\partial_p^2\Big)\end{aligned} \tag{5.43}$$

and the diffusion coefficients

$$D_{xx}(t) = \hbar\xi_1^0(t)\xi_2^0(t)(N+1/2)/m, \tag{5.44}$$

$$D_{xp}(t) = \hbar\left(\dot{\xi}_1^0(t)\xi_2^0(t) + \xi_1^0(t)\dot{\xi}_2^0(t)\right)(N+1/2), \tag{5.45}$$

$$D_{pp}(t) = m\hbar\dot{\xi}_1^0(t)\dot{\xi}_2^0(t)(N+1/2). \tag{5.46}$$

The fact that there are also dissipative terms in Eq. (5.42) containing derivatives with respect to x is a consequence of the RWA: Its effect is equivalent to using the coupling Hamiltonian $H_{\rm SB}^{\rm RWA} = \sum_\nu g_\nu (a b_\nu^\dagger + a^\dagger b_\nu)$ instead of (3.1), where a and b_ν are the usual annihilation operators of the system and the bath, respectively. This introduces an additional coupling term $\propto p p_\nu$. In the next section we show how to avoid this RWA, by returning to the original Markov approximation, Eq. (4.3).

5.4 Basis-independent description beyond RWA

In the present case of a bilinear system, driven or not, for which the classical motion is integrable, the knowledge of the classical dynamics opens a more direct access also to the quantal time evolution. Specifically, the Heisenberg position operator $x_{\rm H}(t,t')$ for the corresponding undamped quantum system is given by the solution of the classical equation of motion in the limit $\gamma \to 0$, indicated by the superscript ^{0}. In our case the classical solution is given by (5.12). The corresponding interaction-picture position operator reads

$$x_{\rm H}(t,t') = -x \frac{\partial G^0(t,t')}{\partial t'} + \frac{p}{m} G^0(t,t'), \tag{5.47}$$

where x and p now denote the position and the momentum operator. Inserting this operator into Eq. (4.6), leads to the master equation

$$\begin{aligned} \dot\varrho = &-\frac{\rm i}{\hbar}[H_{\rm S}(t), \varrho] - \frac{\rm i}{2\hbar}\gamma\, [x, [p, \varrho]_+] \\ &- \frac{\gamma}{\hbar^2} D_{pp} [x, [x, \varrho]] + \frac{\gamma}{\hbar^2} D_{xp} [x, [p, \varrho]], \end{aligned} \tag{5.48}$$

with the periodically time-dependent transport coefficients

$$D_{pp}(t) = -\frac{\hbar}{\gamma} \int_0^\infty {\rm d}\tau\, K(\tau)\, \frac{\partial G^0(t-\tau, t')}{\partial t'}\bigg|_{t'=t}, \tag{5.49}$$

$$D_{xp}(t) = -\frac{\hbar}{m\gamma} \int_0^\infty {\rm d}\tau\, K(\tau)\, G^0(t-\tau, t). \tag{5.50}$$

This form of the master equation does not produce a positive semidefinite diffusion matrix. It consequently does not exhibit Lindblad form [93] (see Appendix B.1). Note that within a Markov approximation, the master equation is periodic with the driving period $T = 2\pi/\Omega$. This is in contrast to the non-Markovian exact master equation [28]. In this latter case, the effective master equation has the structure of (5.48) with coefficients D_{xp} and D_{pp} which depend in a non-periodic way on the time elapsed since the preparation at t_0. In Wigner representation, this corresponds to a time-dependent diffusion coefficient, see Eq. (5.56), below.

To evaluate these expressions, we substitute the undamped limit of Eq. (5.11),

$$G^0(t,t') = \sum_{n,n'=-\infty}^{\infty} c_n^0 c_{n'}^0 \sin\left[\mu^0 (t-t') + \Omega(nt - n't')\right]. \tag{5.51}$$

The explicit time dependence in $G(t,t')$ results in a $2\pi/\Omega$-periodic time dependence of the coefficients D_{pp} and D_{xp}. Averaging the transport coefficients over one period of the driving is equivalent to the moderate rotating-wave approximation introduced in Section 4.3.2.

After inserting the noise kernel (3.17) and assuming an Ohmic bath, $I(\omega) = m\gamma\omega$, we find for D_{pp} in an average over one period of the driving,

$$D_{pp} = \frac{1}{2} m\hbar \sum_{n=-\infty}^{\infty} \left[c_n^0(\mu^0 + n\Omega)\right]^2 \coth \frac{\hbar(\mu^0 + n\Omega)}{2k_{\mathrm{B}}T}. \tag{5.52}$$

This form makes explicit that the diffusion D_{pp} accounts for the quasienergies $\hbar(\mu^0 + n\Omega)$. Thus the quasienergy spectrum approach is reflected solely by a driving-induced modification of the momentum diffusion D_{pp}.

The evaluation of the cross diffusion D_{xp} is more complex. Its logarithmic divergence is regularized by a Drude cutoff to obtain

$$D_{xp} = -\frac{\hbar}{2\pi} \sum_{n=-\infty}^{\infty} \mathsf{P} \int_{-\infty}^{\infty} \mathrm{d}\omega \coth\left(\frac{\hbar\omega}{2k_{\mathrm{B}}T}\right) \frac{\omega}{\omega^2 - (\mu^0 + n\Omega)^2} \frac{\omega_{\mathrm{D}}^2}{\omega^2 + \omega_{\mathrm{D}}^2}, \tag{5.53}$$

where P denotes Cauchy's principal part. The integral in Eq. (5.53) is solved by contour integration in the upper half plane. Expressing the resulting sums by the psi function $\psi(x) = \mathrm{d}\ln\Gamma(x)/\mathrm{d}x$ [92], we obtain

$$D_{xp} = -\frac{\hbar}{\pi}\left[\psi\left(1 + \frac{\hbar\omega_{\mathrm{D}}}{2\pi k_{\mathrm{B}}T}\right) + C\right], \tag{5.54}$$

where C is the Euler constant. We have neglected terms of the order $(\mu^0 + n\Omega)/\omega_{\mathrm{D}}$, i.e., we have to choose the cutoff ω_{D} much larger than the relevant frequencies $\mu^0 + n\Omega$.

Interestingly enough, $m\gamma D_{xp}$ coincides with the Drude regularized divergent part of the stationary momentum variance of a dissipative harmonic oscillator [54,55,60]. In contrast to the Fokker-Planck equation with RWA in the last subsection, the terms with $\partial_x x$ and ∂_x^2 are now absent. In addition, the cross diffusion D_{xp} in (5.50) is completely different, and unrelated to the one in the RWA case (5.45). It originates from a principal part that has been neglected in the derivation of the Floquet-Markov equation in (4.18).

5.4.1 Wigner representation and Fokker-Planck equation

In order to achieve a description close to the classical phase-space dynamics, we discuss the time evolution of the density operator in Wigner representation. Applying the transformations (A.25)–(A.28) to the master equation (5.48), we obtain a c-number equation of motion,

$$\partial_t W(x,p,t) = \mathcal{L}(t) W(x,p,t), \tag{5.55}$$

with the differential operator

$$\mathcal{L}(t) = -\frac{1}{m}p\partial_x + \gamma\partial_p p + k(t)x\partial_p + \gamma D_{pp}\partial_p^2 + \gamma D_{xp}\partial_x\partial_p. \tag{5.56}$$

Equation (5.56) has the structure of an effective Fokker-Planck operator. However, for any non-zero D_{xp}, the diffusion matrix is not positive semidefinite; correspondingly the Fokker-Planck-like equation (5.55) with Eq. (5.56) has no equivalent Langevin representation.

As is the case for the master equation from which it has been derived, the coefficients of the Fokker-Planck operator retain the periodicity of the driving, so that (5.55) has solutions of Floquet form. This fact will be exploited in the following subsection to construct the solutions.

5.4.2 Wigner-Floquet solutions

The Fokker-Planck equation for the density operator in Wigner representation, Eq. (5.55) with Eq. (5.56), offers the opportunity to make full use of the well-known and intuitive results for the corresponding classical stochastic system. In particular, a solution of the Fokker-Planck equation can be obtained directly by solving the equivalent Langevin equation [45, 94], or by using the formula for the conditional probability of a Gauss process [94]. In the present case, however, the fact that the diffusion matrix of (5.56) is not positive semidefinite requires to take a different route.

Since Eq. (5.55) with Eq. (5.56) represents a differential equation with time-periodic coefficients, it complies with the conditions of the Floquet theorem. Consequently, there exists a complete set of solutions of the form

$$W_\alpha(x,p,t) = \mathrm{e}^{-\mu_\alpha t}u_\alpha(x,p,t), \quad u_\alpha(x,p,t) = u_\alpha(x,p,t+T), \tag{5.57}$$

henceforth referred to as Wigner-Floquet functions.

We construct a solution for (5.55) of this form with $\mu_{00} = 0$ by the method of characteristics [95] in Appendix C. In the limit $t_0 \to -\infty$, the terms in the first line of (C.18), which contain the initial condition, vanish and we obtain the asymptotic solution

$$\begin{aligned} W_{00}(x,p,t) = {} & \frac{1}{2\pi}\begin{vmatrix} \sigma_{xx}(t) & \sigma_{xp}(t) \\ \sigma_{xp}(t) & \sigma_{pp}(t) \end{vmatrix}^{-1/2} \\ & \times \exp\left\{ -\frac{1}{2}\begin{pmatrix} x \\ p \end{pmatrix}\begin{pmatrix} \sigma_{xx}(t) & \sigma_{xp}(t) \\ \sigma_{xp}(t) & \sigma_{pp}(t) \end{pmatrix}^{-1}\begin{pmatrix} x \\ p \end{pmatrix}\right\} \end{aligned} \tag{5.58}$$

with the variances

$$\sigma_{xx}(t) = \frac{2\gamma D_{pp}}{m^2}\int_{-\infty}^{t} \mathrm{d}t' \left[G(t,t')\right]^2, \tag{5.59}$$

$$\sigma_{xp}(t) = \frac{2\gamma D_{pp}}{m}\int_{-\infty}^{t} \mathrm{d}t' G(t,t')\frac{\partial}{\partial t}G(t,t'), \tag{5.60}$$

$$\sigma_{pp}(t) = -m\gamma D_{xp} + 2\gamma D_{pp}\int_{-\infty}^{t} \mathrm{d}t' \left[\frac{\partial}{\partial t}G(t,t')\right]^2. \tag{5.61}$$

Note that in (5.59)–(5.61) the difference in using D_{pp} and $D = D_{pp} + \gamma D_{xp}$ [see Eq. (C.14)] is meaningless, since it is a correction of order γ. By inserting the Fourier representation (5.11) for $G(t, t')$, one finds that the variances are asymptotically time periodic.

Starting from W_{00}, we construct further Wigner-Floquet functions: By solving the characteristic equations (see Appendix C), we find the two time-dependent differential operators

$$Q_{1+}(t) = f_1(t)\partial_x + m\dot{f}_1(t)\partial_p, \tag{5.62}$$
$$Q_{2+}(t) = f_2(t)\partial_x + m\dot{f}_2(t)\partial_p, \tag{5.63}$$

where the solutions $f_i(t)$ of the classical equation of motion are given by (5.9). The operators $Q_{i+}(t)$ have the properties

$$[\mathcal{L}(t) - \partial_t\,, Q_{1+}(t)] = [\mathcal{L}(t) - \partial_t\,, Q_{2+}(t)] = 0 \tag{5.64}$$

and

$$Q_{1+}(t+T) = \mathrm{e}^{(-\gamma/2+\mathrm{i}\mu)T} Q_{1+}(t), \tag{5.65}$$
$$Q_{2+}(t+T) = \mathrm{e}^{(-\gamma/2-\mathrm{i}\mu)T} Q_{2+}(t). \tag{5.66}$$

Taking the commutation relation (5.64) into account, the functions

$$W_{nn'}(x,p,t) = Q_{1+}^{n}(t)\, Q_{2+}^{n'}(t)\, W_{00}(x,p,t), \quad n, n' = 0, 1, 2, \ldots \tag{5.67}$$

also solve Eq. (5.55).

Due to Eqs. (5.65), (5.66) they are of Floquet structure with the Floquet spectrum

$$\mu_{nn'} = (n+n')\gamma/2 - \mathrm{i}(n-n')\mu. \tag{5.68}$$

This spectrum is independent of the diffusion constants, as expected for an operator of type (5.56) [96], and therefore is the same as in the case of the classical parametrically driven Brownian oscillator [97].

The expression for the eigenfunctions in the high-temperature limit of the (undriven) classical Brownian harmonic oscillator in Refs. [96, 98] is also of the structure (5.67). We can recover this solution by inserting the classical diffusion constant $mk_{\mathrm{B}}T$ and the undriven limit $\varepsilon \to 0$ for the classical solution, given in Section 5.1.

5.4.3 Influence of the driving on the master equation

The master equation in operator notation (5.48) and the Fokker-Planck equation (5.55) given in this section result from a Markov approximation with respect to the quasienergy spectrum. Nevertheless, they are formally independent of the Floquet basis. This allows for a detailed analysis of the difference between the Markovian approach with respect to the unperturbed spectrum and the quasienergy spectrum approach beyond mere differences in representation.

Parametrical driving

The Markov approximation with respect to the unperturbed spectrum can be obtained from the (in general more complicated) quasienergy spectrum approach by replacing the coefficients of friction and diffusion by their corresponding limits for zero driving amplitude ε. We obtain a master equation of the form (5.48) and accordingly a Fokker-Planck equation of the form (5.55), where the momentum diffusion coefficient D_{pp} is replaced by its limit for $\varepsilon \to 0$,

$$D'_{pp} = \lim_{\varepsilon \to 0} D_{pp} = \frac{1}{2} m\hbar\omega_0 \coth\left(\frac{\hbar\omega_0}{2k_{\mathrm{B}}T}\right). \tag{5.69}$$

In general $D'_{pp} \neq D_{pp}$, which we verify by numerical studies in Section 5.6. Thus parametric driving of a dissipative harmonic oscillator modifies the momentum diffusion in the master equation.

Additional additive driving

The Markovian master equation within the quasienergy spectrum approach undergoes a further modification when the parametric oscillator is subject to an additional additive driving $-xF(t)$, i.e.,

$$H_F(t) = H_{\mathrm{S}}(t) - xF(t). \tag{5.70}$$

With $H_{\mathrm{S}}(t)$ being a time-independent harmonic oscillator, i.e., $k(t) = m\omega_0^2$, the corresponding Markovian master equation in RWA for the dissipative system was already given in [26]. Herein we generalize these results for the combined time-dependent system Hamiltonian in (5.70).

It is known that the only effect of the driving force $F(t)$ on the (quasi-) energy spectrum of a parametrically driven harmonic oscillator is an overall level shift [82]. Thus the level separations remain unaffected and we expect no change in the dissipative part of the master equation (5.48).

The classical equation of motion, which is also obeyed by the interaction-picture position operator, now reads

$$m\ddot{x} + k(t)x = F(t), \tag{5.71}$$

and can be integrated to yield the interaction-picture operators

$$x_{\mathrm{H}}(t,t') = -x\frac{\partial G^0(t,t')}{\partial t'} + \frac{p}{m}G^0(t,t') + \frac{1}{m}\int_{t'}^{t} \mathrm{d}t''\, G^0(t,t'')F(t''), \tag{5.72}$$

$$p_{\mathrm{H}}(t,t') = -x\, m\frac{\partial^2 G^0(t,t')}{\partial t\, \partial t'} + p\frac{\partial G^0(t,t')}{\partial t} + \int_{t'}^{t} \mathrm{d}t''\, \frac{\partial G^0(t,t'')}{\partial t}F(t''). \tag{5.73}$$

Thus we obtain a c-number correction to the interaction-picture position operator (5.47), given by the third term. After inserting (5.73) into (3.38), the Markovian

master equation emerges as

$$\dot{\varrho} = \ldots + \frac{\mathrm{i}}{\hbar} F(t)[x, \varrho] \tag{5.74}$$

$$+ \frac{\mathrm{i}}{\hbar} \int_0^\infty \mathrm{d}\tau\, \gamma(\tau)\, [x, \varrho] \frac{2}{m} \int_t^{t-\tau} \mathrm{d}t' G^0(t-\tau, t') F(t'). \tag{5.75}$$

The dots denote the old result for $F(t) \equiv 0$, given by the right hand side of Eq. (5.48). The term in the first line stems from the reversible part of the master equation (4.3); the second one is a correction of the driving force due to interaction with the bath. Thus the equation of motion for the density operator has the structure

$$\dot{\varrho} = \ldots + \frac{\mathrm{i}}{\hbar} \tilde{F}(t)[x, \varrho] \tag{5.76}$$

with an effective total driving force

$$\tilde{F}(t) = F(t) + \int_0^\infty \mathrm{d}\tau\, \gamma(\tau) \int_t^{t-\tau} \mathrm{d}t'\, \frac{\partial G^0(t-\tau, t')}{\partial t} F(t'). \tag{5.77}$$

Note that the dissipative parts of (5.76) are not affected by the additive driving force $F(t)$. This makes explicit, that we must use a parametric time-dependence to study differences in the dissipative parts resulting from the Markov approximation with respect to the energy spectrum versus the Markov approximation with respect to the quasienergy spectrum.

With an Ohmic bath, $\gamma(\tau) = 2\gamma\delta(\tau)$, the inner integral in (5.77) vanishes and we obtain $\tilde{F}(t) = F(t)$. Thus in contrast to an explicit parametric time dependence $k(t)$ in the quadratic part of the Hamiltonian, the time dependence of an additive force, in this case, does not change the Markovian master equation of the dissipative system.

5.5 Asymptotics

5.5.1 The conservative limit

In contrast to the Markov approximation with RWA in Section 5.3, the variances in both Markov approximations without RWA still depend on the friction γ. To obtain the conservative limit $\gamma \to 0$ of these, we insert the Green function (5.11) into (5.59) and get

$$\sigma_{xx}(t) = -\frac{\gamma D_{pp}}{2m^2} \sum_{n,n'} c_n c_{n'} \left(f_1^2(t) \frac{\mathrm{e}^{\gamma t - \mathrm{i}[2\mu + (n+n')\Omega]t}}{\gamma - \mathrm{i}[2\mu + (n+n')\Omega]} \right.$$

$$\left. - 2 f_1(t) f_2(t) \frac{\mathrm{e}^{\gamma t - \mathrm{i}(n-n')\Omega t}}{\gamma - \mathrm{i}(n-n')\Omega} + f_2^2(t) \frac{\mathrm{e}^{\gamma t + \mathrm{i}[2\mu + (n+n')\Omega]t}}{\gamma + \mathrm{i}[2\mu + (n+n')\Omega]} \right). \tag{5.78}$$

In the limit of weak damping, $\gamma \ll |\mu + n\Omega|$ for any integer n, only the case $n = n'$ of the second term in the brackets remains. Note that this condition is violated in

parameter regions where the Floquet index becomes a multiple of Ω, as is the case along the borderlines of the regions of stability in parameter space (cf. Fig. 5.1).

For the position variance, we get

$$\sigma_{xx}(t) = B\frac{D_{pp}}{m^2}\,\xi_1^0(t)\xi_2^0(t), \tag{5.79}$$

where

$$B = \sum_{n=-\infty}^{\infty} \left(c_n^0\right)^2 \tag{5.80}$$

denotes a number of order unity.

In an analogous way, we find

$$\sigma_{xp}(t) = B\frac{D_{pp}}{2m}\left(\dot{\xi}_1^0(t)\xi_2^0(t) + \xi_1^0(t)\dot{\xi}_2^0(t)\right), \tag{5.81}$$

$$\sigma_{pp}(t) = BD_{pp}\,\dot{\xi}_1^0(t)\dot{\xi}_2^0(t). \tag{5.82}$$

Besides the prefactor, these variances are the same as for the master equation with RWA in Section 5.3.

Moreover, in this limit $\gamma \to 0$, all diagonal elements $W_{nn}(x,p,t)$ are Floquet functions with the quasienergies $\mu_{nn} = 0$. However, they are different from the Wigner representation of the stationary solutions (5.35) of the corresponding Schrödinger equation, which are also solutions of the coherent equation of motion, Eq. (5.55) with $\gamma = 0$. Due to the degeneracy of the Floquet indices, this is no contradiction. The $\lim_{\gamma\to 0} W_{nn}(x,p,t)$ can be viewed as dissipation-adapted Floquet functions.

For consistency, we check the position-momentum uncertainty relation for the asymptotic solution. It is satisfied if the variances fulfill the inequality

$$\begin{vmatrix} \sigma_{xx}(t) & \sigma_{xp}(t) \\ \sigma_{xp}(t) & \sigma_{pp}(t) \end{vmatrix} = \left(\frac{D_{pp}B}{m}\right)^2 \geq \hbar^2/4, \tag{5.83}$$

which we have verified numerically for the case of the Mathieu oscillator.

5.5.2 The high-temperature limit

In the limit of high temperatures $k_\mathrm{B}T \gg \hbar\omega_\mathrm{D}$, we expect the Fokker-Planck equation for the Wigner function to give the Kramers equation for the classical Brownian motion [97], i.e., an equation of the form (5.55) with diffusion constants $D_{xp} = 0$ and $D_{pp} = mk_\mathrm{B}T$.

In the refined approach (Section 5.4), the Fokker-Planck equation is already of the required structure. With $\psi(1) = -C$ [92], the cross diffusion D_{xp} vanishes in the high-temperature limit. For D_{pp}, we use $\coth x = 1/x + \mathcal{O}(x)$ and get

$$D_{pp} = mk_\mathrm{B}T\sum_n \left(c_n^0\right)^2(\mu^0 + n\Omega). \tag{5.84}$$

With the sum rule (5.8), this reduces to $D_{pp} = mk_\mathrm{B}T$.

In the quasienergy spectrum approach with RWA in Section 5.3, the variances and diffusion constants scale with $N + 1/2$. This factor, in the high-temperature limit, reads

$$N + \frac{1}{2} = \sum_n \left(c_n^0\right)^2 \frac{k_\mathrm{B}T}{\hbar} = B\frac{k_\mathrm{B}T}{\hbar}. \tag{5.85}$$

Therefore the diffusion constants D_{xx} and D_{xp} remain finite and the Fokker-Planck operator (5.42) does not approach the Kramers limit for high temperatures. Nevertheless the asymptotic variances in RWA coincide for high temperatures, with the classical result in the limit $\gamma \to 0$.

5.6 Numerical results

In this section, we compare our approximate results to exact ones, obtained from the path-integral solution in Ref. [28]. Specifically, we give the numerical results for the Mathieu oscillator, i.e., we choose

$$k(t) = m\left(\omega_0^2 + \varepsilon\cos\Omega t\right). \tag{5.86}$$

By inserting (5.86) and the *ansatz* (5.6) into (5.4), we obtain the tridiagonal recurrence relation

$$\varepsilon c_{n-1} + 2\left(\omega_0^2 - \gamma^2/4 - (\mu + n\Omega)^2\right)c_n + \varepsilon c_{n+1} = 0. \tag{5.87}$$

From this equation, the classical Floquet index μ and the Fourier coefficients c_n are determined numerically by continued fractions [45].

In the figures, time and driving parameters are given in the units which are commonly used in mathematical literature [85] to obtain the scaled Mathieu equation $\ddot{x} + (\bar{\omega}_0^2 + 2\bar{\varepsilon}\cos(2\bar{t}))x = 0$. Variances are plotted in units of the corresponding ground-state variance for zero driving amplitude (cf. Appendix A).

We showed in Section 5.4 that the influence of the driving on the master equation results in a modification of the momentum diffusion. Figure 5.2 compares the diffusion coefficient D'_{pp}, obtained from a Markov approximation with respect to the unperturbed spectrum, to the diffusion coefficient D_{pp}, which results from the quasienergy spectrum approach. The numerical values are given in units of the classical momentum diffusion coefficient $mk_\mathrm{B}T$. The parameters ω_0^2 and ε are varied along the full line in the inset. Note that within the unstable regimes, perturbation theory is not valid. Nevertheless, Eq. (5.52) gives a smooth interpolation. The discrepancies become most significant for strong driving and large ω_0^2. Both for low driving amplitude $\varepsilon \ll \omega_0^2$ and high temperature $T \gg \hbar\omega_0/k_\mathrm{B}$, the difference vanishes.

The variances $\sigma_{xx}(t)$ and $\sigma_{pp}(t)$ of the Markov approximations without RWA are compared to the exact results [28] in the Figs. 5.3a and 5.3b. The chosen driving parameters $\omega^2 = 6.5\,\Omega^2$ and $\varepsilon = 7\,\Omega^2$ lie inside the fifth stable zone ($\mu = 4.53513\,\Omega/2$). The temperature $k_\mathrm{B}T = 0.5\,\hbar\Omega$ is sufficiently large, but with quantum effects still

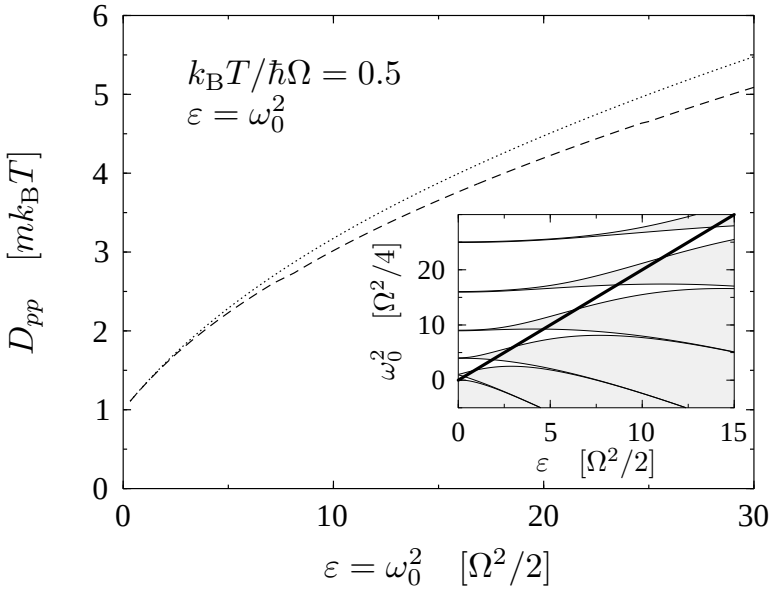

Figure 5.2: The diffusion constants D_{pp} for the simple (dotted) and D'_{pp} for the improved (dashed) Markov approximation in units of the classical diffusion constant $mk_\mathrm{B}T$ for $k_\mathrm{B}T = 0.5\,\hbar\Omega$. The parameters ω_0^2 and ε are indicated by the full line in the inset (cf. Fig. 5.1).

appreciable. We note that the improved Markovian treatment in Section 5.4, which accounts for the quasienergy differences, agrees better with the exact prediction. In the Figure we depict asymptotic times $t > 100/\Omega$, where transient effects have already decayed. The asymptotic covariance elements retain the periodicity $T = 2\pi/\Omega$ of the external driving. The relative error

$$\eta_{xx}(t) = \frac{\sigma_{xx}^{\mathrm{Markov}}(t) - \sigma_{xx}^{\mathrm{exact}}(t)}{\sigma_{xx}^{\mathrm{exact}}(t)} \tag{5.88}$$

of the position variance for these two Markov approximations is depicted in Fig. 5.4. For the chosen parameters it is reduced by the use of the improved Markov scheme by approximately 30%. Note that the maximal deviations do not occur in the extrema, but happen to occur in the regions with negative slope.

As depicted in Fig. 5.5, the quality of both Markov approximations worsens with increasing dissipation strength γ. This reflects the breakdown of the weak-coupling approach.

Results for the Markovian treatment within RWA, given in Section 5.3, are depicted for the position variance $\sigma_{xx}(t)$ in Fig. 5.6. The driving parameters are the same as in Fig. 5.3. For this example, the quality of agreement to the exact result is similar for both Markov approximations. Nevertheless, the solution without RWA yields—up to a scale—a better overall agreement with the exact behavior over a full driving period T.

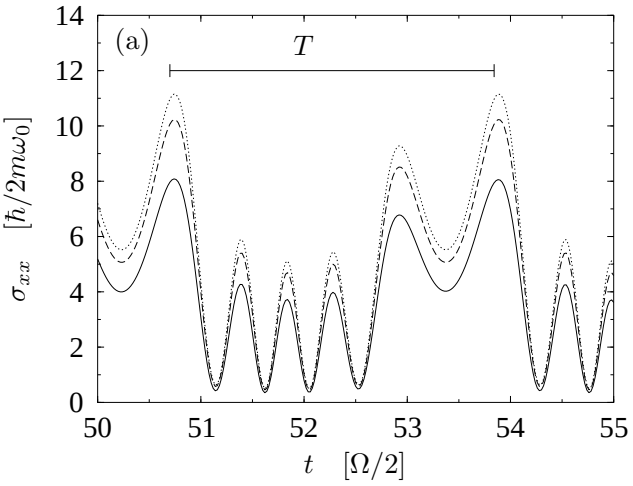

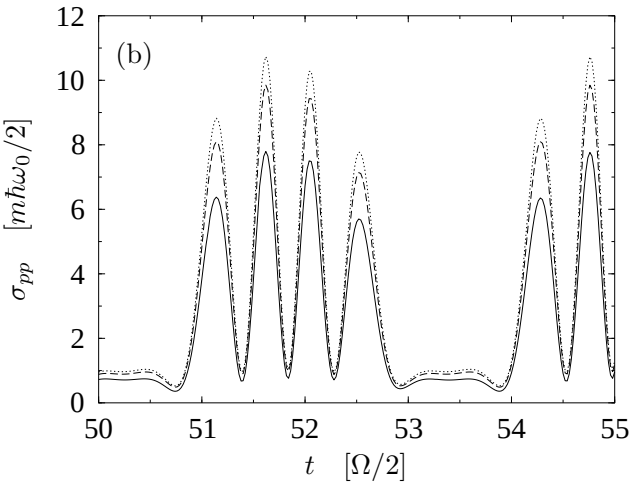

Figure 5.3: The asymptotic variances $\sigma_{xx}(t)$ (a) and $\sigma_{pp}(t)$ (b) with period $T = 2\pi/\Omega$ for the simple (dotted) and the improved (dashed) Markov approximation, compared to the exact result (full line) for the parameters $\varepsilon = 7\,\Omega^2$, $\omega_0^2 = 6.5\,\Omega^2$, $k_{\rm B}T = 0.5\,\hbar\Omega$ and $\gamma = \Omega/20$. The scaled driving period $T = 2\pi/\Omega$ is indicated in panel (a).

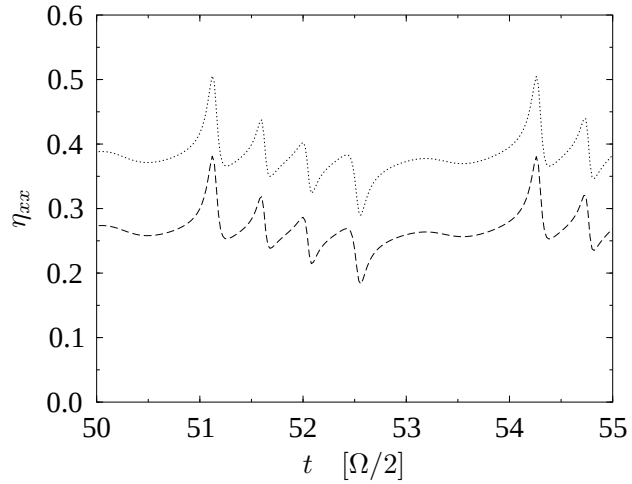

Figure 5.4: Relative error $\eta_{xx}(t)$ for the position variances of Fig. 5.3a.

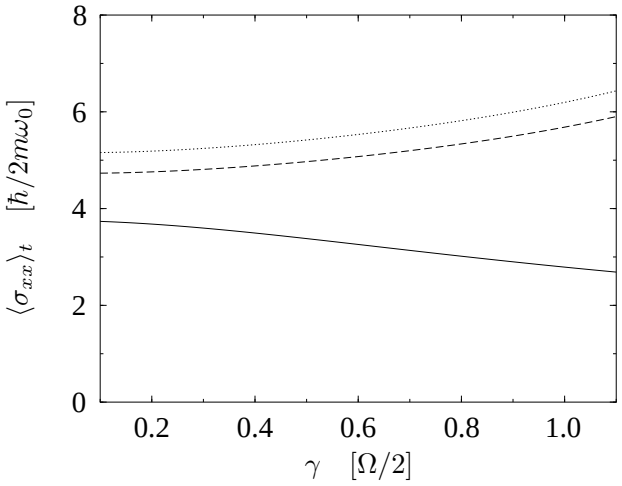

Figure 5.5: The time averaged variance $\langle\sigma_{xx}\rangle_t$ for the simple (dotted) and the improved (dashed) Markov approximation, compared to the exact result (full line) for the parameters $\varepsilon = 7\,\Omega^2$, $\omega_0^2 = 6.5\,\Omega^2$ and $k_\mathrm{B}T = 0.5\,\hbar\Omega$.

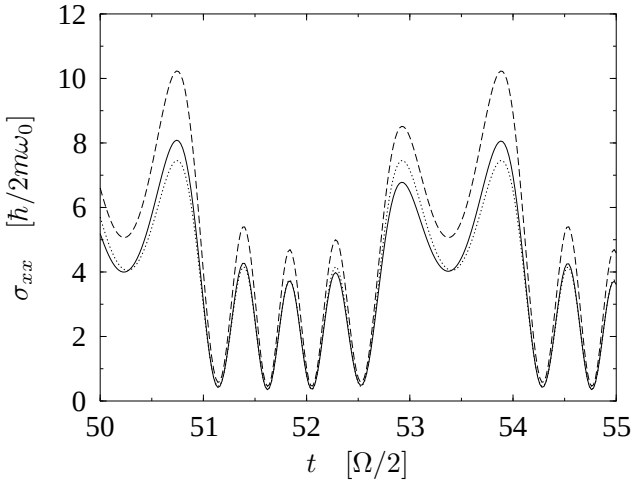

Figure 5.6: Position variances obtained with the Markov approximation with respect to the quasienergy spectrum with (dotted) and without (dashed) RWA, compared to the exact result (full line) for $\gamma = \Omega/20$ and $k_\mathrm{B}T = 0.5\,\hbar\Omega$. The driving parameters are $\varepsilon = 7\,\Omega^2$ and $\omega_0^2 = 6.5\,\Omega^2$.

5.7 Conclusion

The principal distinction to be made among possible Markovian approaches to the driven dissipative dynamics, refers to the degree to which changes in dynamical and spectral properties of the central system due to the driving are taken into account. In the crudest treatment introduced in Section 4.1, where the dissipative terms in the master equation are derived ignoring the explicit time dependence of the Hamiltonian, and the driving only appears in the coherent term. An improved master equation results from the Floquet-Markov scheme which we obtained in Section 4.2 by coupling the central system and the driving as one whole to the heat bath. The energy-domain quantity relevant for all subsequent developments is then the quasienergy spectrum, obtained within the Floquet formalism, instead of the unperturbed spectrum. In the time domain, the quantities entering the dissipative terms of the master equation, such as Heisenberg-picture operators of the central system, gain an explicit time dependence with the periodicity of the driving.

Besides the differences in representation, the use of the improved Floquet-Markov

approximation in Section 5.4 mainly results in a modified momentum diffusion that depends on the quasienergy spectrum instead of the unperturbed spectrum of the central system. The difference becomes significant in the limits of strong driving amplitude and low temperature. An additive time-dependent external force, applied in addition to or instead of the parametric driving, undergoes a renormalization which vanishes, however, in the case of an Ohmic bath.

Even within the improved Markov approach, finer levels of approximation can be distinguished. A significant simplification of the master equation is achieved by a rotating-wave approximation, i.e. here, by neglecting reservoir-induced virtual transitions between Floquet states of the central system that violate quasienergy conservation. The resulting master equation has Lindblad form, with creation and annihilation operators acting on Floquet states, and thus manifestly generates a dynamical semigroup. This is not the case if the RWA is avoided. Apparently a drawback, the lack of a Lindblad structure in the master equation without RWA faithfully reflects the failure of the Markov approximation on short time scales.

An analogous situation as with the Lindblad form of the master equation arises with its Floquet structure. If all coefficients are at most periodically time dependent, then the equation of motion for the reduced density operator complies with the conditions for applicability of the Floquet theorem. As a consequence, the solutions can be cast in Floquet form, i.e., can be written as eigenfunctions of a generalized non-unitary Floquet operator that generates the evolution of the density operator over a single period. Since all variants of the Markov approximation discussed here truncate the memory of the central system on time scales shorter than the period of the driving, the corresponding master equations have Floquet structure throughout. The exact path-integral solution, in contrast, allows for memory effects of unlimited duration and thereby generally prevents the consistent definition of a propagator over a single period.

Additional insight is gained by discussing the dynamics in terms of phase-space distributions, specifically in terms of the Wigner representation of the density operator and its equation of motion. In this representation, the Floquet formalism is a useful device to construct and classify solutions. Since all Fokker-Planck equations obtained are time periodic, as are the corresponding master equations, their solutions may be written as eigenstates of a Wigner-Floquet operator (the Fokker-Planck operator evolving the Wigner function, integrated over a single period), or Wigner-Floquet states in short. They represent the quasiprobability distributions closest to the Floquet solutions of the corresponding classical Fokker-Planck equation.

Wigner-Floquet states with Floquet index zero correspond to asymptotic solutions. They are not literally stationary but retain the periodic time dependence of the driving. Since we are here dealing with a linear system, the centers of gravity of the asymptotic quasiprobability distributions follow the corresponding classical limit cycles. In the case of parametric driving, these limit cycles are trivial and correspond to a fixed point at the origin. A time dependence arises only by the periodic variation of the shape of the asymptotic distributions.

Concluding from a numerical comparison of certain dynamical quantities, for the

specific case of the Mathieu oscillator, the attributes "simple" and "improved" for the two basic Markovian approaches prove adequate. Results for the Markov approximation based on the quasienergy spectrum show consistently better agreement with the exact path-integral solution than those for the Markov approximation with respect to the unperturbed spectrum. However, even in parameter regimes where the respective approximations are expected to become problematic, the differences in quality are not huge and the agreement with the exact solution is generally good. Technical advantages of the Markov approximation in general and of its various ramifications—easy analytical and numerical tractability, desirable formal properties such as Floquet or Lindblad form of the master equation—can justify to tolerate their quantitative inaccuracy.

6 The harmonically driven double-well potential

In this chapter we use the Floquet-Markov scheme to investigate the interplay of chaos and dissipation in a bistable quantum system. The harmonically driven quartic double well will serve as our working model. In Section 6.1 we introduce its Hamiltonian and the underlying symmetries. Moreover, we briefly review coherent driven tunneling as well as its modification caused by the influence of classical chaos.

For moderate driving near the classical resonances, chaos already plays a significant role for the classical dynamics although the motion near the bottom of the wells is still regular. Thus, we have a mixed phase space, where the coexistence of regular and chaotic regions leads to a variety of uncommon coherence phenomena. Most prominent among them is chaotic tunneling [13–17, 30–33, 99–105], the coherent exchange of probability between symmetry-related regular islands that are separated by a chaotic layer, not by a static potential barrier. Chaotic tunneling comes about by an interplay of classical nonlinear, typically bistable, dynamics and quantum coherence. Tunneling is extremely sensitive to any disruption of coherence as it occurs due to the unavoidable coupling to the environment: In presence of dissipation, coherent tunneling becomes a transient that fades out on the way to an asymptotic state [11, 12].

The quasispectrum associated with chaotic tunneling exhibits a characteristic feature: Quasienergies of chaotic singlets intersect tunnel doublets which are supported by regular tori. We study coherent and dissipative chaotic tunneling in the vicinity of such singlet-doublet crossings in Section 6.2. While in the coherent case the dynamics is well described in a three-state approximation, the coupling to the environment indirectly couples the three states to all other states. On the basis of numerical results for the full driven double well with dissipation, we reveal the limitations of the three-level approximation and identify additional features of the full dynamics not covered by it. In particular, we consider the long-time asymptotics and the phase-space structure associated with it.

Switching on friction has a dramatic consequence for the classical phase space: A volume element contracts exponentially in time and therefore all trajectories converge towards a submanifold of phase space with zero volume, the so-called attractor [3]. Depending on friction strength and details of the system, this attractor may be of quite different nature. If the dissipative dynamics is also chaotic, the attractor has in general fractal geometry—it forms a so-called strange attractor; for sufficiently strong friction, the attractor typically shrinks to a limit cycle or a set of isolated fixed points. On a quantum level, the structures associated with classical attractors are smeared out on a scale $\hbar$ but leave their trace in the asymptotic state of the corresponding dissipative quantum map [106]. We study the classical-quantum correspondence of the asymptotic state in Section 6.3.

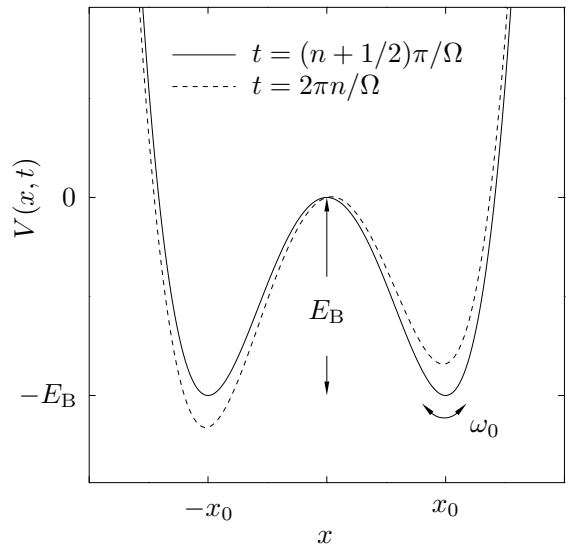

Figure 6.1: Sketch of the driven double well potential described by the time-dependent Hamiltonian (6.1) at various times.

6.1 The model

As a prototypical working model, we consider the quartic double well with a spatially homogeneous driving force, harmonic in time. It is defined by the Hamiltonian

$$H(t) = H_\mathrm{DW} + H_F(t), \tag{6.1}$$

$$H_\mathrm{DW} = \frac{p^2}{2m} - \frac{1}{4}m\omega_0^2 x^2 + \frac{m^2\omega_0^4}{64E_\mathrm{B}}x^4, \tag{6.2}$$

$$H_F(t) = Sx\cos(\Omega t). \tag{6.3}$$

The potential term of the static bistable Hamiltonian H_DW possesses two minima at $x = \pm x_0$, $x_0 = (8E_\mathrm{B}/m\omega_0^2)^{1/2}$, separated by a barrier of height E_B (cf. Fig. 6.1). The parameter ω_0 denotes the (angular) frequency of small oscillations near the bottom of a well. Apart from mere scaling, the classical phase space of H_DW only depends on the presence or absence, and the signs, of the x^2 and the x^4 term. Besides that, it has no free parameter. This is obvious from the scaled form of the classical equations of motion,

$$\dot{\bar{x}} = \bar{p}, \tag{6.4}$$

$$\dot{\bar{p}} = \frac{1}{2}\bar{x} - \frac{1}{2}\bar{x}^3 - F\cos(\bar{\Omega}\bar{t}), \tag{6.5}$$

where the dimensionless quantities $\bar{x}$, $\bar{p}$ and $\bar{t}$ are given by x/x_0, $p/m\omega_0 x_0$ and $\omega_0 t$, respectively. The influence of the driving on the classical phase-space structure is fully characterized by the rescaled amplitude and frequency of the driving,

$$F = \frac{S}{\sqrt{8m\omega_0^2 E_\mathrm{B}}}, \qquad \bar{\Omega} = \frac{\Omega}{\omega_0}. \tag{6.6}$$

This implies that the classical dynamics is independent of the barrier height E_B.

In the quantum-mechanical case, however, this holds no longer true: The finite size of Planck's constant results in a finite number of doublets with energy below the barrier top. It is approximately given by

$$D = \frac{E_{\mathrm{B}}}{\hbar\omega_0}, \tag{6.7}$$

and distinguishes the semiclassical from the deep quantum regime. This is evident from the classical scales for position, x_0, and momentum, $m\omega_0 x_0$, introduced above: The corresponding action scale is $m\omega_0 x_0^2$ and therefore, the position-momentum uncertainty relation in the scaled phase space $(\bar{x}, \bar{p})$ reads

$$\Delta\bar{x}\,\Delta\bar{p} \geq \frac{\hbar_{\mathrm{eff}}}{2} \tag{6.8}$$

where

$$\hbar_{\mathrm{eff}} = \frac{\hbar}{m\omega_0 x_0^2} = \frac{1}{8D} \tag{6.9}$$

denotes the effective quantum of action. The classical limits hence amounts to $D \to \infty$.

In the following, we restrict ourselves to moderate driving amplitudes, such that the variation of the potential at the bottom of the wells is much smaller than the barrier height. This implies that the bistable character of the potential is retained at any time.

6.1.1 Symmetries

The model Hamiltonian (6.1) obviously is $2\pi/\Omega$-periodic in time, thus possesses discrete time-translational invariance. This enables a treatment within the Floquet-Markov scheme, introduced in Chapter 4. In addition, we find two more discrete symmetries, which allow for an improvement of numerical efficiency and also for a classification of the Floquet states as even or odd.

Time-reversal symmetry

It is well known that the energy eigenfunctions of an (undriven) Hamiltonian which obeys time-reversal symmetry, can be chosen as real [8, 79]. This has, apart from computational advantages, also direct physical consequences for the level statistics of quantum systems with chaotic classical counterpart [8, 79]. Time-reversal symmetry is typically broken by a magnetic field (recall that a magnetic field is described by an axial vector and changes sign under time reversion) or by an explicit time-dependence of the Hamiltonian. However, for the sinusoidal shape of the driving together with the initial phase chosen above, time-reversal symmetry

$$\mathsf{T}: \quad x \to x, \quad p \to -p, \quad t \to -t \tag{6.10}$$

is retained and the Floquet Hamiltonian obeys $\mathcal{H}(t) = \mathcal{H}^*(-t)$ [cf. Eq. (2.11)]. If now $\phi(x,t)$ is a Floquet state in position representation with quasienergy ϵ, then $\phi^*(x,-t)$

also is a Floquet state with the same quasienergy. This means that we can always choose the Floquet states by linear combination such that $\phi(x,t) = \phi^*(x,-t)$, which translates to $\phi(x,\omega) = \phi^*(x,\omega)$ in the frequency regime, i.e., the Fourier coefficients of the Floquet states can be chosen real.

Generalized parity

The undriven Hamiltonian H_{DW} is invariant under the parity P: $x \to -x$, $p \to -p$, $t \to t$. This symmetry is destroyed by a linerarly coupled driving field. With the above choice of $H_F(t)$, however, a more general, dynamical symmetry remains [10, 107, 108]. It is defined by the operation

$$\mathsf{P}_\Omega : \quad x \to -x, \quad p \to -p, \quad t \to t + \pi/\Omega \tag{6.11}$$

and represents a generalized parity acting in the extended phase space spanned by x, p, and phase, i.e., time $t \bmod(2\pi/\Omega)$ or in the composite Hilbert space $\mathcal{R} \otimes \mathcal{T}$, respectively. While such a discrete symmetry is of minor importance in classical physics, its influence on the quantum mechanical quasispectrum $\{\epsilon_\alpha(F)\}$ is more distinct: It devides the composite Hilbert space in an even and an odd subspace, thus allowing for a classification of the Floquet states as even or odd. Quasienergies from different symmetry classes may intersect, whereas quasienergies with the same symmetry typically form avoided crossings [79]. However, the fact that the generalized parity acts on the composite Hilbert space results in a particularity: If $|\phi(t)\rangle$ is e.g. an even Floquet state, then $|\phi^{(1)}(t)\rangle = \exp(\mathrm{i}\Omega t)|\phi(t)\rangle$ turns out to be odd. Thus, two equivalent Floquet states from neighboring Brillouin zones possess different generalized parity. This means that a classification of the corresponding solutions of the Schrödinger equation, $|\psi(t)\rangle = \exp(-\mathrm{i}\epsilon t/\hbar)|\phi(t)\rangle$, as even or odd requires a restriction to a single Brillouin zone.

The invariance of the system under the generalized parity is also of considerable help in the numerical treatment of the Floquet matrix (2.53) [16, 100]. To obtain a complete set of Floquet states, it is sufficient to compute all eigenvectors of the Floquet Hamiltonian in the even subspace whose eigenvalues lie in the first two Brillouin zones. The even Floquet states are given by the eigenvectors of $\mathcal{H}_{\mathrm{e}}$ from the first Brillouin zone; the odd Floquet states are obtained by shifting the (even) ones from the second to the first Brillouin zone, which changes their generalized parity. Thus, we have to diagonalize the even supermatrix

$$\mathcal{H}_{\mathrm{e}} = \begin{pmatrix} \ddots & \vdots & \vdots & \vdots & \vdots & \vdots & \\ \cdots & E_{\mathrm{e}} + 2\hbar\Omega & X_{\mathrm{eo}} & 0 & 0 & 0 & \cdots \\ \cdots & X_{\mathrm{eo}} & E_{\mathrm{o}} + \hbar\Omega & X_{\mathrm{oe}} & 0 & 0 & \cdots \\ \cdots & 0 & X_{\mathrm{oe}} & E_{\mathrm{e}} & X_{\mathrm{eo}} & 0 & \cdots \\ \cdots & 0 & 0 & X_{\mathrm{eo}} & E_{\mathrm{o}} - \hbar\Omega & X_{\mathrm{oe}} & \cdots \\ \cdots & 0 & 0 & 0 & X_{\mathrm{oe}} & E_{\mathrm{e}} - 2\hbar\Omega & \cdots \\ & \vdots & \vdots & \vdots & \vdots & \vdots & \ddots \end{pmatrix}, \tag{6.12}$$

which for the same number of Floquet channels has only half the dimension of the original Floquet matrix (2.53). The matrices

$$E_{\mathrm{e}} = \begin{pmatrix} E_0 & 0 & 0 & \cdots \\ 0 & E_2 & 0 & \cdots \\ 0 & 0 & E_4 & \cdots \\ \vdots & \vdots & \vdots & \ddots \end{pmatrix}, \quad E_{\mathrm{o}} = \begin{pmatrix} E_1 & 0 & 0 & \cdots \\ 0 & E_3 & 0 & \cdots \\ 0 & 0 & E_5 & \cdots \\ \vdots & \vdots & \vdots & \ddots \end{pmatrix}, \tag{6.13}$$

$$X_{\mathrm{eo}} = \frac{S}{2} \begin{pmatrix} x_{0,1} & x_{0,3} & x_{0,5} & \cdots \\ x_{2,1} & x_{2,3} & x_{2,5} & \cdots \\ x_{4,1} & x_{4,3} & x_{4,5} & \cdots \\ \vdots & \vdots & \vdots & \ddots \end{pmatrix}, \quad X_{\mathrm{oe}} = \frac{S}{2} \begin{pmatrix} x_{1,0} & x_{1,2} & x_{1,4} & \cdots \\ x_{3,0} & x_{3,2} & x_{3,4} & \cdots \\ x_{5,0} & x_{5,2} & x_{5,4} & \cdots \\ \vdots & \vdots & \vdots & \ddots \end{pmatrix}, \tag{6.14}$$

which are part of the supermatrix $\mathcal{H}_{\mathrm{e}}$, denote the undriven Hamiltonian H_{DW} and the coupling to the driving field $H_1 = Sx/2$, decomposed into the even and odd eigenstates of H_{DW}.

6.1.2 Tunneling, driving, and dissipation

With the driving $H_F(t)$ switched off, the classical phase space generated by H_{DW} exhibits the constituent features of a bistable Hamiltonian system. There is a separatrix at $E = 0$. It forms the border between two sets of trajectories: One set, with $E < 0$, comes in symmetry-related pairs, each partner of which oscillates in either one of the two potential minima. The other set consists of unpaired trajectories, with $E > 0$, that encircle both wells in a spatially symmetric fashion.

Due to the integrability of the undriven double well, Eq. (6.2), we can gain a qualitative picture of its eigenstates from simple torus quantization: The unpaired tori correspond to singlets with positive energy, whereas the symmetry-related pairs below the top of the barrier correspond to degenerate pairs of eigenstates. Neighboring pairs are separated in energy approximately by $\hbar\omega_0$, which reflects the almost harmonic potential shape near the bottom of the wells. Exact quantization, however, predicts that the partners of these pairs have small but finite overlap. Therefore, the true eigenstates come in doublets, each of which consists of an even and an odd state, $|\Phi_n^+\rangle$ and $|\Phi_n^-\rangle$. The energies of the nth doublet are separated by a small tunnel splitting Δ_n. We can always choose the globals phases such that the superpositions

$$|\Phi_n^{\mathrm{R,L}}\rangle = \frac{1}{\sqrt{2}} \left(|\Phi_n^+\rangle \pm |\Phi_n^-\rangle \right) \tag{6.15}$$

are localized in the right and the left well, respectively. As time evolves, the states $|\Phi_n^+\rangle$, $|\Phi_n^-\rangle$ acquire a relative phase $\exp(-\mathrm{i}\Delta_n t/\hbar)$ and $|\Phi_n^{\mathrm{R}}\rangle$, $|\Phi_n^{\mathrm{L}}\rangle$ are transformed into one another after a time $\pi\hbar/\Delta_n$. Thus, the particle tunnels forth and back between the wells with a frequency $\Delta_n/\hbar$. This introduces an additional, purely quantum mechanical frequency-scale, the tunnel rate $\Delta_0/\hbar$ of a particle which resides in the ground-state doublet. Typically, tunnel rates are extremely small compared

to the frequencies of the classical dynamics, all the more in the semiclassical regime we are interested in.

A driving of the form (6.3), even if its influence on the classical phase space is minor, can entail significant consequences for the tunnel dynamics: It may enlarge the tunnel rate by orders of magnitude or even suppress tunneling at all. For adiabatically slow driving, $\Omega \ll \Delta_0/\hbar$, tunneling is governed by the time-average of the instantaneous tunnel splitting, which is always larger than its unperturbed value Δ_0 and results in an enhancement of the tunneling rate [107]. If the driving is faster, $\Delta_0/\hbar \lesssim \Omega \ll \omega_0$, the opposite holds true: The relevant time scale is now given by the inverse of the quasienergy splitting of the ground-state doublet $\hbar/|\epsilon_1 - \epsilon_0|$. It has been found [107,109] that in this case for finite driving amplitude $|\epsilon_1 - \epsilon_0| < \Delta_0$, thus tunneling is always decelerated. It even happens that the quasienergies of the ground-state doublet (which are of different generalized parity) intersect as a function of the driving amplitude F, thus the splitting vanishes and tunneling is brought to a complete standstill by the purely coherent influence of the driving [10].

The small energy scales associated with make tunneling extremely sensitive to any disruption of coherence, as it occurs due to the unavoidable coupling to the environment. As an immediate consequence, the symmetry underlying the formation of tunnel doublets is generally broken, and an additional energy scale is introduced, the effective finite width attained by each discrete level. Tunneling and related coherence phenomena are thus rendered transients that occur—if at all—on the way towards an asymptotic equilibrium state and fade out on a time scale t_{decoh}. In general, this time scale gets shorter for higher temperatures, reflecting the growth of the transition rates (4.23) [53]. However, there exist counterintuitive effects. For example, for driven tunneling in the vicinity of an exact crossing of the ground-state doublet, the coherent suppression of tunneling [10, 12, 107] can be stabilized with higher temperatures [76–78] until levels outside the doublet start to play a role.

So far, we have considered only driving frequencies much smaller than the frequency scale ω_0 of the relevant classical resonances, i.e., a parameter regime where classical motion is predominantly regular. Coherent tunneling is in this case well described within a two-state approximation [107,109]. In the dissipative case, however, a two-state approximation of course fails for temperatures $k_{\mathrm{B}}T \gtrsim \hbar\omega_0$, where thermal activation to higher doublets becomes relevant.

6.1.3 The onset of chaos

Driving with a frequency $\Omega \approx \omega_0$ has an even stronger influence on the dynamics of the bistable system. It enters already on the level of classical mechanics since small oscillations near the bottom of the wells become resonant and classical chaos comes into play. This corresponds in a quantum description to resonant multiple excitation of inter-doublet transitions until levels near the top of the barrier are significantly populated.

Increasing the amplitude of the driving from zero onwards has two principal consequences for the classical dynamics: The separatrix is destroyed as a closed

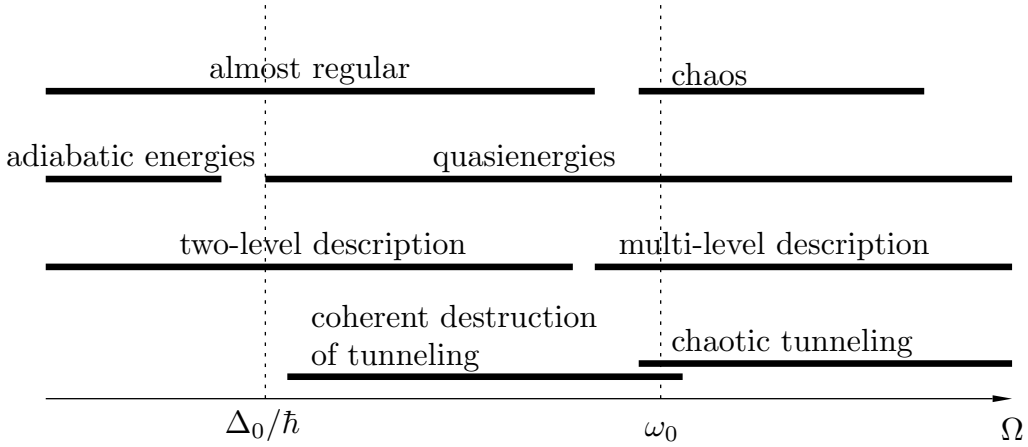

Figure 6.2: Tunneling phenomena and the according appropriate levels of description for the non-dissipative driven double-well potential, Eq. (6.1). The bars depict the corresponding regimes of the driving frequency Ω. See Section 6.1 for a detailed discussion.

curve and replaced by a homoclinic tangle [110] of stable and unstable manifolds. As a whole, it forms a chaotic layer in the vicinity and with the topology of the former separatrix (cf. Fig. 6.6). This opens the way for diffusive transport between the two potential wells. Due to the nonlinearity of the potential, there is an infinite set of resonances of the driving with the unperturbed motion, both inside and outside the wells [111,112]. Since the period of the unperturbed, closed trajectories diverges for $E \to 0$, the resonances accumulate towards the separatrix of the unperturbed system. By its sheer phase-space area, the first resonance (the one for which the periods of the driving and of the unperturbed oscillation are in a ratio of 1:1) is prominent among the others and soon (in terms of increasing amplitude F) exceeds the size of the "order-zero" regular areas near the bottom of each well [16].

Both major tendencies in the evolution of the classical phase space—extension of the chaotic layer and growth of the first resonance—leave their specific traces in the quasienergy spectrum. The tunnel doublets characterizing the unperturbed spectrum for $E < 0$ pertain to states located on pairs of symmetry-related quantizing tori in the regular regions within the wells. With increasing size of the chaotic layer, the quantizing tori successively resolve in the chaotic sea. The corresponding doublets disappear as distinct structures in the spectrum as they attain a splitting of the same order as the mean level separation. The gradual widening of the doublets proceeds as a smooth function of the driving amplitude [16, 100]. This function roughly obeys a power law [34, 113, 114]. As soon as a pair of states is no longer supported by any torus-like manifold, including fractal [115] and vague tori [116], the corresponding eigenvalues detach themselves from the regular ladder to which they formerly belonged. They can then fluctuate freely in the spectrum and thereby "collide" with other chaotic singlets or regular doublets.

The appearance of a regular region, large enough to accommodate several eigenstates, around the first resonance introduces a second ladder of doublets into the spectrum. Size and shape of the first resonance vary in a way different from the

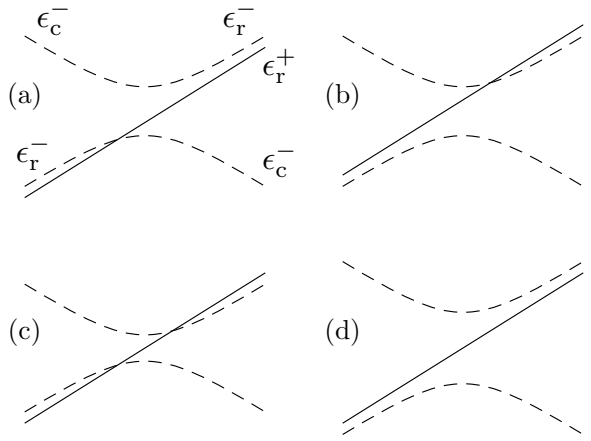

Figure 6.3: Possible configurations of quasienergy crossings between a chaotic singlet and a regular doublet. Different line types signify different parity. See Section 6.2.1 for the labeling of the levels. Note that only for configurations (a),(b), the order of the regular doublet is restored in passing through the crossing. In configurations (c),(d), it is reversed.

main regular region. The corresponding doublet ladder therefore moves in the spectrum independently of the doublets that pertain to the main regular region, and of the chaotic singlets. This gives rise to additional singlet-doublet and even to doublet-doublet encounters.

6.2 Chaotic tunneling near singlet-doublet crossings

Near a crossing, level separations deviate vastly, in both directions, from the typical tunnel splitting (cf. Fig. 6.8, below). This is reflected in time-domain phenomena ranging from the suppression of tunneling to a strong increase in its rate and to complicated quantum beats [31–33]. Singlet-doublet crossings, in turn, drastically change the non-dissipative quasienergy scales and replace the two-level by a three-level structure. As a consequence, the familiar way tunneling fades out in the presence of dissipation is also significantly altered. Near a crossing, the coherent dynamics can last much longer than for the unperturbed doublet, despite the presence of the same dissipation as outside the crossing, establishing "chaos-induced coherence." Depending on temperature, it can also be destroyed on a much shorter time scale.

For the parameters chosen in our numerical studies, higher resonances are negligible in size. Therefore, the borderline between the chaotic layer along the former separatrix and the regular regions within and outside the wells is quite sharply defined. The "coastal strip" formed by hierarchies of regular islands around higher resonances remains narrow (cf. Fig. 6.6, below) on a scale of the chosen effective quantum of action. For the tunneling dynamics, the role of states located in the border region [102, 103] is therefore not significant in our studies.

6.2.1 Three-level crossings

Among the various types of quasienergy crossings that occur according to the above scenario, those involving a regular doublet and a chaotic singlet are the most com-

mon. In order to give a quantitative account of such crossings and the associated coherent dynamics, and for later reference in the context of the incoherent dynamics, we shall now discuss them in terms of a simple three-state model, devised much in the spirit of Ref. [30].

Far to the left of the crossing, we expect the following situation: There is a doublet of Floquet states

$$|\psi_{\mathrm{r}}^{+}(t)\rangle = \mathrm{e}^{-\mathrm{i}\epsilon_{\mathrm{r}}^{+}t/\hbar}|\phi_{\mathrm{r}}^{+}(t)\rangle, \tag{6.16}$$

$$|\psi_{\mathrm{r}}^{-}(t)\rangle = \mathrm{e}^{-\mathrm{i}(\epsilon_{\mathrm{r}}^{+}+\Delta)t/\hbar}|\phi_{\mathrm{r}}^{-}(t)\rangle, \tag{6.17}$$

with even (superscript +) and odd (−) generalized parity, respectively, residing on a pair of quantizing tori in one of the regular (subscript r) regions. We have assumed that the quasienergy splitting (as opposed to the unperturbed splitting) is $\epsilon_{\mathrm{r}}^{-} - \epsilon_{\mathrm{r}}^{+} = \Delta > 0$. The global relative phases can be chosen such that the superpositions

$$|\phi_{\mathrm{R,L}}(t)\rangle = \frac{1}{\sqrt{2}}\left(|\phi_{\mathrm{r}}^{+}(t)\rangle \pm |\phi_{\mathrm{r}}^{-}(t)\rangle\right) \tag{6.18}$$

are localized in the right and the left well, respectively, and tunnel back and forth with a frequency $\Delta/\hbar$ given by the tunnel splitting in the presence of the driving.

As the third player, we introduce a Floquet state

$$|\psi_{\mathrm{c}}^{-}(t)\rangle = \mathrm{e}^{-\mathrm{i}(\epsilon_{\mathrm{r}}^{+}+\Delta+\Delta_{\mathrm{c}})t/\hbar}|\phi_{\mathrm{c}}^{-}(t)\rangle, \tag{6.19}$$

located mainly in the chaotic (subscript c) layer, so that its time-periodic part $|\phi_{\mathrm{c}}^{-}(t)\rangle$ contains a large number of harmonics. Without loss of generality, its generalized parity is fixed to be odd. For the quasienergy, we have assumed that $\epsilon_{\mathrm{c}}^{-} = \epsilon_{\mathrm{r}}^{+}+\Delta+\Delta_{\mathrm{c}}$, where $|\Delta_{\mathrm{c}}|$ can be regarded as a measure of the distance from the crossing.

The structure of the classical phase space then implies that the mean energy of the chaotic state should be close to the top of the barrier and far above that of the doublet. We assume, like for the quasienergies, a small splitting of the mean energies pertaining to the regular doublet, $|E_{\mathrm{r}}^{-} - E_{\mathrm{r}}^{+}| \ll E_{\mathrm{c}}^{-} - E_{\mathrm{r}}^{\pm}$.

In order to model an avoided crossing between $|\phi_{\mathrm{r}}^{-}\rangle$ and $|\phi_{\mathrm{c}}^{-}\rangle$, we suppose that there is a non-vanishing fixed matrix element

$$b \equiv \langle\langle\phi_{\mathrm{r}}^{-}|H_{\mathrm{DW}}|\phi_{\mathrm{c}}^{-}\rangle\rangle > 0. \tag{6.20}$$

For the singlet-doublet crossings under study, we typically find that $\Delta \ll b \ll \hbar\Omega$. Neglecting the coupling with all other states, we model the system by the three-state (subscript 3s) Floquet Hamiltonian

$$\mathcal{H}_{3\mathrm{s}} = \epsilon_{\mathrm{r}}^{+} + \begin{pmatrix} 0 & 0 & 0 \\ 0 & \Delta & b \\ 0 & b & \Delta+\Delta_{\mathrm{c}} \end{pmatrix}, \tag{6.21}$$

in the three-dimensional Hilbert space spanned by $\{|\phi_{\rm r}^+(t)\rangle, |\phi_{\rm r}^-(t)\rangle, |\phi_{\rm c}^-(t)\rangle\}$. Its Floquet states read

$$\begin{aligned} |\phi_0^+(t)\rangle &= |\phi_{\rm r}^+(t)\rangle, \\ |\phi_1^-(t)\rangle &= \left(|\phi_{\rm r}^-(t)\rangle \cos\beta - |\phi_{\rm c}^-(t)\rangle \sin\beta\right), \\ |\phi_2^-(t)\rangle &= \left(|\phi_{\rm r}^-(t)\rangle \sin\beta + |\phi_{\rm c}^-(t)\rangle \cos\beta\right). \end{aligned} \tag{6.22}$$

Their quasienergies are

$$\epsilon_0^+ = \epsilon_{\rm r}^+, \quad \epsilon_{1,2}^- = \epsilon_{\rm r}^+ + \Delta + \frac{1}{2}\Delta_{\rm c} \mp \frac{1}{2}\sqrt{\Delta_{\rm c}^2 + 4b^2}, \tag{6.23}$$

and the mean energies are approximately given by

$$\begin{aligned} E_0^+ &= E_{\rm r}^+, \\ E_1^- &= E_{\rm r}^- \cos^2\beta + E_{\rm c}^- \sin^2\beta, \\ E_2^- &= E_{\rm r}^- \sin^2\beta + E_{\rm c}^- \cos^2\beta, \end{aligned} \tag{6.24}$$

where contributions of the matrix element b have been neglected. The angle β describes the mixing between the Floquet states $|\phi_{\rm r}^-\rangle$ and $|\phi_{\rm c}^-\rangle$ and is a measure of the distance to the avoided crossing. By diagonalizing the Hamiltonian (6.21), we obtain

$$2\beta = \arctan\left(\frac{2b}{\Delta_{\rm c}}\right), \quad 0 < \beta < \frac{\pi}{2}. \tag{6.25}$$

For $\beta \to \pi/2$, corresponding to $-\Delta_{\rm c} \gg b$, we retain the situation far left of the crossing, as outlined above, with $|\phi_1^-\rangle \approx |\phi_{\rm c}^-\rangle$, $|\phi_2^-\rangle \approx |\phi_{\rm r}^-\rangle$. To the far right of the crossing, i.e., for $\beta \to 0$ or $\Delta_{\rm c} \gg b$, the exact eigenstates $|\phi_1^-\rangle$ and $|\phi_2^-\rangle$ have interchanged their identity with respect to the phase-space structure [31–33]. Here, we have $|\phi_1^-\rangle \approx |\phi_{\rm r}^-\rangle$ and $|\phi_2^-\rangle \approx |\phi_{\rm c}^-\rangle$. The mean energy is essentially determined by the phase-space structure. Therefore, there is also an exchange of E_1^- and E_2^- in an exact crossing, cf. Eq. (6.24), while E_0^+ remains unaffected (Fig. 6.4b). The quasienergies ϵ_0^+ and ϵ_1^- must intersect close to the avoided crossing of ϵ_1^- and ϵ_2^- (Fig. 6.4a). Their crossing is exact, since they pertain to states with opposite parity (cf. Fig. 6.3a,b).

In order to illustrate the above three-state model and to demonstrate its adequacy, we have numerically studied a singlet-doublet crossing that occurs for the double-well potential, Eq. (6.1), with $D = 4$, at a driving frequency $\Omega = 0.982\,\omega_0$ and amplitude $F = 0.015029$ (Fig. 6.5). The phase-space structure of the participating Floquet states (Figs. 6.6, 6.7) meets the assumptions of our three-state theory. A comparison of the appropriately scaled three-state theory (Fig. 6.4) with this real singlet-doublet crossing (Fig. 6.5) shows satisfactory agreement. Note that in the real crossing, the quasienergy of the chaotic singlet decreases as a function of F, so that the exact crossing occurs to the left of the avoided one. This numerical example also shows that the idealized three-state model is not always strictly correct. Following the global tendency of widening of the splittings with increasing driving amplitude [16, 34, 114], it may well happen that even far away from a crossing,

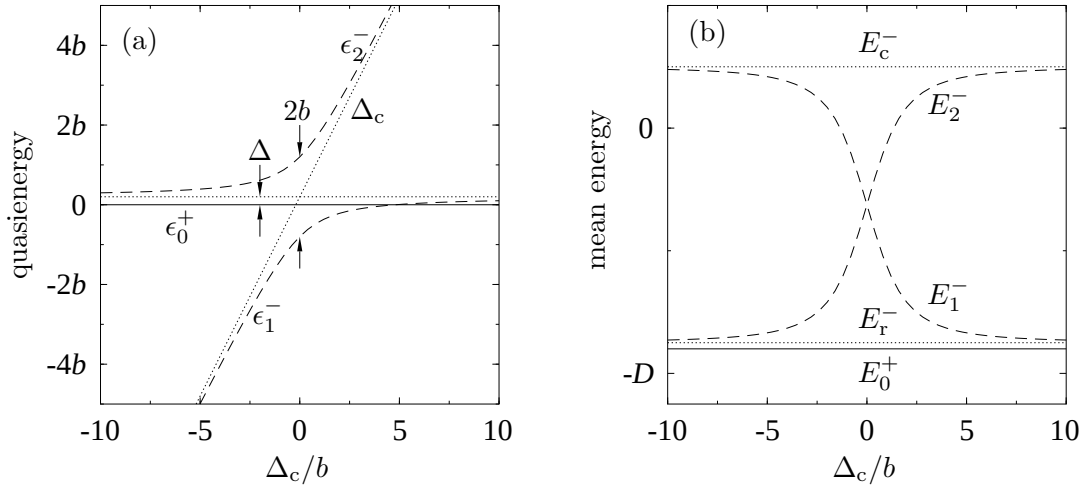

Figure 6.4: A singlet-doublet crossing, according to a three-state model (6.21) in terms of the dependence of the quasienergies (a) and the mean energies (b) on the coupling parameter Δ_c/b. Unperturbed energies are marked by dotted lines, the energies for the case with coupling by full lines for even and dashed lines for odd states.

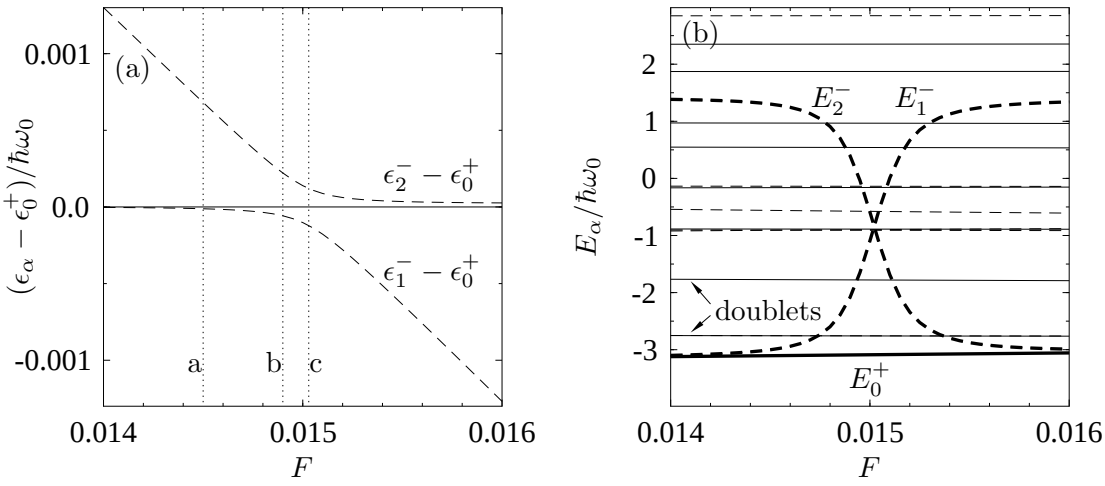

Figure 6.5: Singlet-doublet crossing found numerically for the driven double well, Eq. (6.1), at $D = 4$ and $\Omega = 0.982\,\omega_0$, in terms of the dependence of the quasienergies (a) and the mean energies (b) on the driving amplitude F. Values of the driving amplitude used in Fig. 6.9 are marked by dotted vertical lines. Full and dashed lines indicate energies of even and odd states, respectively. Bold lines give the mean energies of the chaotic singlet and the ground-state doublet depicted in panel (a).

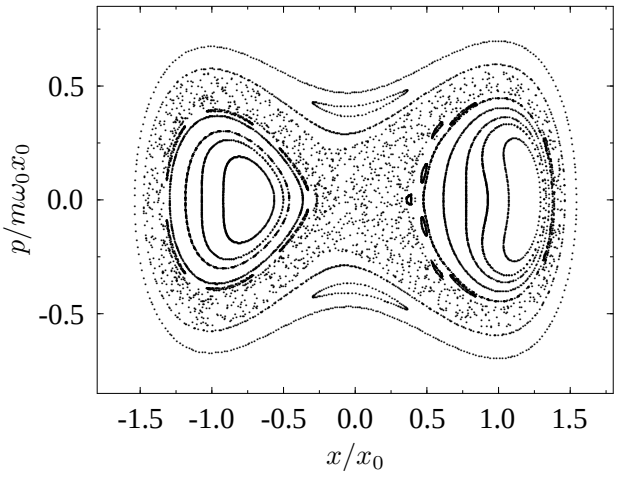

Figure 6.6: Stroboscopic classical phase-space portraits, at $t = 2\pi n/\Omega$, of the harmonically driven quartic double well, Eq. (6.1). The driving parameters $F = 0.015$, $\Omega = 0.982\,\omega_0$, are chosen at the the center of the singlet-doublet crossing under study.

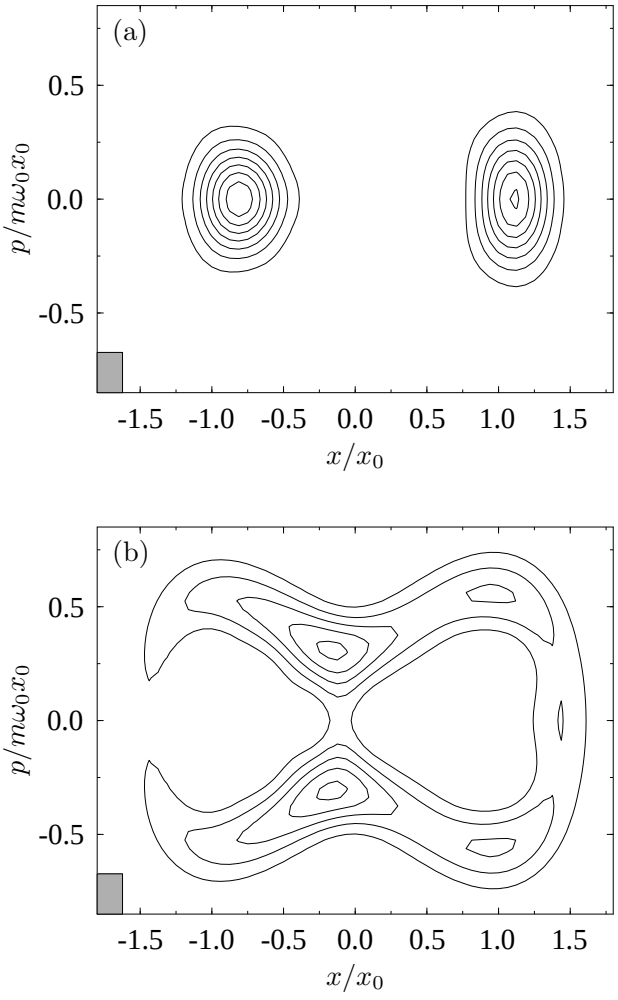

Figure 6.7: Contour plots of the Husimi functions for the Floquet states $|\phi_1^-\rangle \approx |\phi_\mathrm{r}^-\rangle$ (a) and $|\phi_2^-\rangle \approx |\phi_\mathrm{c}^-\rangle$ (b) of the harmonically driven quartic double well, Eq. (6.1), at stroboscopic times $t = 2\pi n/\Omega$. The driving parameters $F = 0.014$, $\Omega = 0.982\,\omega_0$, are in sufficient distance to the singlet-doublet crossing such that the mixing between the regular and the chaotic state is negligible. The rectangle in the lower left corner depicts the size of the effective quantum of action $\hbar_\mathrm{eff}$.

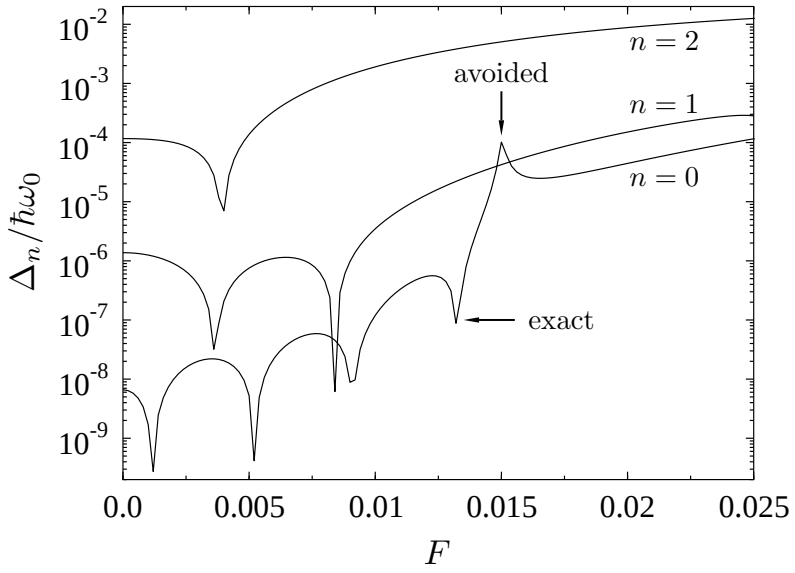

Figure 6.8: Splitting of the lowest doublets for $D = 4$ and $\Omega = 0.982\,\omega_0$. The arrows indicate the locations of the exact and the avoided crossing within a three-level crossing of the type sketched in Fig. 6.3a.

the doublet splitting does not exactly return to its value on the opposite side (see Fig. 6.8). It is even possible that an exact crossing of ϵ_0^+ and ϵ_1^- does not take place at all in the vicinity of the crossing. In that case, the relation of the quasienergies in the doublet gets reversed via the crossing (Fig. 6.3c,d). Nevertheless, the above scenario captures the essential features.

To study the dynamics of the tunneling process, we focus on the state

$$|\psi(t)\rangle = \frac{1}{\sqrt{2}}\left(\mathrm{e}^{-\mathrm{i}\epsilon_0^+ t/\hbar}|\phi_0^+(t)\rangle + \mathrm{e}^{-\mathrm{i}\epsilon_1^- t/\hbar}|\phi_1^-(t)\rangle\cos\beta + \mathrm{e}^{-\mathrm{i}\epsilon_2^- t/\hbar}|\phi_2^-(t)\rangle\sin\beta\right). \quad (6.26)$$

It is constructed such that at $t = 0$, it corresponds to the decomposition of $|\phi_\mathrm{R}\rangle$ in the basis (6.22) at finite distance from the crossing. Therefore, it is initially localized in the regular region in the right well and follows the time evolution under the Hamiltonian (6.21). From Eqs. (6.18), (6.22), we find the probabilities for its evolving into $|\phi_\mathrm{R}\rangle$, $|\phi_\mathrm{L}\rangle$, or $|\phi_\mathrm{c}\rangle$, respectively, to be

$$\begin{aligned}
P_\mathrm{R}(t) &= |\langle\phi_\mathrm{R}(t)|\psi(t)\rangle|^2 \\
&= \frac{1}{2}\Bigg(1 + \cos\frac{(\epsilon_1^- - \epsilon_0^+)t}{\hbar}\cos^2\beta + \cos\frac{(\epsilon_2^- - \epsilon_0^+)t}{\hbar}\sin^2\beta \\
&\quad + \left[\cos\frac{(\epsilon_1^- - \epsilon_2^-)t}{\hbar} - 1\right]\cos^2\beta\sin^2\beta\Bigg), \\
P_\mathrm{L}(t) &= |\langle\phi_\mathrm{L}(t)|\psi(t)\rangle|^2 \\
&= \frac{1}{2}\Bigg(1 - \cos\frac{(\epsilon_1^- - \epsilon_0^+)t}{\hbar}\cos^2\beta - \cos\frac{(\epsilon_2^- - \epsilon_0^+)t}{\hbar}\sin^2\beta
\end{aligned} \quad (6.27)$$

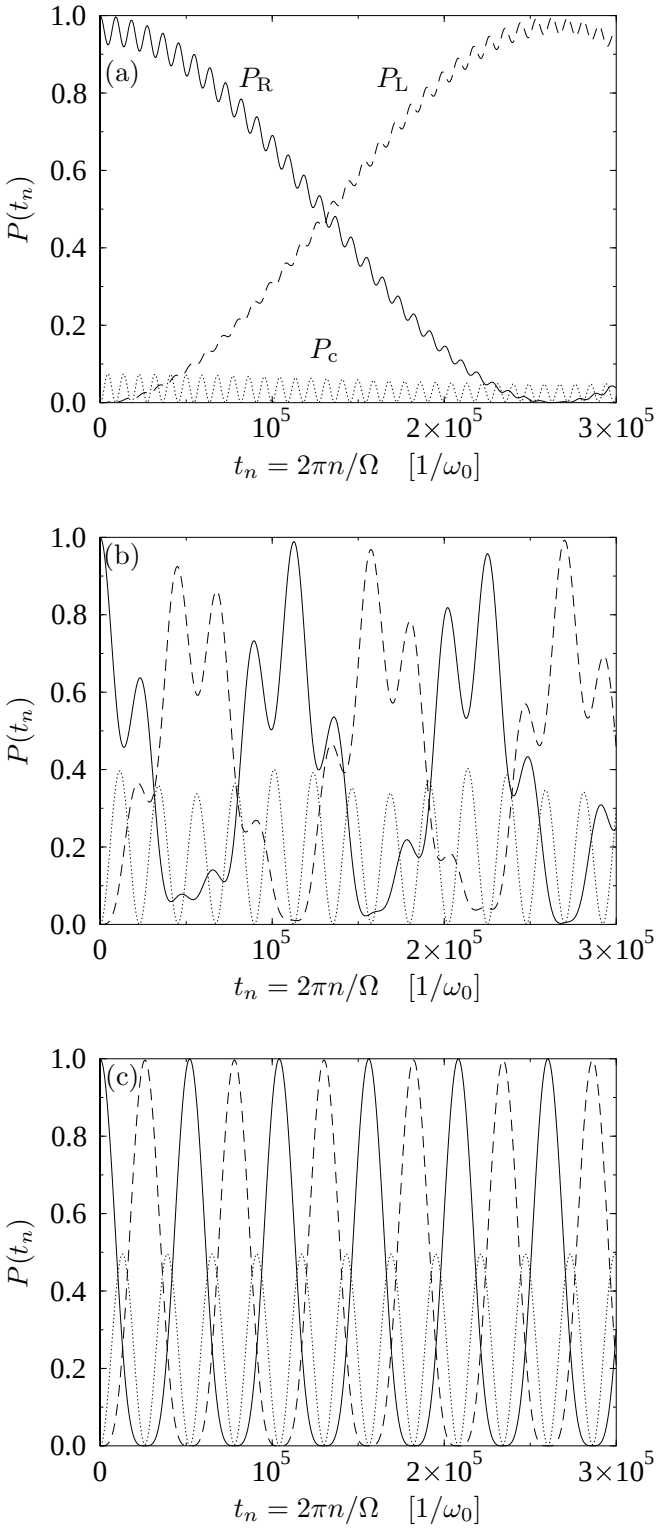

Figure 6.9: Stroboscopic time evolution of a state initially localized in the right well, in the vicinity of the singlet-doublet crossing shown in Fig. 6.5, in terms of the probabilities to be in the right well (which here is identical to the return probability, marked by full lines), in the reflected state in the left well (dashed), or in the chaotic state $|\psi_{\rm c}\rangle$ (dotted). Parameter values are as in Fig. 6.5, and $F = 0.0145$ (a), 0.0149 (b), 0.015029 (c).

$$+\left[\cos\frac{(\epsilon_1^- - \epsilon_2^-)t}{\hbar} - 1\right]\cos^2\beta\sin^2\beta\Bigg),$$

$$P_{\rm c}(t) = |\langle\phi_{\rm c}(t)|\psi(t)\rangle|^2$$
$$= \left[1 - \cos\frac{(\epsilon_1^- - \epsilon_2^-)t}{\hbar}\right]\cos^2\beta\sin^2\beta.$$

We discuss the coherent dynamics of the three-state model for different distances to the crossing and illustrate it by numerical results for the real crossing introduced above.

In sufficient distance from the crossing, there is only little mixing between the regular and the chaotic states, i.e., $\sin\beta \ll 1$ or $\cos\beta \ll 1$. The tunneling process then follows the familiar two-state dynamics involving only $|\phi_{\rm r}^+\rangle$ and $|\phi_{\rm r}^-\rangle$, with tunnel frequency $\Delta/\hbar$ (Fig. 6.9a).

Close to the avoided crossing, $\cos\beta$ and $\sin\beta$ are of the same order of magnitude, and $|\phi_1^-\rangle$, $|\phi_2^-\rangle$ become very similar to one another. Both now have support in the chaotic layer as well as in the symmetry-related regular regions and thus are of a hybrid nature. Here, the tunneling involves all the three states and must at least be described by a three-level system. The exchange of probability between the two regular regions proceeds via a "stop-over" in the chaotic region [15, 30–33]. The three quasienergy differences that determine the time scales of this process are in general all different, leading to complicated beats (Fig. 6.9b).

However, for $\Delta_{\rm c} = -2\Delta$, the two quasienergies $\epsilon_1^- - \epsilon_0^+$ and $\epsilon_0^+ - \epsilon_2^-$ are degenerate. At this point, which marks the center of the crossing, the number of different frequencies in the three-level dynamics reduces to two again. This restores the familiar coherent tunneling in the sense that there is again a simple periodic exchange of probability between the regular regions [31–33]. However, the rate is much larger if compared to the situation far off the crossing, and the chaotic region is now temporarily populated during each probability transfer, twice per tunneling cycle (Fig. 6.9c).

6.2.2 Dissipative chaos-assisted tunneling

The crucial effect of dissipation on a quantum system is the disruption of coherence: a coherent superposition evolves into an incoherent mixture. Thus, phenomena based on coherence, such as tunneling, are rendered transients that fade out on a finite time scale $t_{\rm decoh}$. In general, for driven tunneling in the weakly damped regime, this time scale gets shorter for higher temperatures, reflecting the growth of transition rates [53]. However, in the vicinity of an exact crossing of the ground-state quasienergies, the coherent suppression of tunneling [10, 12, 107] can be stabilized with higher temperatures [76–78] and increasing friction [57, 58] until levels outside the doublet start to play a role. We have studied dissipative chaos-assisted tunneling, using again the real singlet-doublet crossing introduced in Sec. 6.2.1 (see Fig. 6.5) as our working example. The time evolution has been computed numerically by iterating the dissipative quantum map (4.31) for the improved master equation in

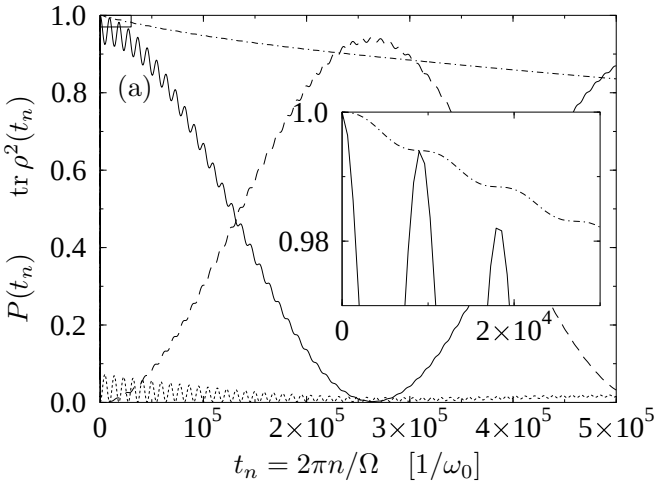

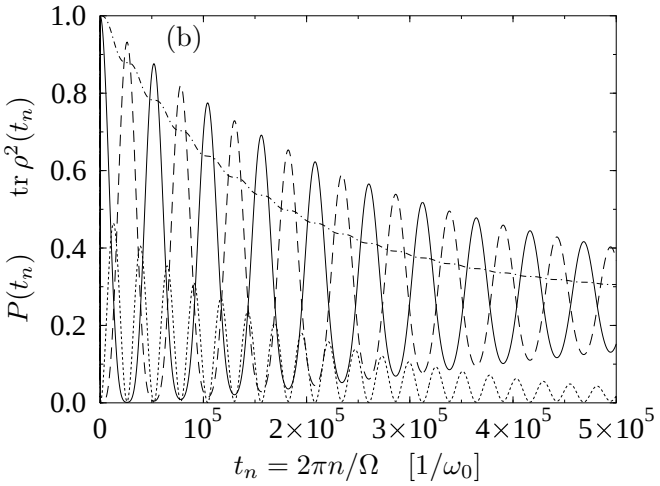

Figure 6.10: Occupation probabilities as in Fig. 6.9a,c, but in the presence of dissipation. The dash-dotted line shows the time evolution of $\mathrm{tr}\,\varrho^2$. The parameter values are $D = 4$, $\Omega = 0.982\,\omega_0$, $\gamma = 10^{-6}\omega_0$, $k_\mathrm{B}T = 10^{-4}\hbar\omega_0$, and $F = 0.0145$ (a), 0.015029 (b). The inset in (a) is a blow up of the rectangle in the upper left corner of that panel.

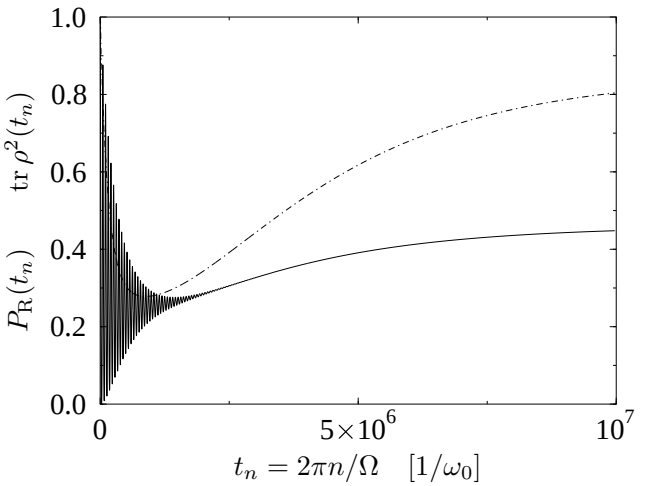

Figure 6.11: Time evolution of the return probability P_R (full line) and the coherence function $\mathrm{tr}\,\varrho^2$ (dash-dotted) during loss and regain of coherence. The parameter values are as in Fig. 6.10b.

moderate rotating-wave approximation, Eq. (4.22). As an initial condition, we have chosen the density operator $\varrho(0) = |\phi_\mathrm{R}\rangle\langle\phi_\mathrm{R}|$, i.e. a state localized in the right well.

In the vicinity of a singlet-doublet crossing, the tunnel splitting increases significantly—the essence of chaos-assisted tunneling. During the tunneling, the chaotic singlet becomes populated periodically with frequency $|\epsilon_2^- - \epsilon_1^-|/\hbar$, cf. Eq. (6.27) and Fig. 6.9. The high mean energy of this singlet results in an enhanced decay of coherence at times when $|\phi_\mathrm{c}\rangle$ is populated (Fig. 6.10). For the relaxation towards the asymptotic state, also the slower transitions within doublets are relevant. Therefore, the corresponding time scale t_relax can be much larger than t_decoh (Fig. 6.11).

To obtain quantitative estimates for the dissipative time scales, we approximate t_decoh by the decay rate of $\operatorname{tr}\varrho^2$, a measure of coherence (see Appendix B.2), averaged over a time t_p,

$$\frac{1}{t_\mathrm{decoh}} = -\frac{1}{t_\mathrm{p}}\int_0^{t_\mathrm{p}} \mathrm{d}t' \frac{\mathrm{d}}{\mathrm{d}t'} \operatorname{tr}\varrho^2(t') \tag{6.28}$$

$$= \frac{1}{t_\mathrm{p}}\Big(\operatorname{tr}\varrho^2(0) - \operatorname{tr}\varrho^2(t_\mathrm{p})\Big)\,. \tag{6.29}$$

Because of the stepwise decay of the coherence (Fig. 6.10), we have chosen the propagation time t_p as an $n$fold multiple of the duration $2\pi\hbar/|\epsilon_2^- - \epsilon_1^-|$ of the chaotic beats. For this procedure to be meaningful, n should be so large that the coherence decays substantially during the time t_p (in our numerical studies to a value of approximately 0.9). The time scale t_relax of the approach to the asymptotic state is given by the reciprocal of the smallest real part of the eigenvalues of the dissipative kernel.

Outside the singlet-doublet crossing we find that the decay of coherence and the relaxation take place on roughly the same time scale (Fig. 6.12). At $F \approx 0.013$, the chaotic singlet induces an exact crossing of the ground-state quasienergies (see Fig. 6.8), resulting in a stabilization of coherence with increasing temperature. At the center of the avoided crossing, the decay of coherence becomes much faster and is essentially independent of temperature. This indicates that transitions from states with mean energy far above the ground state play a crucial role.

6.2.3 Asymptotic state

As the dynamics described by the master equation (4.3) is dissipative, it converges in the long-time limit to an asymptotic state $\varrho_\infty(t)$. In general, this attractor remains time dependent but shares all the symmetries of the central system, i.e. here, periodicity and generalized parity. However, the coefficients of the master equation (4.22) for the matrix elements $\varrho_{\alpha\beta}$, valid within the moderate rotating-wave approximation, are time independent and so the asymptotic solution also is. This means that we have eliminated the explicit time dependence of the attractor by representing it in the Floquet basis and introducing a mild rotating-wave approximation.

To gain some qualitative insight into the asymptotic solution, we focus on the

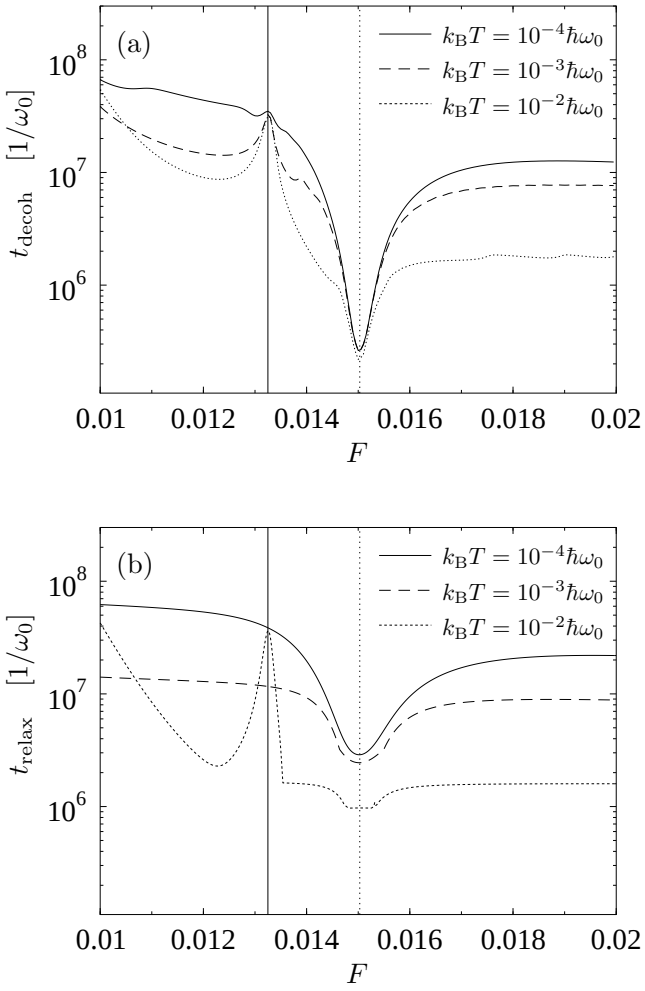

Figure 6.12: Time scales of the decay of the coherence measure $\mathrm{tr}\,\varrho^2$ (a) and of the relaxation towards the asymptotic solution (b) near the singlet-doublet crossing. Near the exact crossing ($F \approx 0.013$, full vertical line) coherence is stabilized, whereas at the center of the avoided crossing ($F \approx 0.015$, dashed vertical line) the decay of coherence is accelerated. The parameter values are $D = 4$, $\Omega = 0.982\,\omega_0$, $\gamma = 10^{-6}\omega_0$, temperature as given in the legend.

diagonal elements

$$\mathcal{L}_{\alpha\alpha,\alpha'\alpha'} = 2\sum_n N_{\alpha\alpha',n}|X_{\alpha\alpha',n}|^2, \quad \alpha \neq \alpha', \tag{6.30}$$

of the dissipative kernel. They give the rates of the direct transitions from $|\phi_{\alpha'}\rangle$ to $|\phi_\alpha\rangle$. Within the full rotating-wave approximation, given in Eqs. 4.28 and 4.29, these are the only non-vanishing contributions to the master equation which affect the diagonal elements $\varrho_{\alpha\alpha}$ of the density matrix.

In the case of zero driving amplitude, the Floquet states $|\phi_\alpha\rangle$ reduce to the eigenstates of the undriven Hamiltonian $H_{\rm DW}$. The only non-vanishing Fourier component is then $|c_{\alpha,0}\rangle$, and the quasienergies ϵ_α reduce to the corresponding eigenenergies E_α. Thus $\mathcal{L}_{\alpha\alpha,\alpha'\alpha'}$ only consists of a single term proportional to $N(\epsilon_\alpha - \epsilon_{\alpha'})$. It describes two kinds of thermal transitions: decay to states with lower energy and, if the energy difference is less than k_BT, thermal activation to states with higher energy. The ratio of the direct transitions forth and back then reads

$$\frac{\mathcal{L}_{\alpha\alpha,\alpha'\alpha'}}{\mathcal{L}_{\alpha'\alpha',\alpha\alpha}} = \exp\left(-\frac{(\epsilon_\alpha - \epsilon_{\alpha'})}{k_BT}\right). \tag{6.31}$$

We have detailed balance and therefore the steady-state solution

$$\varrho_{\alpha\alpha'}(\infty) \sim \mathrm{e}^{-\epsilon_\alpha/k_\mathrm{B}T}\,\delta_{\alpha\alpha'}. \tag{6.32}$$

In particular, the occupation probability decays monotonically with the energy of the eigenstates. In the limit $k_\mathrm{B}T \to 0$, the system tends to occupy the ground state only.

For a strong driving, each Floquet state $|\phi_\alpha\rangle$ contains a large number of Fourier components and $\mathcal{L}_{\alpha\alpha,\alpha'\alpha'}$ is given by a sum over contributions with quasienergies $\epsilon_\alpha - \epsilon_{\alpha'} + n\hbar\Omega$. Thus a decay to states with "higher" quasienergy (recall that quasienergies do not allow for a global ordering) becomes possible due to terms with $n < 0$. Physically, they describe dissipative transitions under absorption of driving-field quanta. Correspondingly, the system tends to occupy Floquet states comprising many Fourier components with low index n. According to Eq. (2.42), these states have low mean energy.

The effects under study are found for a driving with a frequency of the order of unity. Thus for a quasienergy doublet, i.e., far off the three-level crossing, we have $|\epsilon_\alpha - \epsilon_{\alpha'}| \ll \hbar\Omega$, and $\mathcal{L}_{\alpha'\alpha',\alpha\alpha}$ is dominated by contributions with $n < 0$, where the splitting has no significant influence. However, as a consequence of symmetry, the splitting is the main difference between the two partners of the quasienergy doublet. Therefore, with respect to dissipation, both should behave similarly. In particular, one expects an equal population of the doublets even in the limit of zero temperature (Fig. 6.13a). This is in contrast to the undriven case.

In the vicinity of a singlet-doublet crossing the situation is more subtle. Here, the odd partner, say, of the doublet mixes with a chaotic singlet, cf. Eq. (6.22), and thus acquires components with higher energy. Due to the high mean energy E_c^- of the chaotic singlet, close to the top of the barrier, the decay back to the ground state can also proceed indirectly via other states with mean energy below E_c^-. Thus $|\phi_1^-\rangle$ and $|\phi_2^-\rangle$ are depleted and mainly $|\phi_0^+\rangle$ will be populated. However, if the temperature is significantly above the splitting $2b$ of the avoided crossing, thermal activation from $|\phi_0^+\rangle$ to $|\phi_{1,2}^-\rangle$, accompanied by depletion via the states below E_c^-, becomes possible. Thus asymptotically, all these states become populated in a steady flow (Fig. 6.13b,c). The long-time limit of the corresponding classical dynamics converges to one of two limit cycles, each of which is located close to one of the potential minima. In a stroboscopic map they correspond to two isolated fixed points. This behavior is qualitatively different from the asymptotic limit of the dissipative quantum dynamics near the center of the crossing and shows that the occupation of the levels outside the singlet and the doublet at asymptotic times is a pure quantum effect.

An important global characteristic of the asymptotic state is its Shannon entropy $S = -\operatorname{tr}(\varrho_\infty \ln \varrho_\infty)$ or, alternatively, its coherence $\operatorname{tr}\varrho_\infty^2$ (see Appendix B.2). The value of the latter gives approximately the reciprocal of the number of incoherently occupied states. It equals unity only if the attractor is a pure state. According to the above scenario, we expect $\operatorname{tr}\varrho_\infty^2$ to assume the value $1/2$, in a regime with strong driving but preserved doublet structure, reflecting the incoherent population

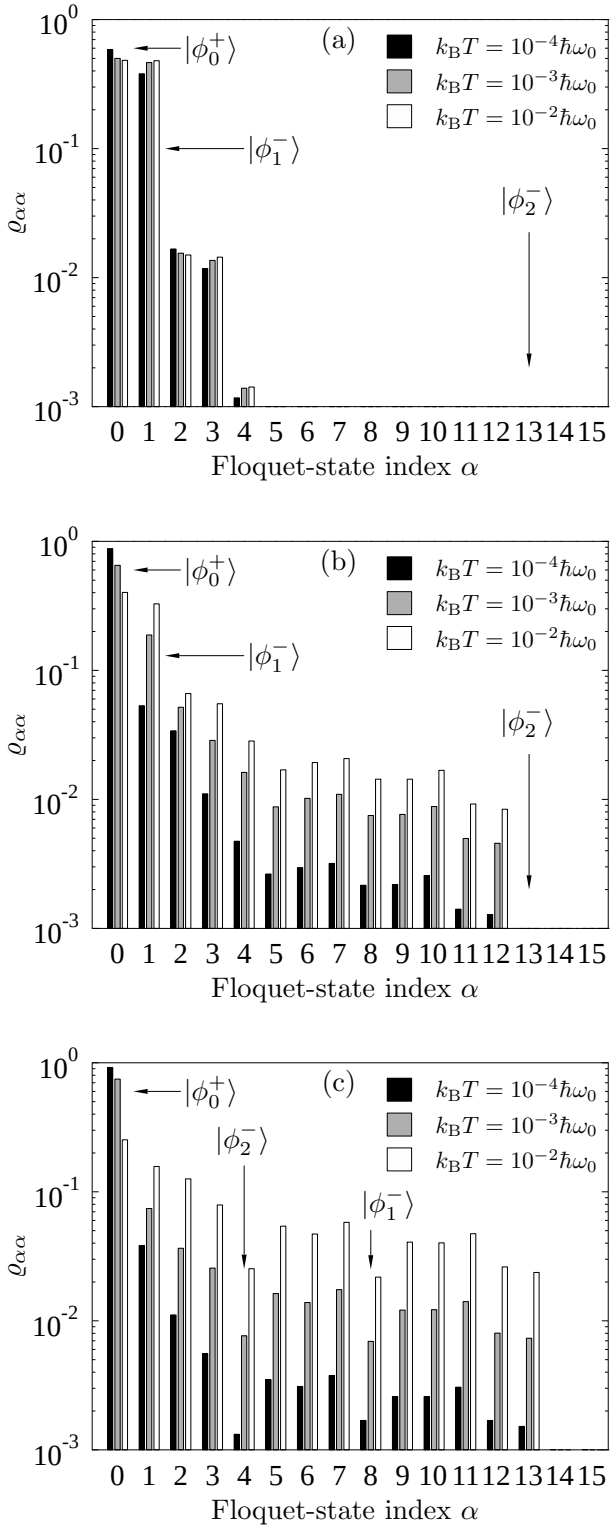

Figure 6.13: Occupation probability $\varrho_{\alpha\alpha}$ of the Floquet states $|\phi_\alpha\rangle$ in the long-time limit. The parameter values are $D = 4$, $\Omega = 0.982\,\omega_0$, $\gamma = 10^{-6}\omega_0$, and $F = 0.013$ (a), 0.0145 (b), 0.015029 (c), temperature as given in the legend.

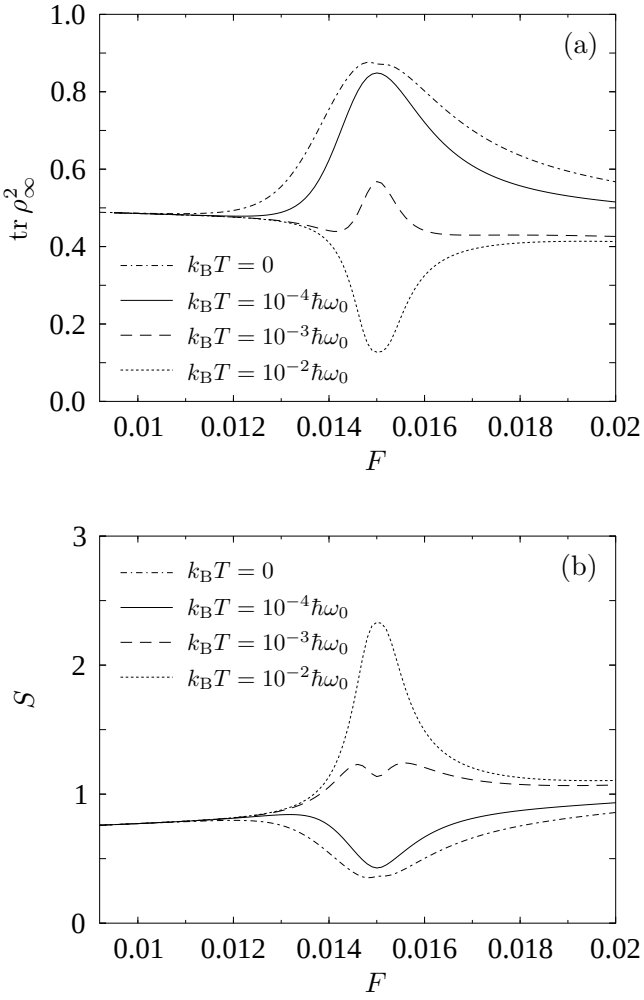

Figure 6.14: Coherence (a) and Shannon entropy (b) of the asymptotic state in the vicinity of a singlet-doublet crossing for different temperatures as given in the legend. The other parameter values are $D = 4$, $\Omega = 0.982\,\omega_0$, and $\gamma = 10^{-6}\omega_0$.

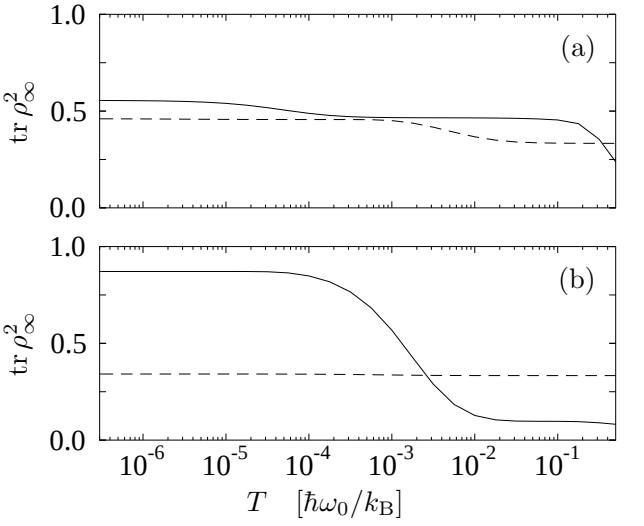

Figure 6.15: Coherence of the asymptotic state in the vicinity of a singlet-doublet crossing for $F = 0.013$ (a) and $F = 0.015029$ (b): exact calculation (full line) compared to the values resulting from a three-level description (dashed) of the dissipative dynamics. The other parameter values are $D = 4$, $\Omega = 0.982\,\omega_0$, and $\gamma = 10^{-6}\omega_0$.

of the ground-state doublet. In the vicinity of the singlet-doublet crossing where the doublet structure is dissolved, its value should be close to unity for temperatures $k_{\mathrm{B}}T \ll 2b$ and much less than unity for $k_{\mathrm{B}}T \gg 2b$ (Figs. 6.14a, 6.15). This means that the crossing of the chaotic singlet with the regular doublet leads to an improvement of coherence if the temperature is below the splitting of the avoided crossing, and a loss of coherence for temperatures above the splitting. This phenomenon amounts to a chaos-induced coherence or incoherence, respectively. The corresponding Shannon entropy (Fig. 6.14b), assumes approximately the value $\ln n$ for n incoherently populated states. Thus outside the crossing, we have $S \approx \ln 2$ and at the center of the crossing the entropy exhibits a significant temperature dependence.

The crucial role of the decay via states not involved in the three-level crossing can be demonstrated by comparing it with the dissipative dynamics including only these three levels (plus the bath). At the crossing, the three-state model results in a completely different type of asymptotic state (Fig. 6.15). The failure of the three-state model in the presence of dissipation clearly indicates that in the vicinity of the singlet-doublet crossing, it is important to take a large set of levels into account.

6.3 Signatures of chaos in the asymptotic state

In recent work it has been demonstrated that a phase-space representation of quantum mechanics, like the Husimi or Wigner distribution, reveals the structures of the corresponding classical phase space [5,30,117–120]. In particular, for the case of regular classical dynamics, the Husimi function of an eigenstate (or of a Floquet state if the system is driven) is localized in phase space along the corresponding quantizing torus; for chaotic motion, it has support in the whole chaotic layer. If the classical dynamics is mixed, one is even able to classify quantum-mechanical states as regular or chaotic according to their localization in phase space [120]. Moreover, the phase-space representation of the asymptotic state of a dissipative quantum map exhibits the structures of the corresponding classical attractor [106]. However, the analogies have their limitations due to the Heisenberg uncertainty principle which does not allow for arbitraryly fine phase-space structures for a quantum system and results in coarse-graining over a "phase-space unit" $2\pi\hbar$.

The asymptotic classical dynamics of the driven dissipative double-well potential is for sufficiently strong driving particularly sensitive to the friction strength: With decreasing friction, the motion changes from regular to chaotic.

6.3.1 Classical attractor

To describe the classical dissipative dynamics of the driven double well, we add an Ohmic friction force $F_\gamma = -\gamma p$ to the conservative equations (6.4), (6.5) and obtain

$$\dot{x} = \frac{1}{m}p, \tag{6.33}$$

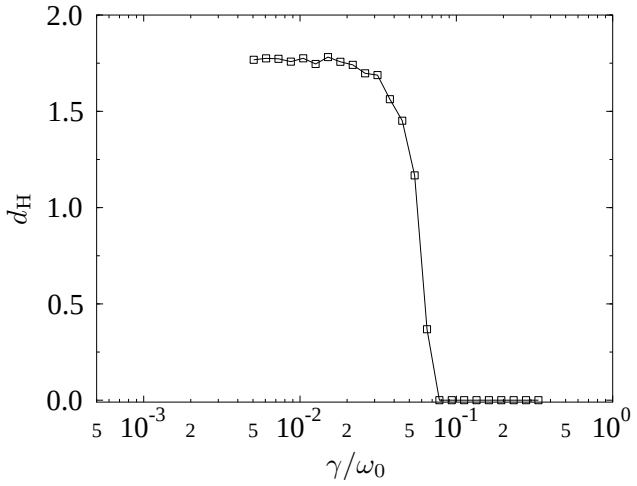

Figure 6.16: Hausdorff dimension of the classical attractor for $F = 0.09$, $\Omega = 0.9\,\omega_0$.

$$\dot{p} = -\gamma p - \frac{\partial V(x,t)}{\partial x}. \tag{6.34}$$

As friction always decelerates a particle, it distinguishes between future and past, thus destroys the time-reversal symmetry (6.10) of the conservative system. Accordingly, dissipation breaks the reflection symmetry at the x-axis of phase-space portraits which we found for the chosen initial phase of the driving (cf. Fig. 6.6).

The lack of time-reversal symmetry in presence of friction is even more evident from the time evolution of a volume element V of phase space. It evolves by having each point on its surface ∂V follow an orbit generated by (6.33), (6.34), which yields by the divergence theorem [3]

$$\frac{\mathrm{d}V}{\mathrm{d}t} = \int_V \mathrm{d}x\,\mathrm{d}p \left(\frac{\partial \dot{x}}{\partial x} + \frac{\partial \dot{p}}{\partial p}\right) = -\gamma V. \tag{6.35}$$

Thus, we obtain an exponential contraction of a phase-space volume V—a constituent feature of dissipative flows. Therefore, the dynamics is asymptotically confined to an attractor, a formation in phase space with zero volume to which all sufficiently close trajectories from the so-called basin of attraction converge for long times. For periodically driven dissipative systems, the attractor is in general also time-dependent with the period of the driving and is properly rendered by its stroboscopic map [121–123].

Depending on the values of the driving parameters and the friction strength, an attractor consists of limit cycles or isolated fixed points. For sufficiently weak dissipation, however, it may even happen that the dissipative dynamics is chaotic and the attractor possess fractal geometry, forming a so-called strange attractor. The type of geometry can be characterized as fractal or regular according to its Hausdorff dimension d_H which is defined by the scaling assumption

$$N \sim l^{-d_\mathrm{H}}, \quad l \to 0. \tag{6.36}$$

Here, N is the number of squares with width l needed to cover the whole attractor.

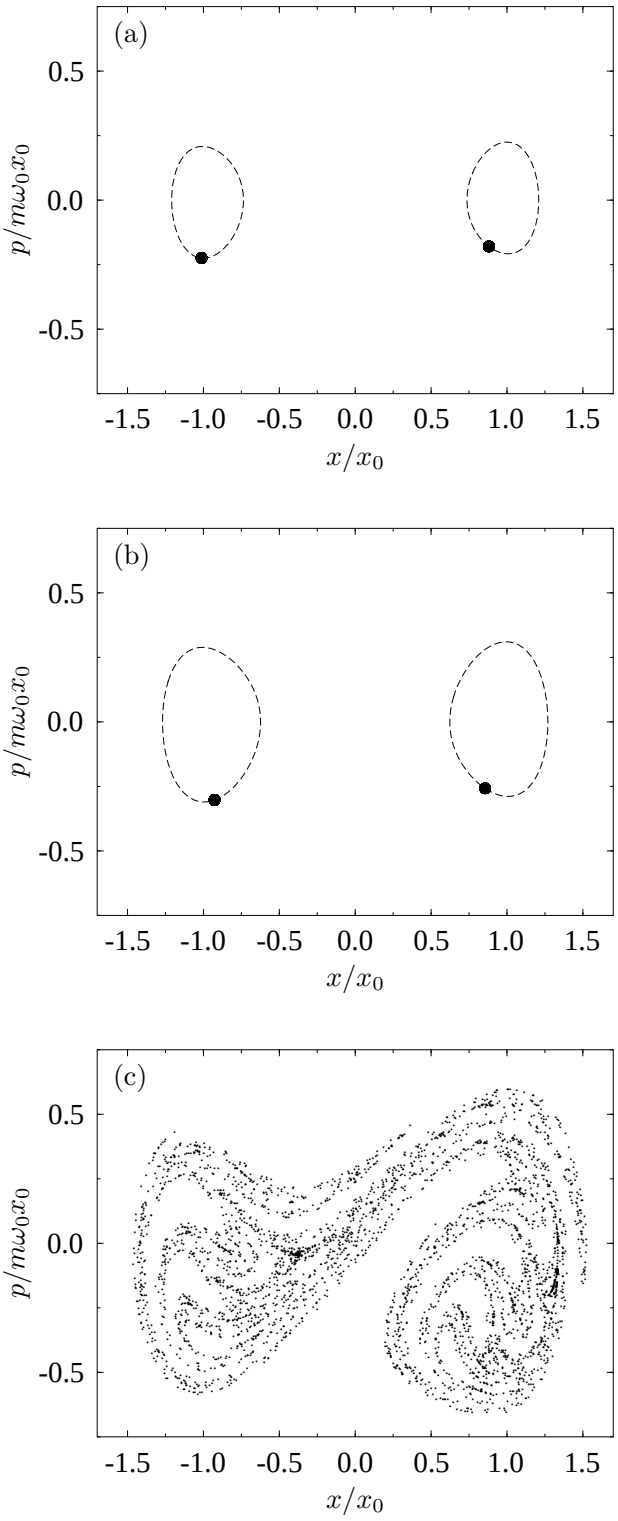

Figure 6.17: Stroboscopic classical phase-space portrait at $t = 2\pi n/\Omega$, of the dissipative harmonically driven quartic double well, Eqs. (6.33), (6.34), for the driving amplitude $F = 0.09$ and frequency $\Omega = 0.9\,\omega_0$. The friction strength is $\gamma = 0.3\,\omega_0$ (a), $0.2\,\omega_0$ (b), $0.03\,\omega_0$ (c). In panels (a) and (b) the stroboscopic portrait is marked by a full dot and the broken lines show the corresponding limit cycles.

It is computed numerically by box counting. Consequently, continuous formations correspond to integer values of d_H. For $d_\mathrm{H} < 2$ the attractor has zero volume.

The Hausdorff dimension of the classical attractor for the parameter values $F = 0.09$ and $\Omega = 0.9\,\omega_0$ for different friction strength γ is depicted in Fig. 6.16. Although the attractor of the driven dissipative double well is periodically time-dependent with the period of the driving, its Hausdorff dimension d_H has no significant time-dependence [121]. Near $\gamma \approx 0.06\,\omega_0$, the classical dynamics undergoes with decreasing γ a transition from regular motion (Fig. 6.17a, 6.17b) to chaos, manifest by a strange attractor (Fig. 6.17c). For this driving amplitude and frequency, the regular islands near the bottom of the wells (cf. Fig. 6.6) are in absence of dissipation already completely resolved in the chaotic sea.

6.3.2 Quantum attractor

In the quantum case, the self-similar fine structures of a strange attractor are in contradiction to the position-momentum uncertainty relation, thus they are smeared out in the Husimi representation of the asymptotic state (Figs. 6.18, 6.19). These "quantum attractors" clearly reflect the structures of the corresponding classical asymptotic state as well as their qualitative change from isolated fixed points to a strange attractor. This transition is, however, in the quantum case not as sharp as in the classical case: Although the asymptotic state for $\gamma = 0.2\,\omega_0$ (Figs. 6.18b, 6.19b) is still mainly located near the fixed points of the classical stroboscopic map, it covers a broader phase-space area that already indicates the shape of the strange attractor. The underlying classical structures in the Husimi functions become more distinct for smaller values of the effective quantum of action $\hbar_\mathrm{eff} = 1/8D$, as expected. Like the phase-space portrait of the dissipative classical dynamics (Fig. 6.17), its quantum-mechanical counterparts obey no reflection symmetry at the x-axis. This feature is in contrast to the Husimi representation of the Floquet states in absence of dissipation (cf. Fig. 6.7) and is caused by finite off-diagonal elements of the asymptotic density matrix in Floquet representation, since diagonal representations share the symmetries of the basis. Thus, off-diagonal matrix elements play a significant role for the asymptotic state. This demonstrates that a description within a full rotating-wave approximation is insufficient, since it would result in a diagonal asymptotic state (see Section 4.3.2).

Because the self-similar structures at an arbitrary small length scale of the classical attractor are washed out in the quantum case, we cannot characterize the quantum attractor by a Hausdorff dimension. A more suitable measure for the qualitative shape of the quantum attractor is the Wehrl entropy S^Q of its Husimi representation [120, 124] (see Appendix A.3.2). Its exponential, $\exp(S^Q)$, gives approximately the number of minimum uncertainty states covered by the Husimi function. Thus, the occupied phase-space area is $2\pi\hbar\exp(S^Q)$. The Wehrl entropy of the asymptotic state for our numerical example for different values of the effective quantum of action is depicted in Fig. 6.20. It becomes larger with decreasing friction γ, reflecting the increasing dispersion of the Husimi functions. In the semiclassical regime, i.e., for

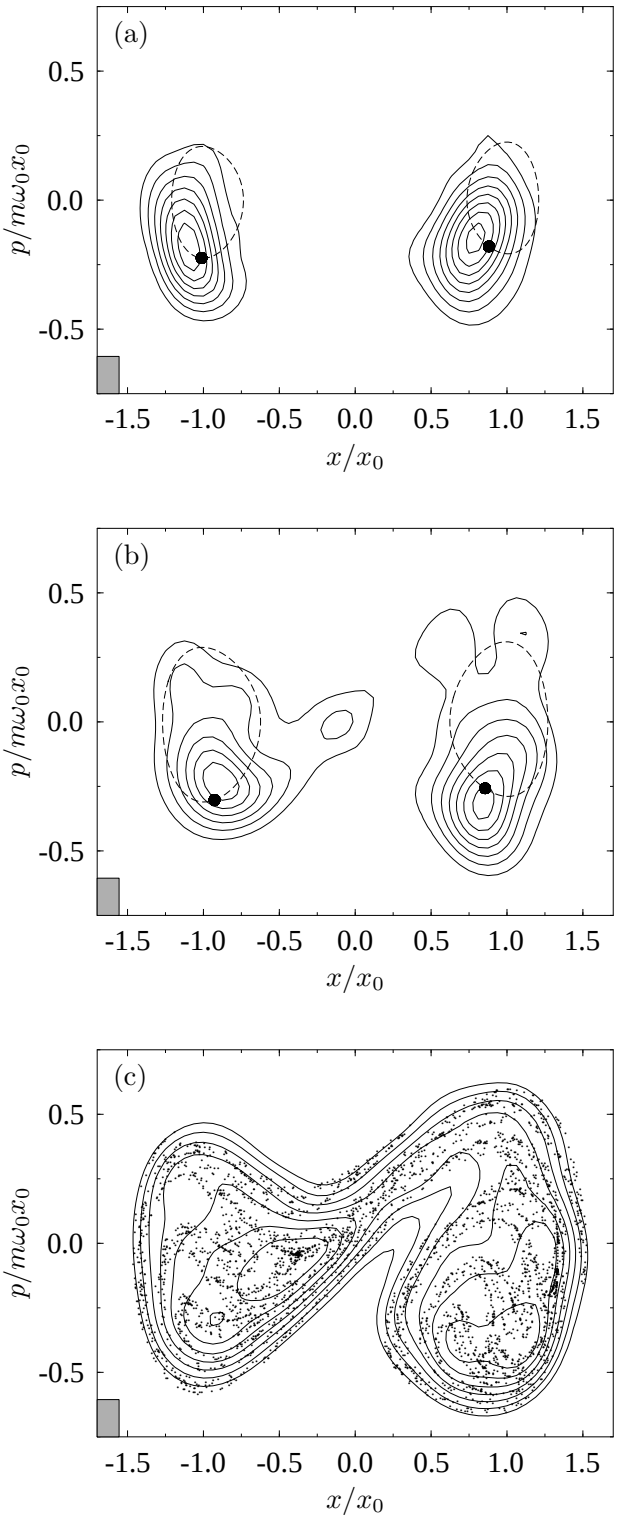

Figure 6.18: Contour plot of the Husimi function of the quantum attractor (full lines) at $t = 2\pi n/\Omega$, $n \to \infty$, superposed on the corresponding classical phase-space portrait, Fig. 6.17. The parameter values $F = 0.09$, $\Omega = 0.9\,\omega_0$, $\gamma = 0.3\,\omega_0$ (a), $0.2\,\omega_0$ (b), $0.03\,\omega_0$ (c) are as in Fig. 6.17. The effective action is $D = 6$. The rectangle in the lower left corner depicts the size of the effective quantum of action $\hbar_{\rm eff} = 1/8D$.

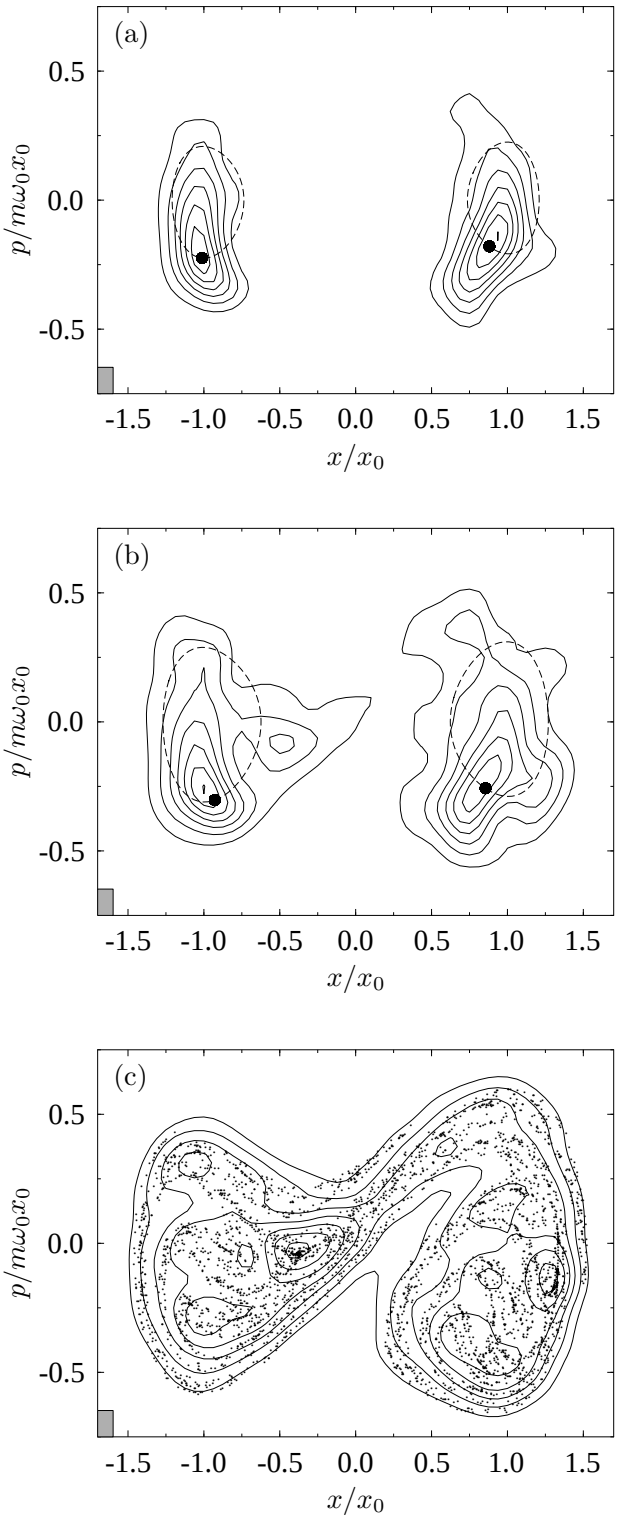

Figure 6.19: Same as Fig. 6.18 for the effective action $D = 12$.

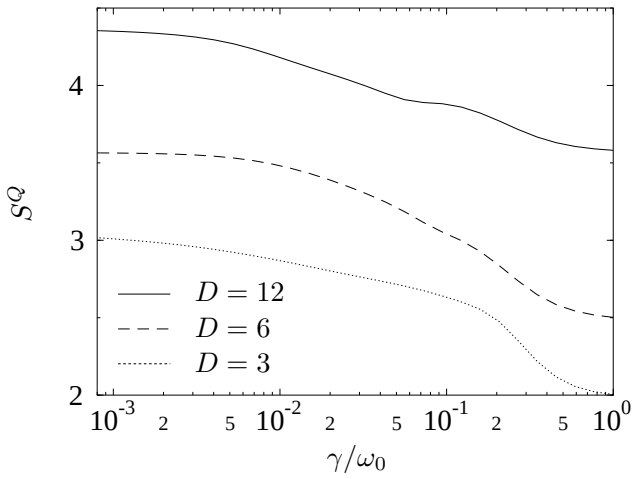

Figure 6.20: Wehrl entropy of the asymptotic state of the dissipative quantum map for different values of the effective quantum of action $\hbar_{\text{eff}} = 1/8D$. Other parameters like in Fig. 6.16.

a sufficiently large value of the effective action D, we observe a kink of the entropy near $\gamma \approx 0.06\,\omega_0$, where the classical attractor undergoes a transition from a set of isolated fixed points to a strange attractor.

Note that for $\gamma \gtrsim 0.1\,\omega_0$, the Markov approximation becomes inaccurate, since γ is of the order of the mean level spacing and the condition (3.33) is violated for at least some of the transitions between Floquet states. Nevertheless, we obtain the qualitative behavior which we expected from classical considerations.

7 Summary and outlook

In this thesis, we put focus on a special class of system: a particle which moves in a one-dimensional potential under the influence of a heat bath and of an external field which is periodic in time. A Markovian approach to quantum dissipation, based on the Floquet solutions of the coherent dynamics, has proven well-adapted to the description of such systems. We have derived this Floquet-Markov approach from an exact path-integral expression and have applied it to the parametrically driven harmonic oscillator and the driven double-well potential.

The study of the parametrically driven harmonic oscillator has been devoted mainly to a thorough understanding of the different approximation schemes. It turned out that the dissipative part of the Markovian master equation depends quantitatively on whether the driving is included in its derivation or not: Considering the driving mainly results in a modified momentum diffusion that depends on the quasienergy spectrum instead of the unperturbed spectrum of the central system without the driving. The difference becomes significant in the limits of strong driving and low temperature. An additional additive time-dependent force undergoes a renormalization which, however, vanishes for strictly Ohmic damping. Concluding from numerical results for the case of a Mathieu oscillator, the attributes "simple" and "improved" for the two basic Markovian approaches prove adequate. To solve the master equation, we have transformed it to Wigner representation, thus obtained a partial differential equation for the Wigner function that corresponds to the density operator, and derived an analytical expression for the Floquet solutions of the resulting Fokker-Planck-like equation. In doing so, we have incidentally obtained the Floquet solutions of the Fokker-Planck equation for the corresponding classical Brownian motion.

A quantum system with more complex dynamics is the quartic double-well potential under the influence of a driving with frequency near resonance. Here, classical chaos plays a significant role for the coherent dynamics. Even for arbitrarily small driving amplitude, the separatrix is replaced by a chaotic layer, but the motion near the bottom of the wells remains regular. Nevertheless, the influence of states located in the chaotic region alters the splittings of the regular doublets and thus the tunnel rates, which is the essence of chaotic tunneling. We have studied chaotic tunneling in the vicinity of crossings of chaotic singlets with tunnel doublets under the influence of an environment. As a simple intuitive model to compare against, we have constructed a three-state system which in the case of vanishing dissipation, provides a faithful description of an isolated singlet-doublet crossing. Dissipation introduces new time scales to the system: one for the loss of coherence and a second one for the relaxation to an asymptotic state. Well outside the crossing, both time-scales are of the same order, reflecting an effective two-state behavior. The center of the

crossing is characterized by a strong mixing of the chaotic state with one state of the tunnel doublet. The high mean energy of the chaotic state introduces additional decay channels to states outside the three-state system. Thus, decoherence becomes far more effective and, accordingly, tunneling fades out much faster.

The study of the asymptotic state, the quantum attractor, demonstrates clearly that a three-state model of the singlet-doublet crossing is insufficient once dissipation is effective. This is so because the coupling to the heat bath enables processes of decay and thermal activation that connect the states in the crossing with other, "external" states of the central system. In the presence of driving, the asymptotic state is no longer literally a state of equilibrium. Rather, incoherent processes create a steady flow of probability involving states within as well as outside the crossing. As a result, the composition of the asymptotic state, expressed for example by its coherence $\mathrm{tr}\,\varrho_\infty^2$, are markedly different at the center of the crossing as compared to the asymptotic state far away from the crossing, even if that is barely visible in the corresponding classical phase-space structure.

With increasing driving amplitude, the dynamics near the bottom of the wells, in absence of dissipation, becomes fully chaotic. This has striking consequences for the dissipative classical dynamics: For sufficiently small dissipation, it remains chaotic, but for strong friction it becomes regular. Accordingly, the geometry of the classical attractor is fractal or regular, respectively. We have observed the signatures of this qualitative difference in the asymptotic state of the corresponding quantum dynamics. However, in contrast to the sudden change of the classical behavior, the quantum attractor undergoes a smooth transition: The structure of the strange attractor is already felt by the Husimi function for parameter values where the classical attractor consists only of two isolated fixed points. For the observation of these semiclassical structures, off-diagonal matrix elements of the asymptotic state in Floquet basis proved crucial. This clearly reflects the failure a full rotating-wave approximation.

Many more phenomena at the overlap of chaos, tunneling, and dissipation await being unraveled. They include four-state crossings formed when two doublets intersect, chaotic Bloch tunneling along extended potentials with a large number of unit cells instead of just two, and the influence of decoherence on a multi-step mechanism of chaotic tunneling. These phenomena are typically observed in the far semiclassical regime, which requires to take very many levels into account. A semiclassical description of the dissipative quantum system may circumvent this problem.

A The harmonic oscillator

In many fields of physics, the harmonic oscillator plays an important role as an exactly solvable model as well as an approximation to a smooth potential minimum. In this work, we use its eigenfunctions as a basis set for numerical computations. Moreover, the ground state of a harmonic oscillator, displaced in phase space (coherent state), forms the initial state for the propagation of the density matrix in Chapter 6. In this appendix, we give a synopsis of basic properties of the harmonic oscillator, described by the Hamiltonian

$$H_{\mathrm{HO}} = \frac{1}{2m}p^2 + \frac{m\omega_{\mathrm{HO}}^2}{2}x^2 \tag{A.1}$$

$$= \hbar\omega_{\mathrm{HO}}\left(a^+a + \frac{1}{2}\right), \tag{A.2}$$

and of the closely related coherent states and quasiprobabilities.

The form (A.2) of the Hamiltonian is achieved by the transformation

$$a = \sqrt{\frac{m\omega_{\mathrm{HO}}}{2\hbar}}\,x + \mathrm{i}\sqrt{\frac{1}{2m\hbar\omega_{\mathrm{HO}}}}\,p, \tag{A.3}$$

$$a^+ = \sqrt{\frac{m\omega_{\mathrm{HO}}}{2\hbar}}\,x - \mathrm{i}\sqrt{\frac{1}{2m\hbar\omega_{\mathrm{HO}}}}\,p, \tag{A.4}$$

$$x = \sqrt{\frac{\hbar}{2m\omega_{\mathrm{HO}}}}(a^+ + a), \tag{A.5}$$

$$p = \mathrm{i}\sqrt{\frac{m\hbar\omega_{\mathrm{HO}}}{2}}(a^+ - a). \tag{A.6}$$

From $[x, p] = \mathrm{i}\hbar$ results the bosonic commutation relation

$$[a, a^+] = 1, \tag{A.7}$$

which yields for the energy eigenstates $|n\rangle$ the relations [125]

$$a|n\rangle = \sqrt{n}\,|n-1\rangle, \tag{A.8}$$

$$a^+|n\rangle = \sqrt{n+1}\,|n+1\rangle. \tag{A.9}$$

These justify the denotation creation and destruction operator (of a quantum) or shift operators (between eigenstates) for a^+ and a. By recursion of (A.9), the so-called number states

$$|n\rangle = \frac{(a^+)^n}{\sqrt{n!}}|0\rangle \tag{A.10}$$

are constructed from the ground state $|0\rangle$, which is defined by $a|0\rangle = 0$.

The state $|n\rangle$ in a semiclassical interpretation [126,127] is a quantized torus with action $\hbar(n + 1/2)$. Therefore, it is restricted to phase-space areas which obey

$$\frac{p^2}{2m} + \frac{1}{2}m\omega_{\mathrm{HO}}^2 x^2 \lesssim n\hbar\omega_{\mathrm{HO}}, \tag{A.11}$$

thus

$$|p| \lesssim p_n = \sqrt{2n\hbar\omega_{\mathrm{HO}} m}\,, \tag{A.12}$$

$$|x| \lesssim x_n = \sqrt{\frac{2n\hbar}{m\omega_{\mathrm{HO}}}}\,. \tag{A.13}$$

A.1 Number states as a basis set

For numerical computations, wave functions and operators are decomposed into a complete set of basis functions. Dealing with polynomial potentials, the eigenfunctions of the harmonic oscillator form a well-suited basis set, as matrix elements of powers of the position operator for these states obey a simple analytical expression resulting from (A.5)–(A.9).

In numerical calculations, one uses N number states (A.10) as a (incomplete) basis set, thus formally approximates infinite matrices by finite ones. Thus, we effectively diagonalize—instead of the Hamiltonian H—the truncated Hamiltonian $\mathcal{P}_N H \mathcal{P}_N$, where $\mathcal{P}_N$ projects on the subspace spanned by the first N basis functions $\{|n\rangle\}_{n=0\ldots N}$. This subspace, according to (A.12), (A.13), corresponds to a finite region of phase space. Consequently, a state with energy E can be approximated reasonably by a linear combination of the first N number states only if its corresponding classical torus is contained in this region of phase space. This results in the conditions

$$E < \frac{p_N^2}{2m} = N\hbar\omega_{\mathrm{HO}}, \tag{A.14}$$

$$E < V(x_N) = -\frac{N\hbar\omega_0^2}{2\omega_{\mathrm{HO}}} + \frac{N^2\hbar^2\omega_0^4}{16E_{\mathrm{B}}\omega_{\mathrm{HO}}^2}. \tag{A.15}$$

To visualize the influence of a finite basis set, we have depicted some eigenvalues of the truncated Hamiltonian $\mathcal{P}_N H_{\mathrm{DW}} \mathcal{P}_N$ for $N = 100$ over the scaling parameter $\omega_{\mathrm{HO}}/\omega_0$ of the basis functions in Fig. A.1. Outside the limits (A.14) and (A.15), the energies depend on the scaling parameter, thus their value is a numerical artefact caused by using a finite basis set. The numerical computations in Chapter 6 were performed using number states with an oscillator frequency

$$\omega_{\mathrm{HO}} = \omega_0 \left(\frac{N\hbar\omega_0}{16E_{\mathrm{B}}}\right)^{1/3}, \tag{A.16}$$

and N was chosen according to the required numerical precision.

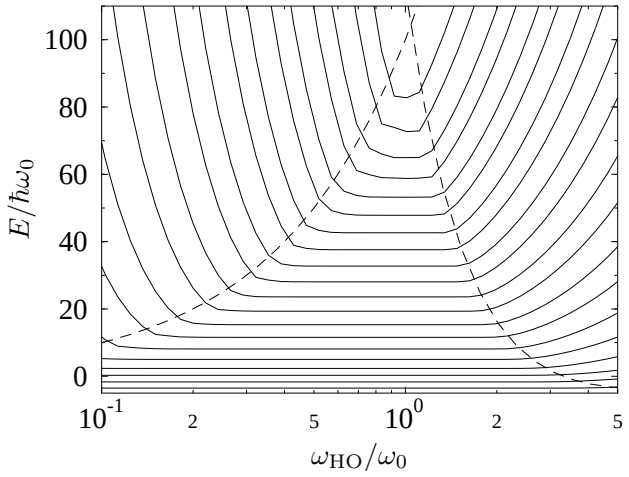

Figure A.1: Some eigenvalues of the truncated Hamiltonian $\mathcal{P}_N H_{\mathrm{DW}} \mathcal{P}_N$ for $N = 100$ and $D = 4$ (full lines). The broken lines give the limits of convergence according to (A.14) and (A.15).

A.2 Coherent states

Due to the Heisenberg uncertainty principle

$$\Delta x \, \Delta p \geq \frac{\hbar}{2} \tag{A.17}$$

a quantum-mechanical state cannot be localized in phase space with arbitrary precision, as would be possible in classical mechanics. The coherent states (or Glauber states) [128, 129]

$$|z\rangle = \mathrm{e}^{za^+ - z^* a}|0\rangle, \quad z \in \mathbb{C} \tag{A.18}$$

obey

$$\langle z|x|z\rangle = \sqrt{\frac{2\hbar}{m\omega_{\mathrm{HO}}}}\,\mathrm{Re}\, z, \qquad \langle z|\Delta x^2|z\rangle = \frac{\hbar}{2m\omega_{\mathrm{HO}}}, \tag{A.19}$$

$$\langle z|p|z\rangle = \sqrt{2m\hbar\omega_{\mathrm{HO}}}\,\mathrm{Im}\, z, \qquad \langle z|\Delta p^2|z\rangle = \frac{m\hbar\omega_{\mathrm{HO}}}{2}. \tag{A.20}$$

Thus according to (A.17), they have minimal uncertainty and approximate a point in phase space at best.

A.3 Quasiprobabilities

The unique representation of a density operator ϱ as a phase-space function is closely related to the question on quasi-classical states. The most prominent example from a variety of possibilities [130–134] is the s-parameterized quasiprobability or Cahill-Glauber distribution [135]

$$W_s(x,p) = \frac{1}{2\pi^2\hbar} \int \mathrm{d}\xi' \mathrm{d}\xi'' \, \mathrm{e}^{z\xi^* - z^*\xi} \chi_s(\xi), \tag{A.21}$$

$$\chi_s(\xi) = \mathrm{tr}\left\{\mathrm{e}^{\xi a^+ - \xi^* a + s\xi^*\xi/2}\varrho\right\}, \quad s \in [-1,1], \tag{A.22}$$

$$z = x\sqrt{\frac{m\omega_{\mathrm{HO}}}{2\hbar}} + \mathrm{i}p\sqrt{\frac{1}{2m\hbar\omega_{\mathrm{HO}}}}. \tag{A.23}$$

It includes the Wigner and the Husimi function as limiting cases. The integration in (A.21) runs over real and imaginary part of ξ. In general, W_s may also assume negative values and for positive s may even be singular—thus a strict probabilistic interpretation is not possible. Quasi-probabilities are used for the calculation of expectation values alike classical phase-space distributions. Thereby the operator ordering is fixed by the parameter s as the s-ordered product

$$\left\{(a^+)^n a^m\right\}_s = \left(\frac{\partial}{\partial z}\right)^n \left(-\frac{\partial}{\partial z^*}\right)^m \exp\left(za^+ - z^*a + \frac{s}{2}z^*z\right)\Big|_{z^*=z=0}, \tag{A.24}$$

which gives an interpolation between normal ordering $(a^+)^n a^m = \{(a^+)^n a^m\}_1$ and anti-normal ordering $a^m(a^+)^n = \{(a^+)^n a^m\}_{-1}$ of creation and annihilation operators [136].

For each operator acting on the density matrix ϱ, there exists a corresponding differential operator acting on $W_s(x,p)$ [137]. From Eq. (A.21) with Eq. (A.22) we obtain the relations

$$x\varrho \longleftrightarrow \left(x + \frac{\mathrm{i}\hbar}{2}\partial_p - \frac{s\hbar}{2m\omega_{\mathrm{HO}}}\partial_x\right) W_s(x,p), \tag{A.25}$$

$$p\varrho \longleftrightarrow \left(p - \frac{\mathrm{i}\hbar}{2}\partial_x - \frac{sm\hbar\omega_{\mathrm{HO}}}{2}\partial_p\right) W_s(x,p), \tag{A.26}$$

$$\varrho x \longleftrightarrow \left(x - \frac{\mathrm{i}\hbar}{2}\partial_p - \frac{s\hbar}{2m\omega_{\mathrm{HO}}}\partial_x\right) W_s(x,p), \tag{A.27}$$

$$\varrho p \longleftrightarrow \left(p + \frac{\mathrm{i}\hbar}{2}\partial_x - \frac{sm\hbar\omega_{\mathrm{HO}}}{2}\partial_p\right) W_s(x,p). \tag{A.28}$$

For powers of x and p they hold iteratively. It is obvious from these operator correspondences that, except for the case $s = 0$, the s-parameterized quasiprobability depends on the choice of the oscillator frequency ω_{HO}.

A.3.1 Wigner function

For $s = 0$, W_s results in the Wigner function [130, 133]

$$W(x,p) = \frac{1}{2\pi\hbar}\int \mathrm{d}x' \mathrm{e}^{\mathrm{i}px'/\hbar}\langle x + x'/2|\varrho|x - x'/2\rangle = W_0(x,p). \tag{A.29}$$

It is independent of the oscillator frequency ω_{HO}, thus basis independent. In numerical computations of Wigner functions or their reconstruction from experimental data, a negative s with small absolute value is often used to ensure numerical convergence.

A.3.2 Husimi function and Wehrl entropy

The Husimi function is defined as the expectation value of the density operator with coherent states [131] and coincides with the quasiprobability W_{-1},

$$Q(x,p) = \frac{1}{2\pi\hbar}\langle z|\varrho|z\rangle = W_{-1}(x,p), \tag{A.30}$$

where $z(x,p)$ is given by (A.23). It is non-negative, due to the positivity of the density operator [133]. The fact that already the diagonal matrix elements hold the full information on the quantum state reflects the over-completeness of the coherent states [128].

In a semiclassical limit, the Husimi function of a state is localized in phase space along the corresponding Lagrangian manifolds. Thus, in case of regular classical dynamics, the Husimi function of an eigenstate is located on the corresponding quantizing torus; for the case of irregular classical dynamics, it is smeared out over the whole chaotic layer [5]. This allows for a classification of single eigenstates as regular or chaotic if the classical dynamics is mixed. For driven systems, the respective assignment of Floquet states to regions in classical phase space holds true [120].

For a classification of quantum mechanical states according to their phase-space structure, it is desirable to have a direct measure for localization properties. One possibility is provided by the Wehrl entropy S^Q of the state which is defined as the entropy of the corresponding Husimi function [120, 124],

$$S^Q = -\int \mathrm{d}x\,\mathrm{d}p\, Q(x,p)\ln[2\pi\hbar Q(x,p)]. \tag{A.31}$$

The number of minimum uncertainty states occupied by the Husimi function is approximately given by $\exp(S^{\mathrm{Q}})$, thus the occupied phase-space area is $2\pi\hbar\exp(S^Q)$. Consequently, for a coherent state the Wehrl entropy assumes its minimum value $S^Q_{\mathrm{min}} = 1$.

B The density operator

An observer, who is not fully aware of the state of a system, can at best describe it by a density operator ϱ [138]. Its eigenvalues p_i give the probability for the system to reside in the corresponding eigenstate. Therefore, the eigenvalues of a proper density operator have to suffice the intrinsic restrictions of probabilities,

$$0 \leq p_i \leq 1, \tag{B.1}$$

$$\sum_i p_i = \operatorname{tr} \varrho = 1, \tag{B.2}$$

i.e. positivity and a total probability which equals unity. In the limit of a pure state, where the full quantum-mechanical information (i.e. the wavefunction) is known, one of the probabilities p_i equals unity, all the others vanish.

B.1 Lindblad form

The conditions on a physically meaningful density operator, Eqs. (B.1) and (B.2), as well as its Hermitecity, of course, have to be conserved during time evolution. Lindblad proved [93] that a Markovian master equation with constant coefficients meets this requirement, thus generates a so-called completely positive dynamical semigroup, if and only if it is of the form

$$\dot{\varrho} = -\frac{\mathrm{i}}{\hbar}[H, \varrho] + \sum_i \gamma_i \left(2Q_i \varrho Q_i^\dagger - Q_i^\dagger Q_i \varrho - \varrho Q_i^\dagger Q_i \right). \tag{B.3}$$

The operators Q_i, which are introduced phenomenologically, induce dissipative transitions of the system.

It turned out, however, that many Markovian master equations occurring in the literature [11, 70, 71, 139, 140], including our master equation (4.3), are not of this so-called Lindblad form, thus they do not ensure positivity of an arbitrary density operator at any future time. This apparent contradiction was resolved only recently: A master equation of the form (4.3) violates positivity only for initial conditions that do not meet the requirements under which it has been derived. Namely, if the system is prepared with a position variance Δx smaller than the thermal de Broglie wavelength,

$$\Delta x < \lambda_{\mathrm{dB}} = \hbar / \sqrt{4 m k_{\mathrm{B}} T}, \tag{B.4}$$

positivity will be violated until Δx becomes larger than λ_{dB} [68–71, 141]. Thus, dissipative effects on a length scale $l < \lambda_{\mathrm{dB}}$ cannot be described selfconsistently within a Markov approximation.

B.2 Coherence and entropy

The lack of information inherent in a density operator ϱ can be measured by the Shannon entropy

$$S = -\sum_i p_i \ln p_i = -\operatorname{tr}(\varrho \ln \varrho). \tag{B.5}$$

Consequently, for a pure state $S = 0$. This definition agrees, besides a factor k_B, with the entropy known from statistical thermodynamics. The entropy also gives a proper measure for the coherence of a system, thus for the ability to observe interference effects. However, it has the disadvantage that its direct numerical computation requires diagonalization of the density operator. A numerically less expensive, related quantity is the "linearized entropy"

$$S_\mathrm{lin} = \operatorname{tr} \varrho(1 - \varrho) = 1 - \operatorname{tr} \varrho^2, \tag{B.6}$$

introduced by Zurek *et al.* [142]. It arises formally by Taylor expansion of (B.5) if ϱ describes an almost pure state. In the case of many incoherently populated states, all $p_i \ll 1$ and both entropies differ drastically. Nevertheless, the related quantity

$$C = \operatorname{tr} \varrho^2 = 1 - S_\mathrm{lin} \tag{B.7}$$

is a proper measure for the coherence of a density operator. Its value approximately gives the reciprocal of the number of incoherently populated states and equals unity if the system resides in a pure state.

C Solution of the Fokker-Planck equation

In this appendix, we solve the equation of motion (5.55) for the Wigner function by the method of characteristics. We write $W(x,p,t)$ as

$$W(x,p,t) = \int \mathrm{d}X\mathrm{d}P\, \mathrm{e}^{\mathrm{i}xX+\mathrm{i}pP}\mathrm{e}^{S(X,P,t)}. \tag{C.1}$$

By this ansatz, equation (5.55) is transformed to the quasilinear partial differential equation

$$\mathcal{F}(X, S_X, P, S_P, t, S_t) = 0 \tag{C.2}$$

for $S(X,P,t)$, where $\mathcal{F}$ is given by

$$\mathcal{F} = S_t - XS_P + \gamma PS_P + \omega^2(t)PS_X + \gamma D_{pp}P^2 + \gamma D_{xp}XP. \tag{C.3}$$

We denote the partial derivatives of $S(X,P,t)$ with respect to X, P, and t by S_X, S_P, and S_t, respectively.

The characteristic equations [95] of (C.2) are given by

$$\dot{t} = \frac{\partial\mathcal{F}}{\partial S_t} = 1, \tag{C.4}$$

$$\dot{X} = \frac{\partial\mathcal{F}}{\partial S_X} = \omega^2(t)P, \tag{C.5}$$

$$\dot{P} = \frac{\partial\mathcal{F}}{\partial S_P} = \gamma P - X, \tag{C.6}$$

$$\dot{S}_X = -\frac{\partial\mathcal{F}}{\partial X} = S_P - \gamma D_{xp}P, \tag{C.7}$$

$$\dot{S}_P = -\frac{\partial\mathcal{F}}{\partial P} = -\gamma S_P - \omega^2(t)S_X - 2\gamma D_{pp}P - \gamma D_{xp}X, \tag{C.8}$$

$$\dot{S}_t = -\frac{\partial\mathcal{F}}{\partial t} = -\frac{\mathrm{d}\omega^2(t)}{\mathrm{d}t}PS_X, \tag{C.9}$$

whose solutions give the characteristics of the partial differential equation (C.2).

Equation (C.4) signifies that the characteristics can be parameterized by the time t. Instead of equation (C.9), we will use (C.2) to get an expression for S_t. So we only have to solve (C.5)–(C.8). The solutions of these equations can be traced back to the fundamental solutions $f_i(t)$ of the classical equation of motion (5.3).

From (C.5) and (C.6), we find

$$\ddot{P} - \gamma\dot{P} + \omega^2(t)P = 0. \tag{C.10}$$

This is simply the classical equation of motion with a negative damping constant. Therefore the solutions for X and P read

$$P(t) = -c_{1+}\mathrm{e}^{\gamma t} f_2(t) + c_{2+}\mathrm{e}^{\gamma t} f_1(t), \tag{C.11}$$

$$X(t) = c_{1+}\mathrm{e}^{\gamma t} \dot{f}_2(t) - c_{2+}\mathrm{e}^{\gamma t} \dot{f}_1(t), \tag{C.12}$$

where c_{i+} denote integration constants.

From (C.7) and (C.8) we find for S_X

$$\ddot{S}_X + \gamma \dot{S}_X + \omega^2(t) S_X = -2\gamma D P, \tag{C.13}$$

which is the classical equation of motion with an inhomogeneity. The effective diffusion constant D is given by

$$D = D_{pp} + \gamma D_{xp}. \tag{C.14}$$

With the integration constants c_{i-}, we integrate (C.13) with the Green function (5.10) to

$$S_X(t) = c_{1-} f_1(t) + c_{2-} f_2(t) - 2\gamma D \int_{t_0}^{t} \mathrm{d}t'\, G(t,t') P(t'), \tag{C.15}$$

and get by use of (C.7)

$$S_P(t) = c_{1-} \dot{f}_1(t) + c_{2-} \dot{f}_2(t) - 2\gamma D \int_{t_0}^{t} \mathrm{d}t'\, \frac{\partial G(t,t')}{\partial t} P(t') + \gamma D_{xp} P(t). \tag{C.16}$$

By inserting

$$P(t') = G(t,t') X(t) + \frac{\partial G(t,t')}{\partial t} P(t), \tag{C.17}$$

obtained from Eqs. (C.11) and (C.12), we get a result for S_X and S_P that only depends on the endpoints of the characteristics. Now together with Eq. (C.2), we have an expression for $\operatorname{grad} S(X,P,t) = (S_X, S_P, S_t)$, which can be integrated to

$$\begin{aligned} S(X,P,t) = {} & \Big[c_{1-} f_1(t) + c_{2-} f_2(t)\Big] X + \Big[c_{1-} \dot{f}_1(t) + c_{2-} \dot{f}_2(t)\Big] P \\ & - \frac{1}{2}\sigma_{xx}(t,t_0) X^2 - \sigma_{xp}(t,t_0) XP - \frac{1}{2}\sigma_{pp}(t,t_0) P^2, \end{aligned} \tag{C.18}$$

with

$$\sigma_{xx}(t,t_0) = 2\gamma D \int_{t_0}^{t} \mathrm{d}t' \left[G(t,t')\right]^2, \tag{C.19}$$

$$\sigma_{xp}(t,t_0) = 2\gamma D \int_{t_0}^{t} \mathrm{d}t' G(t,t') \frac{\partial}{\partial t} G(t,t'), \tag{C.20}$$

$$\sigma_{pp}(t,t_0) = -\gamma D_{xp} + 2\gamma D \int_{t_0}^{t} \mathrm{d}t' \left[\frac{\partial}{\partial t} G(t,t')\right]^2. \tag{C.21}$$

By inserting $S(X,P,t)$ into (C.1), we find a time-dependent solution for the Wigner function $W(x,p,t)$.

The integration constants $c_{i\pm}$ are constant along the characteristics by construction. Thus, the Poisson brackets between the expressions $c_{i\pm}(X, S_X, P, S_P, t)$ and $\mathcal{F}(X, S_X, P, S_P, t, S_t)$ vanish [95]. By transforming back from Fourier space to real space, one finds that the operators $\hat{c}_{i\pm} \equiv c_{i\pm}(-\mathrm{i}\partial_x, -\mathrm{i}x, -\mathrm{i}\partial_p, -\mathrm{i}p, t)$ commute with the operator $\partial_t - L(t)$, whose nullspace is the solution of the equation of motion. Therefore, the $\hat{c}_{i\pm}$ are shift operators in the subspace of solutions, i.e., if $W(x, p, t)$ is a solution of (5.55), then $\hat{c}_{i\pm}W(x, p, t)$ is also a solution. For the $\hat{c}_{i\pm}$ we find

$$\hat{c}_{1+} = \frac{1}{2}\Big[f_1(t)\partial_x + \dot{f}_1(t)\partial_p\Big], \tag{C.22}$$

$$\hat{c}_{2+} = \frac{1}{2}\Big[f_2(t)\partial_x + \dot{f}_2(t)\partial_p\Big], \tag{C.23}$$

$$\begin{aligned}\hat{c}_{1-} = {} & \mathrm{i}\dot{f}_2(t)\Big[x + \sigma_{xx}(t, t_0)\partial_x + \sigma_{xp}(t, t_0)\partial_p\Big] \\ & - \mathrm{i}f_2(t)\Big[p + \sigma_{xp}(t, t_0)\partial_x + \sigma_{pp}(t, t_0)\partial_p\Big],\end{aligned} \tag{C.24}$$

$$\begin{aligned}\hat{c}_{2-} = {} & -\mathrm{i}\dot{f}_1(t)\Big[x + \sigma_{xx}(t, t_0)\partial_x + \sigma_{xp}(t, t_0)\partial_p\Big] \\ & + \mathrm{i}f_1(t)\Big[p + \sigma_{xp}(t, t_0)\partial_x + \sigma_{pp}(t, t_0)\partial_p\Big].\end{aligned} \tag{C.25}$$

Note that because of the linear structure of the characteristic equations, there is no ambiguity concerning the ordering of operators. The operators $Q_{i+}(t)$, used in Section 5.4.2 to construct the Floquet solutions of the Fokker-Planck equation, are proportional to the $\hat{c}_{i+}$.

References

[1] G. Casati, B. V. Chirikov, F. M. Izrailev, and J. Ford, in *Stochastic Behavior in Classical and Quantum Hamiltonian Systems*, Vol. 93 of *Lecture Notes in Physics*, edited by G. Casati and J. Ford (Springer, Berlin, 1979), p. 334.

[2] T. Dittrich and R. Graham, *Long Time Behavior in the Quantized Standard Map with Dissipation*, Ann. Phys. (N.Y.) **200**, 363 (1990).

[3] H.-G. Schuster, *Deterministic chaos: an introduction*, 2nd ed. (VCH, Weinheim, 1989).

[4] E. Heller, *Bound-State Eigenfunctions of Classically Chaotic Hamiltonian Systems: Scars of Periodic Orbits*, Phys. Rev. Lett. **53**, 1515 (1984).

[5] K. Takahashi and N. Saitô, *Chaos and Husimi Distribution Function in Quantum Mechanics*, Phys. Rev. Lett. **55**, 645 (1985).

[6] F. J. Dyson, *The Threefold Way: Algebraic Structure of Symmetry Groups and Ensembles in Quantum Mechanics*, J. Math. Phys. **3**, 1199 (1962).

[7] M. V. Berry and M. Robnik, *Semiclassical level spacings when regular and chaotic orbits coexist*, J. Phys. A **17**, 2413 (1984).

[8] M. L. Mehta, *Random matrices and the statistical theory of energy levels* (Academic Press, New York, 1967).

[9] F. Hund, *Zur Deutung der Molekelspektren III: Bemerkungen über das Schwingungs- und Rotationsspektrum bei Molekeln mit mehr als zwei Kernen*, Z. Phys. **43**, 805 (1927).

[10] F. Grossmann, T. Dittrich, P. Jung, and P. Hänggi, *Coherent Destruction of Tunneling*, Phys. Rev. Lett. **67**, 516 (1991).

[11] A. O. Caldeira and A. L. Leggett, *Quantum Tunnelling in a Dissipative System*, Ann. Phys. (N.Y.) **149**, 374 (1983).

[12] M. Grifoni and P. Hänggi, *Driven Quantum Tunneling*, Phys. Rep. **304**, 219 (1998).

[13] O. Bohigas, S. Tomsovic, and D. Ullmo, *Dynamical quasidegeneracies and separation of regular and irregular quantum levels*, Phys. Rev. Lett. **64**, 1479 (1990).

[14] O. Bohigas, S. Tomsovic, and D. Ullmo, *Classical transport effects on chaotic levels*, Phys. Rev. Lett. **65**, 5 (1990).

[15] S. Tomsovic and D. Ullmo, *Chaos-assisted tunneling*, Phys. Rev. E **50**, 145 (1994).

[16] R. Utermann, T. Dittrich, and P. Hänggi, *Tunneling and the Onset of Chaos in a Driven Bistable System*, Phys. Rev. E **49**, 273 (1994).

[17] W. A. Lin and L. E. Ballentine, *Quantum tunneling and chaos in a driven anharmonic oscillator*, Phys. Rev. Lett. **65**, 2927 (1990).

[18] J. Plata and J. M. Gomez Llorente, *Classical-quantum correspondence for barrier crossing in a driven bistable potential*, J. Phys. A **25**, L303 (1992).

[19] V. B. Magalinskiĭ, *Dynamical model in the theory of the Brownian motion*, Zh. Eksp. Teor. Fiz. **36**, 1942 (1959), [Sov. Phys. JETP **9**, 1381 (1959)].

[20] R. Zwanzig, *Ensemble method in the theory of irreversibility*, J. Chem. Phys. **33**, 1338 (1960).

[21] R. P. Feynman and F. L. Vernon, *The theory of a general quantum system interacting with a linear dissipative system*, Ann. Phys. (N.Y.) **24**, 118 (1963).

[22] R. Blümel, R. Graham, L. Sirko, U. Smilansky, H. Walther, and K. Yamada, *Microwave excitation of Rydberg atoms in presence of noise*, Phys. Rev. Lett. **62**, 341 (1989).

[23] A. G. Fainshtein, N. L. Manakov, and L. P. Rapoport, *Some general properties of quasi-energetic spectra of quantum systems in classical monochromatic fields*, J. Phys. B **11**, 2561 (1978).

[24] N. L. Manakov, V. D. Ovsiannikov, and L. P. Rapoport, *Atoms in a laser field*, Phys. Rep. **141**, 319 (1986).

[25] T. Dittrich, P. Hänggi, G.-L. Ingold, B. Kramer, G. Schön, and W. Zwerger, *Quantum Transport and Dissipation* (Wiley-VCH, Weinheim, 1998).

[26] R. Graham and R. Hübner, *Generalized Quasi-Energies and Floquet States for a Dissipative System*, Ann. Phys. (N.Y.) **234**, 300 (1994).

[27] S. Kohler, T. Dittrich, and P. Hänggi, *Floquet-Markovian description of the parametrically driven, dissipative harmonic quantum oscillator*, Phys. Rev. E **55**, 300 (1997).

[28] C. Zerbe and P. Hänggi, *Brownian parametric quantum oscillators with dissipation*, Phys. Rev. E **52**, 1533 (1995).

[29] J. I. Cirac and P. Zoller, *Quantum Computations with Cold Trapped Ions*, Phys. Rev. Lett. **74**, 4091 (1995).

[30] O. Bohigas, S. Tomsovic, and D. Ullmo, *Manifestations of classical phase space structures in quantum mechanics*, Phys. Rep. **223**, 43 (1993).

[31] M. Latka, P. Grigolini, and B. J. West, *Chaos and avoided level crossing*, Phys. Rev. E **50**, 596 (1994).

[32] M. Latka, P. Grigolini, and B. J. West, *Chaos-induced avoided level crossing and tunneling*, Phys. Rev. A **50**, 1071 (1994).

[33] M. Latka, P. Grigolini, and B. J. West, *Control of dynamical tunneling in a bichromatically driven pendulum*, Phys. Rev. E **50**, R3299 (1994).

[34] S. Kohler, R. Utermann, P. Hänggi, and T. Dittrich, *Coherent and incoherent chaotic tunneling near singlet-doublet crossings*, Phys. Rev. E **58**, 7219 (1998).

[35] G. Floquet, Ann. de l'Ecole Norm. Sup. **12**, 47 (1883).

[36] G. Casati and L. Molinari, *"Quantum Chaos" with Time-Periodic Hamiltonians*, Prog. Theor. Phys. Suppl. **98**, 287 (1989).

[37] S.-I. Chu, *Generalized Floquet theoretical approach to intense-field multiphoton and nonlinear optical processes*, Adv. Chem. Phys. **73**, 739 (1989).

[38] J. S. Howland, *Stationary Scattering Theory for Time-dependent Hamiltonians*, Math. Ann. **207**, 315 (1974).

[39] J. H. Shirley, *Solution of the Schrödinger Equation with a Hamiltonian Periodic in Time*, Phys. Rev. **138**, B979 (1965).

[40] H. Sambe, *Steady States and Quasienergies of a Quantum-Mechanical System in an Oscillating Field*, Phys. Rev. A **7**, 2203 (1973).

[41] D. J. Moore, *Time dependence in quantum mechanics—Floquet theory and the Berry phase*, Helv. Phys. Acta **66**, 3 (1993).

[42] W. Magnus and S. Winkler, *Hill's Equation* (Dover, New York, 1979).

[43] J. von Neumann, *Mathematical foundations of quantum mechanics* (Princeton Univ. Press, Princeton, 1955).

[44] C. Cohen-Tannoudji, J. Dupont-Roc, and G. Grynberg, *Atom photon interaction: basic processes and applications* (Wiley, New York, 1992).

[45] H. Risken, *The Fokker-Planck Equation*, Vol. 18 of *Springer Series in Synergetics* (Springer, Berlin, 1984).

[46] N. Moiseyev, *Time-independent scattering theory for general time-dependent Hamiltonians*, Comments At. Mol. Phys. **31**, 87 (1995).

[47] U. Peskin and N. Moiseyev, *The solution of the time-dependent Schrödinger equation by the (t, t') method: Theory, computational algorithm and applications*, J. Chem. Phys. **99**, 4590 (1993).

[48] H. Goldstein, *Classical Mechanics*, 2nd ed. (Addison-Wesley, Reading, 1980).

[49] U. Weiss, *Quantum Dissipative Systems*, Vol. 2 of *Series in Modern Condensed Matter Physics* (World Scientific, Singapore, 1993).

[50] W. H. Louisell, *Quantum Statistical Properties of Radiation* (Wiley & Sons, New York, 1973).

[51] F. Haake, in *Quantum Statistics in Optics and Solid-State Physics*, Vol. 66 of *Springer Tracts in Modern Physics*, edited by G. Höhler (Springer, Berlin, 1973).

[52] H. Grabert, in *Projection Operator Techniques in Nonequilibrium Statistical Mechanics*, Vol. 95 of *Springer Tracts in Modern Physics*, edited by G. Höhler (Springer, Berlin, 1982).

[53] P. Hänggi, P. Talkner, and M. Borkovec, *Reaction-rate theory: fifty years after Kramers*, Rev. Mod. Phys. **62**, 251 (1990).

[54] H. Grabert, U. Weiss, and P. Talkner, *Quantum Theory of the Damped Harmonic Oscillator*, Z. Phys. B **55**, 87 (1984).

[55] P. Riseborough, P. Hänggi, and U. Weiss, *Exact Results for a Damped Quantum Mechanical Harmonic Oscillator*, Phys. Rev. A **31**, 471 (1985).

[56] G. A. Voth, *Feynman Path Integral of Quantum Mechanical Transition-State Theory*, J. Phys. Chem. **97**, 8365 (1993).

[57] D. E. Makarov and N. Makri, *Control of dissipative tunnelling dynamics by continuous wave electromagnetic fields: Localization and large-amplitude coherent motion*, Phys. Rev. E **52**, 5863 (1995).

[58] N. Makri, *Stabilization of localized states in dissipative tunneling systems interacting with monochromatic fields*, J. Chem. Phys. **106**, 2286 (1997).

[59] R. Zwanzig, *Nonlinear Generalized Langevin Equations*, J. Stat. Phys. **9**, 215 (1973).

[60] H. Grabert, P. Schramm, and G.-L. Ingold, *Quantum Brownian Motion: The Funtional Integral Approach*, Phys. Rep. **168**, 115 (1988).

[61] R. Benguria and M. Kac, *Quantum Langevin Equation*, Phys. Rev. Lett. **46**, 1 (1981).

[62] A. Schmid, *On a Quasiclassical Langevin Equation*, J. Low Temp. Phys. **49**, 609 (1982).

[63] G. W. Ford and M. Kac, *On the Quantum Langevin Equation*, J. Stat. Phys. **46**, 803 (1987).

[64] P. Hänggi, *Generalized Langevin Equations: A Useful Tool for the Perplexed Modeller of Nonequilibrium Fluctuations?*, in *Stochastic Dynamics*, Vol. 484 of *Lecture Notes in Physics*, edited by L. Schimansky-Geier and T. Pöschel (Springer, Berlin, 1997), p. 15.

[65] R. P. Feynman and A. R. Hibbs, *Quantum Mechanics and Path Integrals* (McGraw-Hill, New York, 1965).

[66] L. S. Schulman, *Techniques and Applications of Path Integrals* (Wiley & Sons, New York, 1981).

[67] N. Makri and D. E. Makarov, *Tensor propagator for iterative quantum evolution of reduced density matrices. I. Theory*, J. Chem. Phys. **102**, 4600 (1995).

[68] P. Pechukas, in *Proc. NATO ASI "Large-scale molecular systems"*, edited by W. Gans (Plenum Press, New York, 1991), Vol. B258, p. 123.

[69] P. Pechukas, *Reduced Dynamics Need Not Be Completely Positive*, Phys. Rev. Lett. **73**, 1060 (1994).

[70] L. Diósi, *Caldeira-Leggett master equation and medium temperatures*, Physica A **199**, 517 (1993).

[71] L. Diósi, *On High-Temperature Markovian Equation for Quantum Brownian Motion*, Europhys. Lett. **22**, 1 (1993).

[72] M. Grifoni, M. Sassetti, J. Stockburger, and U. Weiss, *Nonlinear response of a periodically driven damped two-state system*, Phys. Rev. E **48**, 3497 (1993).

[73] M. Grifoni, M. Sassetti, P. Hänggi, and U. Weiss, *Cooperative effects in the nonlinearly driven spin-boson system*, Phys. Rev. E **52**, 3596 (1995).

[74] T.-S. Ho, K. Wang, and S.-I. Chu, *Floquet-Liouville supermatrix approach: Time development of density-matrix operator and multiphoton resonance spectra in intense laser fileds*, Phys. Rev. A **33**, 1798 (1986).

[75] R. Blümel, A. Buchleitner, R. Graham, L. Sirko, U. Smilansky, and H. Walther, *Dynamical localization in the microwave interaction of Rydberg atoms: The influence of noise*, Phys. Rev. A **44**, 4521 (1991).

[76] T. Dittrich, B. Oelschlägel, and P. Hänggi, *Driven Dissipative Tunneling*, Europhys. Lett. **22**, 5 (1993).

[77] B. Oelschlägel, T. Dittrich, and P. Hänggi, *Damped periodically driven quantum transport in bistable systems*, Acta Physica Polonica B **24**, 845 (1993).

[78] T. Dittrich, P. Hänggi, B. Oelschlägel, and R. Utermann, *Driven Tunneling: New Possibilities for Coherent and Incoherent Quantum Transport*, in *25 Years of Non-Equilibrium Statistical Mechanics*, Vol. 445 of *Lecture Notes in Physics*, edited by J. J. Brey (Springer, Berlin, 1995), p. 269.

[79] F. Haake, *Quantum Signatures of Chaos*, Vol. 54 of *Springer Series in Synergetics* (Springer, Berlin, 1991).

[80] R. Graham, *Global and Local Dissipation in a Quantum Map*, Z. Phys. B **59**, 75 (1985).

[81] V. S. Popov and A. M. Perelomov, *Parametric exitation of a quantum oscillator*, Zh. Eksp. Teor. Fiz. **55**, 589 (1968), [Sov. Phys. JETP **29**, 719 (1969)].

[82] V. S. Popov and A. M. Perelomov, *Parametric exitation of a quantum oscillator II*, Zh. Eksp. Teor. Fiz. **57**, 1684 (1969), [Sov. Phys. JETP **30**, 910 (1970)].

[83] V. S. Perelomov, A. M. Popov, *Group-theoretical aspects of the variable frequency oscillator problem*, Teor. Mat. Fiz. **1**, 360 (1969).

[84] W. Paul, *Electromagnetic traps for charged and neutral particles*, Rev. Mod. Phys. **62**, 531 (1990).

[85] N. W. McLachlan, *Theory and Applications of Mathieu Functions* (Dover Publications Inc., New York, 1964).

[86] H. R. Lewis, Jr., *Classical and Quantum Systems with Time-Dependent Harmonic-Oscillator-Type Hamiltonians*, Phys. Rev. Lett. **18**, 510, 636 (1967).

[87] H. R. Lewis, Jr. and W. B. Riesenfeld, *An Exact Quantum Theory of the Time-Dependent Harmonic Oscillator and of a Charged Particle in a Time-Dependent Electromagnetic Field*, J. Math. Phys. **10**, 1458 (1969).

[88] L. S. Brown, *Quantum Motion in a Paul Trap*, Phys. Rev. Lett. **66**, 527 (1991).

[89] G. Schrade, V. I. Man'ko, W. P. Schleich, and R. J. Glauber, *Wigner Functions in the Paul Trap*, Quantum Semiclass. Opt. **7**, 307 (1995).

[90] J. G. Hartley and J. R. Ray, *Coherent States for the time-dependent harmonic oscillator*, Phys. Rev. D **25**, 382 (1982).

[91] D. B. Monteoliva, B. Mirbach, and H.-J. Korsch, *Global and local dynamical invariants and quasienergy states of time-periodic Hamiltonians*, Phys. Rev. A **57**, 746 (1998).

[92] I. M. Gradshteyn, I. S. Ryzhik, *Table of Integrals, Series, and Products*, 5th ed. (Academic Press, San Diego, 1994).

[93] G. Lindblad, *On the Generators of Quantum Dynamical Semigroups*, Commun. Math. Phys. **48**, 119 (1976).

[94] P. Hänggi and H. Thomas, *Stochastic Processes: Time Evolution, Symmetries and Linear Response*, Phys. Rep. **88**, 206 (1982).

[95] E. Kamke, *Differentialgleichungen, Vol. II: Partielle Differentialgleichungen*, 6th ed. (Teubner, Stuttgart, 1979).

[96] L. H'walisz, P. Jung, P. Hänggi, P. Talkner, and L. Schimansky-Geier, *Colored noise driven systems with inertia*, Z. Phys. B **77**, 471 (1989).

[97] C. Zerbe, P. Jung, and P. Hänggi, *Brownian parametric oscillators*, Phys. Rev. E **49**, 3626 (1994).

[98] U. M. Titulaer, *A systematic solution procedure for the Fokker-Planck equation of a Brownian particle in the high friction case*, Physica A **91**, 321 (1978).

[99] W. A. Lin and L. E. Ballentine, *Quantum tunneling and regular and irregular quantum dynamics of a driven double-well oscillator*, Phys. Rev. A **45**, 3637 (1992).

[100] P. Hänggi, R. Utermann, and T. Dittrich, *Tunnel Splittings and Chaotic Transport in Periodically Driven Bistable Systems*, Physica B **194-196**, 1013 (1994).

[101] E. M. Zanardi, J. Gutiérrez, and J. M. Gomez Llorente, *Mixed dynamics and tunneling*, Phys. Rev. E **52**, 4736 (1995).

[102] E. Doron and S. D. Frischat, *Semiclassical description of tunneling in mixed systems: Case of the annular billiard*, Phys. Rev. Lett **75**, 3661 (1995).

[103] S. D. Frischat and E. Doron, *Dynamical tunneling in mixed systems*, Phys. Rev. E **57**, 1421 (1998).

[104] F. Leyvraz and D. Ullmo, *The level splitting distribution in chaos-assisted tunneling*, J. Phys. A **29**, 2529 (1996).

[105] R. Roncaglia, L. Bonci, F. M. Izrailev, B. J. West, and P. Grigolini, *Tunneling versus chaos in the kicked Harper model*, Phys. Rev. Lett. **73**, 802 (1994).

[106] T. Dittrich and R. Graham, *Quantum Effects in the Steady State of the Dissipative Standard Map*, Europhys. Lett. **4**, 263 (1987).

[107] F. Grossmann, P. Jung, T. Dittrich, and P. Hänggi, *Tunneling in a Periodically Driven Bistable System*, Z. Phys. B **84**, 315 (1991).

[108] A. Peres, *Dynamical quasidegeneracies and quantum tunneling*, Phys. Rev. Lett. **67**, 158 (1991).

[109] F. Großmann and P. Hänggi, *Localization in a Driven Two-Level Dynamics*, Europhys. Lett. **18**, 571 (1992).

[110] A. J. Lichtenberg and M. A. Liebermann, *Regular and Stochastic Motion*, Vol. 38 of *Applied Mathical Sciences* (Springer, New York, 1983).

[111] D. F. Escande, *Stochasticity in classical Hamiltonian systems: universal aspects*, Phys. Rep. **121**, 165 (1985).

[112] L. E. Reichl and W. M. Zheng, in *Directions in Chaos*, edited by H. B. Lin (World Scientific, Singapore, 1987), Vol. 1, p. 17.

[113] M. Wilkinson, *Tunnelling between tori in phase space*, Physica D **21**, 341 (1986).

[114] M. Wilkinson, *Narrowly avoided crossings*, J. Phys. A **20**, 635 (1987).

[115] L. E. Reichl, *The Transition to Chaos: In Conservative and Classical Systems: Quantum Manifestations* (Springer, New York, 1992).

[116] R. B. Shirts and W. P. Reinhardt, *Approximate constants of motion for classically chaotic vibrational dynamics: Vague tori, semiclassical quantization, and classical intramolecular energy flow*, J. Chem. Phys. **77**, 5204 (1982).

[117] S.-J. Chang and K.-J. Shi, *Time Evolution and Eigenstates of a Quantum Iterative System*, Phys. Rev. Lett. **55**, 269 (1985).

[118] S.-J. Chang and K.-J. Shi, *Evolution and exact eigenstates of a resonant quantum system*, Phys. Rev. A **34**, 7 (1986).

[119] B. Mirbach and H. J. Korsch, *Semiclassical quantization of KAM resonances in time-periodic systems*, J. Phys. A **27**, 6579 (1994).

[120] T. Gorin, H. J. Korsch, and B. Mirbach, *Phase-space localization and level spacing distributions for a driven rotor with mixed regular/chaotic dynamics*, Chem. Phys. **217**, 145 (1997).

[121] F. C. Moon and G.-X. Li, *The fractal dimension of the two-well potential strange attractor*, Physica D **17**, 99 (1985).

[122] F. C. Moon and G.-X. Li, *Fractal Basin Boundaries and Homoclinic Orbits for Periodic Motion in a Two-Well Potential*, Phys. Rev. Lett. **55**, 1439 (1985).

[123] W. Szemplinska-Stupnicka, *Cross-Well Chaos and Escape Phenomena in Driven Oscillators*, Nonlinear Dynamics **3**, 225 (1992).

[124] A. Wehrl, *On the relation between classical and quantum-mechanical entropy*, Reps. Math. Phys. **16**, 353 (1979).

[125] A. Messiah, *Quantum Mechanics*, 3rd ed. (Wiley & Sons, New York, 1965), Vol. I.

[126] M. V. Berry, *Semi-classical mechanics in phase space: a study of Wigner's function*, Proc. R. Soc. A **287**, 237 (1977).

[127] M. Brack and R. K. Bhaduri, *Semiclassical Physics*, Vol. 96 of *Frontiers in Physics* (Addison-Wesley, New York, 1997).

[128] R. J. Glauber, *Coherent and Incoherent States of a Radiation Field*, Phys. Rev. **131**, 2766 (1963).

[129] E. C. G. Sudarshan, *Equivalence of semiclassical and quantum mechanical description of statistical light beams*, Phys. Rev. Lett. **10**, 277 (1963).

[130] E. P. Wigner, *On the Quantum Correction for Thermodynamic Equilibrium*, Phys. Rev. **40**, 749 (1932).

[131] K. Husimi, Proc. Phys. Math. Soc. Japan **22**, 264 (1940).

[132] P. J. Drummond and C. W. Gardiner, *Generalised P-representations in quantum optics*, J. Phys. A **13**, 2353 (1980).

[133] M. Hillery, R. F. O'Connell, M. Scully, and E. P. Wigner, *Distribution Functions in Physics: Fundamentals*, Phys. Rep. **106**, 121 (1984).

[134] C. W. Gardiner, *Handbook of Stochastic Methods*, Vol. 13 of *Springer Series in Synergetics*, 2nd ed. (Springer, Berlin, 1985).

[135] K. E. Cahill and R. J. Glauber, *Density Operators and Quasiprobability Distributions*, Phys. Rev. **177**, 1883 (1969).

[136] K. E. Cahill and R. J. Glauber, *Ordered Expansions in Boson Amplitude Operators*, Phys. Rev. **177**, 1857 (1969).

[137] H. Weyl, *Quantenmechanik und Gruppentheorie*, Z. Phys. **46**, 1 (1927).

[138] E. Fick, *Einführung in die Grundlagen der Quantentheorie*, 6th ed. (Aula, Wiesbaden, 1988).

[139] R. Alicki and K. Lendi, in *Quantum Dynamical Semigroups and Applications*, Vol. 286 of *Lecture Notes in Physics*, edited by W. Beiglböck (Springer, Berlin, 1987).

[140] P. Talkner, *The Failure of the Quantum Regression Hypothesis*, Ann. Phys. (N.Y.) **167**, 390 (1986), see Appendix C therein.

[141] V. Ambegaokar, *Quantum Brownian Motion and its Classical Limit*, Berichte der Bunsengesellschaft **95**, 400 (1991).

[142] W. H. Zurek, S. Habib, and J. P. Paz, *Coherent states via decoherence*, Phys. Rev. Lett. **70**, 1187 (1993).

Acknowledgment

First, I would like to thank Prof. Dr. Peter Hänggi and Prof. Dr. Thomas Dittrich for accepting me as a *Doktorand* and for giving me the opportunity to work on an intriguing project. I gained a lot from their experience. I'm grateful to Thomas also for collaborating with me, even while staying at several remote places all over the world.

Christine Zerbe provided the numerical code for the exact solution of the dissipative, parametrically driven harmonic oscillator.

During the time I spent in Augsburg, I enjoyed many discussions on dissipative quantum mechanics and driven quantum systems with Milena Grifoni, Ludwig Hartmann, Gert-Ludwig Ingold, Michael Thorwart, Ralf Utermann, and Dietmar Weinmann. Especially Gert has always been a competent and interested partner for discussions and questions during his *Teerunde*.

Ralf Utermann not only built up a great computer environment, but also kept it `(mostly :-)` well tuned. With him, Peter Schmitteckert, and André Wobst, I had lots of fruitful discussions about efficient computing and object-oriented programming.

The members of the groups Theoretische Physik I and Theoretische Physik II—present and former ones—provided a stimulating and pleasant working atmosphere.

Thomas Dittrich, Gert-Ludwig Ingold, and Sonja Thunnessen were of indispensible help in proofreading and improving the English of this thesis.

Last, but not least, I'm grateful to the DFG-Schwerpunkt "Zeitabhängige Phänomene und Methoden in Quantensystemen der Physik und Chemie" for founding my position at the Universität Augsburg from September '95 to February '99 under grant no. Di 511/1 and Di 511/2 as well as for the possibility to participate in conferences in Freiburg, Berlin, Dresden, Würzburg, and Haifa.